5-2016

Development of the MASW Method for Pavement Evaluation

Benjamin J. Davis
University of Arkansas, Fayetteville

Development of the MASW Method for Pavement Evaluation

A thesis submitted in partial fulfillment
of the requirements for the degree of
Master of Science in Civil Engineering

by

Benjamin Davis
University of Arkansas
Bachelor of Science in Civil Engineering, 2013

May 2016
University of Arkansas

This thesis is approved for recommendation to the Graduate Council

Dr. Clinton M. Wood
Thesis Director

Dr. Micah Hale
Committee Member

Dr. Michelle Bernhardt
Committee Member

Abstract

The purpose of this research is to establish a recommended procedure for performing multichannel analysis of surface waves (MASW) on pavements as well as evaluating the ability of MASW to detect a change in shear wave velocity as damage in concrete increases. The tests for establishing a recommended procedure for performing MASW on pavements was conducted at five sites at the University of Arkansas Engineering Research Center in Fayetteville, Arkansas. The five sites consisted of three materials: asphalt, concrete, and soil (two sites were on asphalt, two were on concrete, and one was on soil). The methods evaluated at these sites include the source type, distance from the source to the first receiver in the array (i.e., source offset), the spacing between receivers in the array, and the minimum number of receivers in the array. It was determined that for the data collected on asphalt, the optimum procedure included a 230g metal-tipped hammer, 2.5 cm receiver spacing, a minimum of 24 receivers, and source offsets of 12.5 cm, 25 cm, and 50 cm. For concrete, the optimum procedure included a 230g metal-tipped hammer, 5 cm receiver spacing, a minimum of 18 receivers, and source offsets of 12.5 cm, 25 cm, 50 cm, and 75 cm. For soil, the optimum procedure included a 230g metal-tipped hammer, 5 cm receiver spacing, a minimum of 12 receivers, and source offsets of 12.5 cm, 25 cm, and 50 cm. Additionally, it was determined from a limited data set of six tests, that MASW has the ability to detect a decrease in shear wave velocity as damage increases up to a strain level of at least 0.09%. However, MASW testing done on concrete with expansions of 0.09% and 0.29% showed only a 2% difference in shear wave velocity between the two large strain sections. Given the data collected it cannot be determined if MASW can be used to differentiate between concrete sections with strains larger than 0.09% (i.e., sections with heavy damage).

Table of Contents

1 Introduction 1

2 Literature Review 4

2.1 Introduction 4

2.2 Nondestructive Testing 4

2.2.1 Chain Dragging 4

2.2.2 Falling Weight Deflectometer (FWD) 5

2.2.3 Ground Penetrating Radar (GPR) 6

2.2.4 Electrical Resistivity 7

2.3 Seismic Waves 8

2.3.1 Basic wave mechanics 12

2.3.2 Rayleigh Waves 13

2.3.3 Love Waves 14

2.3.4 Lamb Waves 15

2.4 Seismic Wave Testing Methods 17

2.4.1 Steady-State Rayleigh Wave Method 18

2.4.2 Ultrasonic Pulse Velocity (UPV) 19

2.4.3 Impact Echo 19

2.4.4 Spectral Analysis of Surface Waves (SASW) 21

2.4.5 Multichannel Analysis of Surface Waves (MASW) 22

2.4.6 Multichannel Simulation with One Receiver (MSOR) 23
2.5 MASW 24
2.5.1 Geotechnical Site Characterization 24
2.5.2 Pavement Testing 24
2.5.3 Equipment- Source Type 25
2.5.4 Equipment- Receivers 25
2.5.5 Near-field effects 27
2.5.6 Equipment- Data Acquisition System (DAQ) 28
2.5.7 Acquisition 28
2.5.8 Data Processing 28
2.5.9 Inversion 29
2.5.10 Comparison of MASW Tests 30
2.6 Alkali-Silica Reaction (ASR) 31
2.6.1 Efforts in Nondestructive Testing of ASR 32
2.7 Conclusions 33
3 Methods and Materials 35
3.1 Introduction 35
3.2 MASW 35
3.2.1 Equipment 38
3.2.2 Testing 39

3.2.3 Data Acquisition using SignalCalc 730 and Analysis 42
3.2.4 MASW- ASR 43
3.3 ASR Resonance 45
3.3.1 Prism Expansion- ASTM C1293 47
3.3.2 Shear Wave Velocity- ASTM C215 49
3.4 Conclusions 51
4 Analysis of MASW Testing Procedure on Pavement and Soil 52
4.1 Overview 52
4.2 Source Type 53
4.2.1 Asphalt 54
4.2.2 Concrete 56
4.2.3 Soil 58
4.3 Receiver Spacing 59
4.3.1 Asphalt 60
4.3.2 Concrete 63
4.3.3 Soil 65
4.3.4 Conclusions 66
4.4 Source Offset 66
4.4.1 Asphalt 67
4.4.2 Concrete 72

4.4.3 Soil 76
4.4.4 Conclusions 77
4.5 Number of Receivers 78
4.5.1 Asphalt 78
4.5.2 Concrete 80
4.5.3 Soil 83
4.5.4 Conclusions 84
4.6 Lateral influence of Rayleigh wave propagation 84
4.6.1 Sand 86
4.6.2 Clay 87
4.7 Overall Conclusions 87
5 Relationship between ASR Expansion and Shear Wave Velocity in Concrete 89
5.1 Overview 89
5.2 Discussion 89
5.3 MASW Case Study Overview 93
5.4 Discussion 93
5.5 Conclusions 95
6 Summary and Conclusions 96
7 Future Research 101
Works Cited 102

Table of Figures

Figure 2-1. a) Chain dragging method and b) Hammer sounding method (Gucunski 2013. Used with permission)..... 5

Figure 2-2. Falling Weight Deflectometer (Used with permission from FHWA)..... 6

Figure 2-3. Ground Penetrating Radar (GPR) (Gucunski 2013. Used with permission)..... 7

Figure 2-4. Schematic of electrical resistivity (Gucunski 2013). 8

Figure 2-5. Illustration of Body and Surface Waves. 9

Figure 2-6. Dispersive property of surface waves (Rix 1991)..... 11

Figure 2-7. Properties of a wave. 13

Figure 2-8. Rayleigh wave schematic (Bolt 1976). 14

Figure 2-9. Love wave schematic (USGS). 15

Figure 2-10. Example of Lamb wave particle motion (Ryden et al., 2004). 15

Figure 2-11. Typical Lamb wave dispersion for the first, second, and third modes of symmetric (S) and antisymmetric (A) (Ryden et al., 2004)..... 17

Figure 2-12. Basic steady state Rayleigh wave test method (Foti 2000)..... 18

Figure 2-13. Schematic of ultrasonic pulse velocity (UPV) method (Kreitman 2011). 19

Figure 2-14. Basic SASW testing configuration..... 22

Figure 2-15. Basic MASW testing procedure..... 23

Figure 2-16. Change in accelerometer resonance due to coupling method (www.pcb.com). 27

Figure 2-17. a) Macro cracking due to ASR among other causes and b) Microcracking due to ASR (Used with permission from USGS). 32

Figure 3-1. Location of MASW testing sites: “ENRC West Concrete”, “CTTP Soil”, “CTTP Asphalt”, “ENRC Asphalt”, and “ENRC East Concrete.” 36

Figure 3-2. Site pictures of: a) “CTTP Soil”, b) “CTTP Asphalt”, c) “ENRC Asphalt”, d) “ENRC West Concrete”, and e) “ENRC East Concrete.” 37

Figure 3-3. a) Picture of “Soil Box” and b) Schematic of “Soil Box”..... 38

Figure 3-4. a) Love wave orientation of accelerometer and b) Rayleigh wave orientation of accelerometer. 39

Figure 3-5. Template for placing masonry nails in soil. 41

Figure 3-6. Sources used in investigation: a) 1160 gram hammer and b) 230 gram hammer. 41

Figure 3-7. a) Edited dispersion curve using the MATLAB script “PlotAndCutPoints” and b) Unedited dispersion curve developed using the MATLAB script “UofA_MASW.”..... 43

Figure 3-8. Location of MASW tested ASR affected sites on 1-49. 44

Figure 3-9. a) Schematic of barrier wall tested on I-49 near Exit 45, b) Site C-1 visually classified as having “minimal” ASR damage, c) Site C-2 visually classified as having “moderate” ASR damage, and d) Site C-3 visually classified as having “severe” ASR damage. 45

Figure 3-10. 14 day expansion of prisms with unreactive sand to Jobe sand ratios of 8:2, 6:4, and 10:0 (Phillips et al. 2015). 46

Figure 3-11. a) Casting of prisms and b) cured prisms. 48

Figure 3-12. Five gallon bucket for accelerated ASR prisms. 48

Figure 3-13. Water bath for accelerated ASR prisms illustrating a) temperature variable switch and b) the immersion heater and 0.5 m^3/hr. pump. 49

Figure 3-14. ASR prism being tested for expansion. 49

Figure 3-15. Schematic of accelerometer placement and strike point (ASTM C215)..... 50

Figure 3-16. Example output of SignalCalc 240 with the fundamental frequency highlighted. . 51

Figure 4-1. Schematic of MASW parameters evaluated..... 53

Figure 4-2. Sources used in the investigation: a) 1160g hammer and b) 230g hammer..... 54

Figure 4-3. Comparison of the dispersion and COV curves for a 230g and 1160g hammer at ENRC Asphalt. A receiver array of 24 receivers with a 2.5 cm receiver spacing and source offsets of 12.5 cm, 25 cm, and 50 cm (averaged together) were used for the comparison..... 55

Figure 4-4. Comparison of the dispersion and COV curves for a 230g and 1160g hammer at CTTP Asphalt. A receiver array of 24 receivers with a 2.5 cm receiver spacing and source offsets of 12.5 cm, 25 cm, and 50 cm (averaged together) were used for the comparison. 56

Figure 4-5. Comparison of the dispersion and COV curves for a 230g and 1160g hammer at ENRC East Concrete. A receiver array of 24 receivers with a 5 cm receiver spacing and source offsets of 12.5 cm, 25 cm, 50 cm, and 75cm (averaged together) were used for the comparison.57

Figure 4-6. Comparison of the dispersion and COV curves for a 230g and 1160g hammer at ENRC West Concrete. A receiver array of 24 receivers with a 5 cm receiver spacing and source offsets of 12.5 cm, 25 cm, 50 cm, and 75cm (averaged together) were used for the comparison.58

Figure 4-7. Comparison of the dispersion and COV curves for a 230g and 1160g hammer at CTTP Soil. A receiver array of 24 receivers with a 5 cm receiver spacing and source offsets of 12.5 cm, 25 cm, and 50 cm (averaged together) were used for the comparison..... 59

Figure 4-8. MASW array with: a) 2.5 cm spacing, b) 5 cm spacing, and c) 10 cm spacing. 60

Figure 4-9. Comparison of the dispersion and COV curves for 2.5 cm, 5 cm, and 10 cm receiver spacings at ENRC Asphalt. A receiver array of 24 receivers, a 230g hammer and source offsets of 12.5 cm, 25 cm, and 50 cm (averaged together) were used for the comparison. 61

Figure 4-10. Comparison of the dispersion and COV curves for 2.5 cm, 5 cm, and 10 cm receiver spacings at CTTP Asphalt. A receiver array of 24 receivers, a 230g hammer and source offsets of 12.5 cm, 25 cm, and 50 cm (averaged together) were used for the comparison..... 62

Figure 4-11. Comparison of the dispersion and COV curves for 2.5 cm, 5 cm, and 10 cm receiver spacings at ENRC East Concrete. A receiver array of 24 receivers, a 230g hammer and source offsets of 12.5 cm, 25 cm, 50 cm, and 75cm (averaged together) were used for the comparison..... 63

Figure 4-12. Comparison of the dispersion and COV curves for 2.5 cm, 5 cm, and 10 cm receiver spacings at ENRC East Concrete. A receiver array of 24 receivers, a 230g hammer and

source offsets of 12.5 cm, 25 cm, 50 cm, and 75cm (averaged together) were used for the comparison. 64

Figure 4-13. Comparison of the dispersion and COV curves for 2.5 cm, 5 cm, and 10 cm receiver spacings at CTTP Soil. A receiver array of 24 receivers, a 230g hammer and source offsets of 12.5 cm, 25 cm, and 50 cm (averaged together) were used for the comparison. 66

Figure 4-14. Source offsets of 12.5 cm (red), 25 cm (blue), 50 cm (green), 75 cm (magenta), 100 cm (black), and 150 cm (cyan) for MASW testing shown with a 5cm receiver spacing and 24 receivers. 67

Figure 4-15. Comparison of the dispersion and COV curves for source offsets of 12.5 cm, 25 cm, 50 cm, 75 cm, 100 cm, and 150 cm at ENRC Asphalt. A 230g hammer and a receiver array of 24 receivers with a 2.5 cm receiver spacing were used for the comparison. 69

Figure 4-16. Comparison of the dispersion and COV curves for source offsets of 12.5 cm, 25 cm, 50 cm, 75 cm, 100 cm, and 150 cm at CTTP Asphalt. A 230g hammer and a receiver array of 24 receivers with a 2.5 cm receiver spacing were used for the comparison. 71

Figure 4-17. Comparison of the dispersion and COV curves for source offsets of 12.5 cm, 25 cm, 5 0cm, 75 cm, 100 cm, and 150 cm at ENRC East Concrete. A 230g hammer and a receiver array of 24 receivers with a 5cm receiver spacing were used for the comparison. 73

Figure 4-18. Comparison of the dispersion and COV curves for source offsets of 12.5 cm, 25 cm, 50 cm, 75 cm, 100 cm, and 150 cm at ENRC West Concrete. A 230g hammer and a receiver array of 24 receivers with a 5 cm receiver spacing were used for the comparison. 75

Figure 4-19. Comparison of the dispersion and COV curves for source offsets of 12.5 cm, 25 cm, 50 cm, 75 cm, 100 cm, and 150 cm at CTTP Soil. A 230g hammer and a receiver array of 24 receivers with a 5 cm receiver spacing were used for the comparison. 77

Figure 4-20a-c. A) MASW array with 12 receivers, B) MASW array with 18 receivers, and C) MASW array with 24 receivers. 78

Figure 4-21. Comparison of the dispersion and COV curves for 12, 18 and 24 receivers at ENRC Asphalt. A 2.5 cm receiver spacing and a 230g hammer offset 12.5 cm, 25 cm, and 50 cm (averaged together) were used for the comparison. 79

Figure 4-22. Comparison of the dispersion and COV curves for 12, 18 and 24 receivers at CTTP Asphalt. A 2.5 cm receiver spacing and a 230g hammer offset 12.5 cm, 25 cm, and 50 cm (averaged together) were used for the comparison. 80

Figure 4-23. Comparison of the dispersion and COV curves for 12, 18 and 24 receivers at ENRC East Concrete. A 5 cm receiver spacing and a 230g hammer offset 12.5 cm, 25 cm, 50 cm, and 75 cm (averaged together) were used for the comparison. 81

Figure 4-24. Comparison of the dispersion and COV curves for 12, 18 and 24 receivers at ENRC West Concrete. A 5 cm receiver spacing and a 230g hammer offset 12.5 cm, 25 cm, 50 cm, and 75 cm (averaged together) were used for the comparison. 82

Figure 4-25. Comparison of the dispersion and COV curves for 12, 18 and 24 receivers at CTTP Soil. A 5 cm receiver spacing and a 230g hammer offset 12.5 cm, 25 cm, and 50 cm (averaged together) were used for the comparison. 83

Figure 4-26a-b. Laboratory testing environment for evaluating the horizontal resolution of Rayleigh waves using: a) sand and b) homogenous red clay. 85

Figure 4-27. Array configuration for determining the horizontal resolution of Rayleigh waves (Blue=Offset 1, Red=Offset 2, Green=Offset 3, Magenta=Offset 4). 86

Figure 4-28. Dispersion curves displaying arrays on sand with horizontal offsets of 1/8 (Offset 1), 1/4 (Offset 2), 1/2 (Offset 3), and 3/4 (Offset 4) of the box width away from the concrete wall. 87

Figure 5-1. Example reduction of shear wave velocity. 90

Figure 5-2. Shear wave velocity and strain results for Prism groups 40R, 20R, and 0C. Trends are shown as the average of the three specimens in each group. 91

Figure 5-3a-c. Typical cracking from ASR in: a) 40R, b) 20R, and c) 0C 92

Figure 5-4. Three barrier wall sites with varying levels of damage located near Exit 45 on Interstate 45 south of Fayetteville, AR. a) Site C-1 visually classified "minimal" ASR damage, b) Site C-2 visually classified "moderate" ASR damage, c) Site C-3 visually classified "severe" ASR damage. 93

Figure 5-5. Dispersion curves of ASR damaged barrier walls sites C-1, C-2, and C-3 for June 2015 (solid) and March 2016 (dashed). 95

Table of Tables

Table 2-1. Summary of previous research in MASW on pavements. 31

Table 3-1. Descriptions of sites used in testing. 38

Table 3-2. Summary of MASW testing procedure. 42

Table 3-3. Coordinates of ASR affected barrier wall sites tested by MASW. 44

Table 3-4. Mix designs for: a) 0C, b) 20R, and c) 40R. .....**Error! Bookmark not defined.**

Table 4-1. Summary of frequency ranges and average COVs for various offsets for ENRC Asphalt. A 230g hammer and a receiver array of 24 receivers with a 2.5 cm receiver spacing were used in the summary. 68

Table 4-2. Summary of frequency ranges and average COVs for various offsets for CTTP Asphalt. A 230g hammer and a receiver array of 24 receivers with a 2.5 cm receiver spacing were used in the summary. 70

Table 4-3. Summary of frequency ranges and average COVs for various offsets for ENRC East Concrete. A 230g hammer and a receiver array of 24 receivers with a 5 cm receiver spacing were used in the summary. 72

Table 4-4. Summary of frequency ranges and average COVs for various offsets for ENRC West Concrete. A 230g hammer and a receiver array of 24 receivers with a 5 cm receiver spacing were used in the summary. 74

Table 4-5. Summary of frequency ranges and average COVs for various offsets for CTTP Soil. A 230g hammer and a receiver array of 24 receivers with a 5 cm receiver spacing were used in the summary. 76

Table 4-6. Recommended MASW testing procedure for asphalt, concrete, and soil. 88

Table 5-1. Strain associated with three ASR affected barrier wall sites. 95

Table 6-1. Recommended MASW testing procedure for asphalt, concrete, and soil. 99

1 Introduction

According to the American Society of Civil Engineers (ASCE), Arkansas roads cost residents $634 million a year in extra vehicle repairs and operating costs, moreover 39 percent of Arkansas roads are in poor or mediocre condition (ASCE 2013). To reduce both of these numbers, the Arkansas State Highway and Transportation Department (AHTD) and other DOTs/highway departments must develop or implement techniques to plan and budget for roadway repairs and future replacement. Effective methods will yield dense and robust measurements while being conducted in a rapid, non-destructive manner that minimizes traffic disturbance.

There are some nondestructive tests (NDTs) in practice right now that are rapid and produce robust results, but only the spectral analysis of surface waves (SASW) and the multichannel analysis of surface waves (MASW) directly (i.e., not through a correlation) produce physical properties of a material such as Poison's ratio or shear modulus. SASW was originally developed to test pavements, but it has several limitations in that it cannot detect higher modes and the data processing method requires a good deal of time and skill. MASW was developed as a continuation of SASW and improves on the deficiencies of SASW. There is extensive research on MASW testing for soils but little research has concentrated on pavements. The purpose of this research is to test four parameters (source type, source offset, receiver spacing, and number of receivers) used in MASW field testing to determine the optimum testing procedure. Additional research was done on the ability of MASW to measure a degradation in shear wave velocity due to an increase in material damage.

The MASW optimum field testing parameter phase of this research focused on three materials common in transportation: asphalt, concrete, and soil. There were two asphalt sites

("CTTP Asphalt" and "ENRC Asphalt"), two concrete sites ("ENRC East Concrete" and "ENRC West Concrete"), and one soil site ("CTTP Soil"). All of the sites are located at the University of Arkansas Engineering Research Center located in Fayetteville, Arkansas. In addition, research was also done on the effect of lateral variability on Rayleigh wave propagation. This was accomplished by constructing a box with dimensions of 1.22 m wide by 2.44 m long by 2.44 m deep with a cast-in-place (CIP) concrete wall along one of the 2.44 m long walls.

The final portion of the research focused on examining the relationship between a degradation in shear wave velocity and material damage. First, concrete prisms were constructed in accordance with ASTM C1293. There were three groups of prisms constructed, one being a control and the other two containing varying amounts of Jobe sand, which is known for causing alkali-silica reaction (ASR). Second, the ability of MASW to detect a degradation in shear wave velocity as material damage increases was determined. This was accomplished by testing three sites located on a barrier wall along Interstate 49 south of Fayetteville, Arkansas. These three sites (known herein as "C-1","C-2", and "C-3") have varying levels of reactivity and their strains are currently being monitored by Ricky Deschenes of the University of Arkansas.

This thesis is divided into seven sections. Section 1 is the introduction. Section 2 is the literature review containing information on commonly used nondestructive test (NDT) methods, the current state of MASW practice, a brief overview on the mechanics of ASR, and efforts in nondestructively classifying the damage associated with ASR. Section 3 contains the methods used in performing MASW on pavement and in measuring the shear wave velocity of concrete prisms. Section 4 contains the results for evaluating the optimum MASW testing parameters, as well as the results from testing the effect of horizontal variability on Rayleigh wave propagation. Section 5 presents the results from comparing shear wave velocity and material damage. Section

6 presents the final conclusions drawn from this thesis. Section 7 presents several opportunities in future research associated with this thesis.

2 Literature Review

2.1 Introduction

The purpose of this literature review is to increase the understanding of several NDT methods and the merits of using NDT methods to monitor damage in concrete pavements and structures. The primary method examined will be MASW. Sections will cover the process of performing MASW as well as current efforts in performing MASW on pavements. Additionally, the final sections will introduce ASR and efforts in monitoring damage.

2.2 Nondestructive Testing

This section will outline a number of different non-destructive test (NDT) methods that are commonly used in testing pavements. The NDTs that are covered include chain dragging and hammer sounding, falling weight deflectometer, ground penetrating radar, electrical resistivity, steady-state Rayleigh wave method, spectral analysis of surface waves, multichannel analysis of surface waves, and the multichannel simulation with one receiver.

2.2.1 Chain Dragging

The simplest NDT method available is chain dragging and hammer sounding. An example of each is presented in Figure 2-1. Each operate off the principle that an impact on a section of delaminated concrete will sound differently than an impact on a section of intact concrete. Intact concrete will produce a clear ringing sound while a delaminated section will produce a muted and hollow sound (Gucunski 2013). Once an approximate area of delamination is determined using the chain drag method, the area is evaluated with hammer sounding to determine definite boundaries of delamination. The methods give a simple pass/fail, but do not produce any engineering values related to the material being tested.

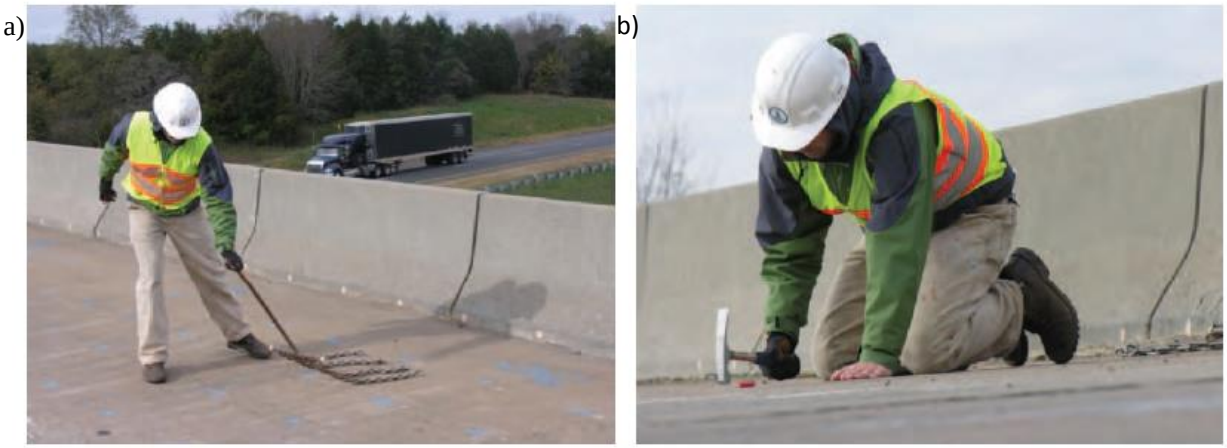

Figure 2-1. a) Chain dragging method and b) Hammer sounding method (Gucunski 2013. Used with permission).

2.2.2 Falling Weight Deflectometer (FWD)

Falling weight deflectometer (FWD) is a NDT that measures the deflection of a pavement under a known loading condition (Figure 2-2). FWD loads the pavement via an internal 150 kg mass that is dropped from a known height onto a rubber pad which rests on the pavement. The force transmitted to the pavement can vary from 0 N to 60,000 N. Peak deflections at multiple points are then measured. The results are used to back calculate the resilient moduli of the pavement layers (Roesset and Shao 1985). FWD is generally considered fully developed and is commercially available.

Figure 2-2. Falling Weight Deflectometer (Used with permission from FHWA).

2.2.3 Ground Penetrating Radar (GPR)

Ground penetrating radar (GPR) uses electromagnetic waves to identify and locate voids and strata boundaries. The method does not produce engineering properties (e.g. shear modulus or mass density). However, the results can be correlated to identify material type and thickness. GPR works by transmitting a high frequency electromagnetic wave into the material of interest and then a portion of the wave is then reflected back to the antenna by an anomaly under the surface. These reflections occur where a material differs in conductivity and relative dielectric permittivity. Conductivity governs how far an electromagnetic wave can penetrate the material while dielectric permittivity governs the speed at which electromagnetic waves propagate (Gucunski 2013). Currently there are a number of different commercial options for GPR.

Figure 2-3. Ground Penetrating Radar (GPR) (Gucunski 2013. Used with permission).

2.2.4 Electrical Resistivity

Electrical Resistivity (ER) measures the resistance to electrical flow of a pavement. The test typically uses a Wenner setup for pavements (see Figure 2-4), which produces an electrical current between the two outside electrodes. The two inside electrodes then measure the potential of the electrical field.

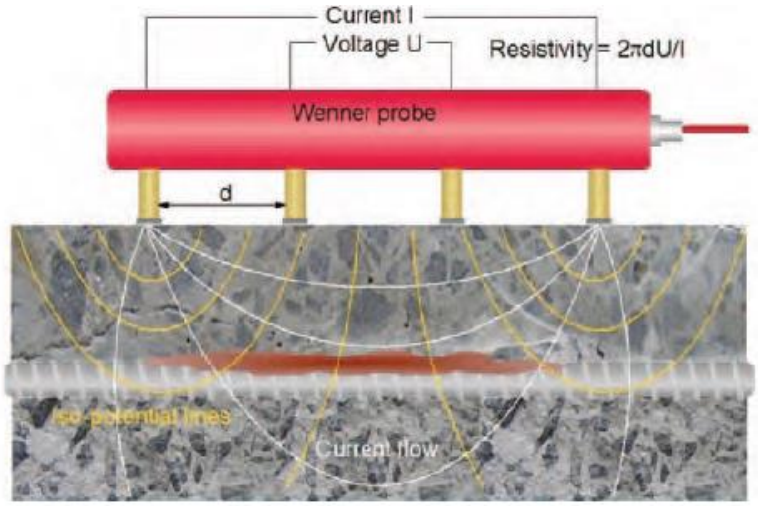

Figure 2-4. Schematic of electrical resistivity (Gucunski 2013).

Much like GPR, resistivity does not provide engineering properties. However, the test is extremely useful in determining the state of corrosion of concrete. In general, as resistivity decreases, the corrosion increases (Gucunski 2013). However, this test is not commercially available for pavement testing and requires a special galvanic coupling to the pavement.

2.3 Seismic Waves

Initial research on seismic waves was first done on earthquakes when seismologists were working to understand the mechanics of an earthquake. Earthquakes produce two types of stress waves, body and surface waves. Body waves are broken into two categories compression (p-waves) and shear (s-waves) waves. There are also several types of surface waves, the most common being Rayleigh waves and Love waves. The difference between the body waves and surface waves is that surface waves propagate along a boundary between a material and free stress boundary while body waves propagate through the body or subsurface (see Figure 2-5). In the 1960s, researchers discovered the potential of surface waves for in-situ geophysical testing when sensors were developed that could measure the velocity of a surface wave across a material. The first surface wave test developed was the steady-state Rayleigh wave method by

Jones (1958, 1962). With this development, engineers and geologists began to evaluate the dynamic properties of near-surface soils. Of particular interest was the shear wave velocity, or V_s, of a material. Shear wave velocity is directly related to shear modulus by Equation 1:

$$G = \rho V_s^2 \quad \text{(Stokoe et al. 2004)} \qquad (1)$$

Where G is shear modulus, ρ is mass density, and V_s is shear wave velocity. Shear modulus helps engineers determine the relationship between stress and strain for a particular material.

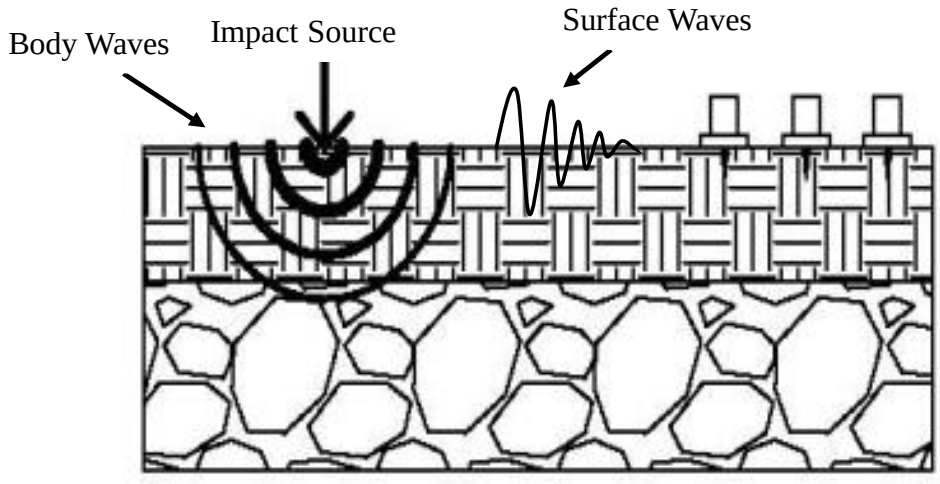

Figure 2-5. Illustration of Body and Surface Waves.

Surface wave testing took another step forward when Nazarian and Stokoe (1984) developed the spectral analysis of surface waves (SASW) method. Since then, many different methods such as impact echo (IE), ultrasonic pulse velocity (UPV), surface wave transmission (SWT), multi-channel simulation with one receiver (MSOR), and the multichannel analysis of surface waves (MASW) have been developed.

For evaluating materials using stress waves, utilizing surface waves over body waves is often more popular for a number of reasons. The primary reason being that surface waves are dispersive. Dispersive means that different frequencies (or wavelengths) travel at different velocities in a layered material. For example, a wave that has a wavelength propagating through

multiple materials will have a velocity that is a weighted average of the velocity of those materials while a wave that has a wavelength propagating through a single material will have a velocity that is only affected by the single material. This principle is illustrated in Figure 2-6. A secondary reason for measuring surface wave velocity is because surface wave energy geometrically attenuates much slower than body waves. Surface waves attenuate at a rate of $\frac{1}{\sqrt{r}}$ while body waves attenuate at a rate of $\frac{1}{r^2}$ where r equals the distance traveled by the wave. Moreover, 67% of the energy created by a vertical surface impact is Rayleigh wave energy, while only 33% is body wave energy (Miller and Pursey 1955). This makes it easier to measure a high signal to noise ratio using surface waves (Rayleigh waves) as opposed to body waves.

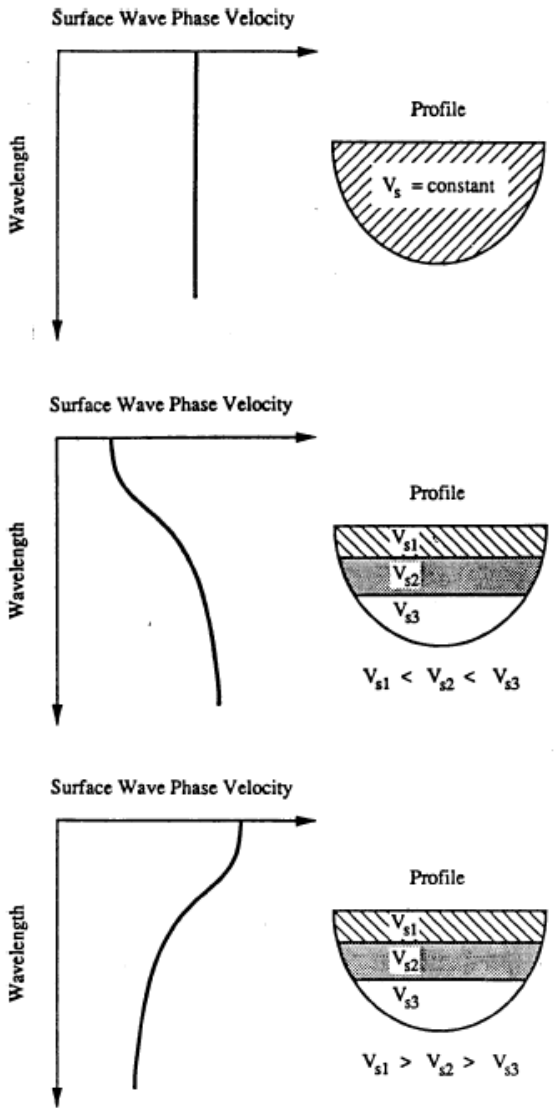

Figure 2-6. Dispersive property of surface waves (Rix 1991).

The following sections will cover basic wave mechanics and types of surface waves (Rayleigh, Love, and Lamb). Rayleigh and Love waves are the most commonly measured surface waves while only a limited amount of research has been done on Lamb wave testing.

2.3.1 Basic wave mechanics

A wave is simply defined as a movement of energy through a material without moving the whole material. A wave will travel at a certain velocity and frequency based on the material's properties. Typically, the stiffer the material, the faster the wave will travel. All waves are defined by the following properties and relationships, which are presented below and in Figure 2-7 for a pure Sine wave.

Peak- Maximum vertical wave motion for one cycle

Trough-Minimum vertical wave motion for one cycle

Amplitude (A) - Difference between the peak and trough divided by two

Wavelength (λ) - Distance between two peaks in a successive cycle

Period (T) - Amount of time passed between two peaks in a successive cycle (typically in seconds)

Frequency (f) - The number of waves that pass a fixed point in one second, or the inverse of T (units are in Hertz or s^{-1})

Angular frequency (ω) - The frequency in radians (radians*s^{-1})

Wave speed (c) - The speed at which a wave travels (may be calculated by either $\frac{\lambda}{T}$ or λf)

Wavenumber (k) - Spatial frequency of a wave or in other words the density of waves in a given distance (may be calculated by $\frac{2\pi}{\lambda}$ or $\frac{1}{\lambda}$)

Phase (Φ) - For a sinusoidal wave that does not begin at t=0, phase is the amount of radians or degrees the wave is offset

Mode- Frequency at which at a standing wave pattern is formed

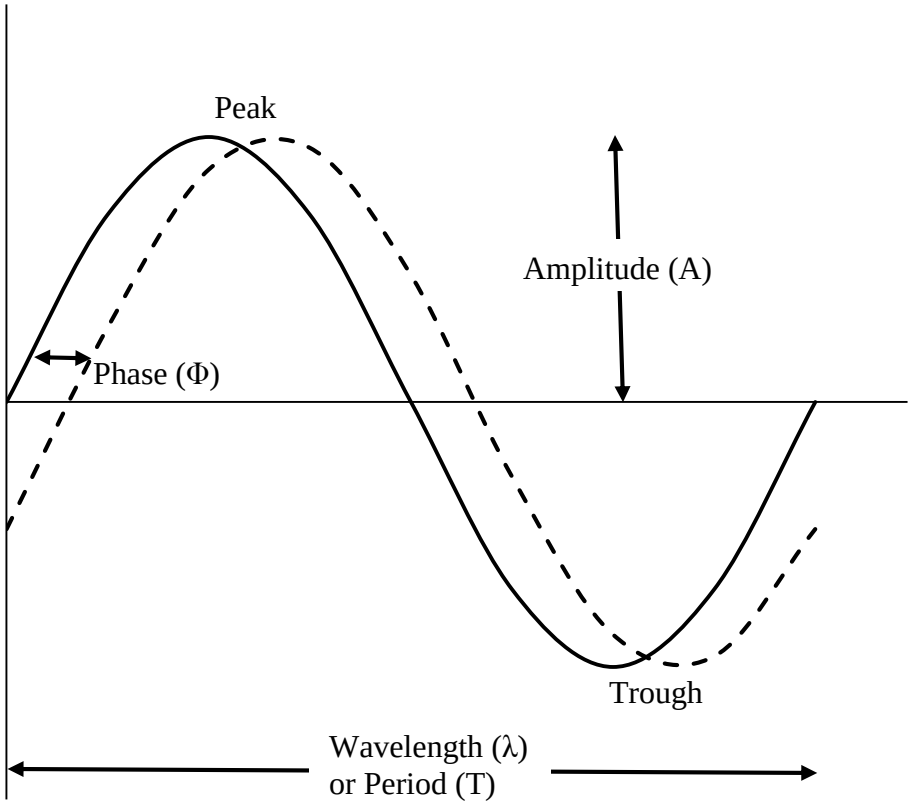

Figure 2-7. Properties of a wave.

2.3.2 Rayleigh Waves

The Rayleigh wave, or R-wave, is the namesake of John William Strutt, the Third Baron Rayleigh. Lord Rayleigh predicted the existence of "waves upon the free surface of an infinite homogenous isotropic elastic solid, their character being such that the disturbance is confined to a superficial region, of thickness comparable with the wavelength" (Strutt 1885). They are generated by the interference of compression waves and vertically polarized shear (SV) waves at the free surface (Liang and Chen 2007). In stress wave testing this is typically instigated by a source (e.g., hammer or Vibroseis) impacting the ground vertically. The waves travel along the

surface in an elliptical retrograde motion as presented in Figure 2-8. The velocity of a Rayleigh wave in a homogenous half-space can be related to shear wave velocity by Equation 2:

$$V_s = (1.13 - 0.16\mu)V_R \quad \text{(Nazarian 1999)} \qquad (2)$$

Where V_s is shear wave velocity, μ is Poisson's ratio, and V_R is Rayleigh wave velocity. Equation 2 may be simplified to $V_s = 1.1 * V_R$.

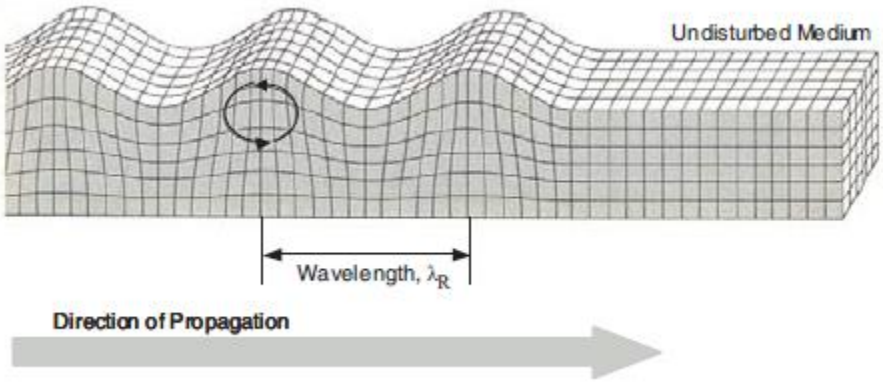

Figure 2-8. Rayleigh wave schematic (Bolt 1976).

2.3.3 Love Waves

Love waves were predicted in 1911 by Augustus Edward Hough Love (Love 1911). The motion is parallel to the free surface and perpendicular to the direction of travel. Love waves are created when two horizontally polarized shear (SH) waves internally reflect off of each other, and the resultant wave motion is presented in Figure 2-9. Since Love waves are created from SH waves and Rayleigh waves are created from SV waves, the two wave types travel orthogonal to each other (Aki and Richards, 1980). Love waves are especially useful in developing an inversion, as they are independent of Poisson's ratio. This simply eliminates one variable present in the Rayleigh wave inversion. Additionally, Love waves are more sensitive to changes in V_s and layer thickness (Liang and Chen 2007). The downside to Love waves is the difficulty

associated with generating them as only 26% of the energy of a seismic impact goes into shear waves.

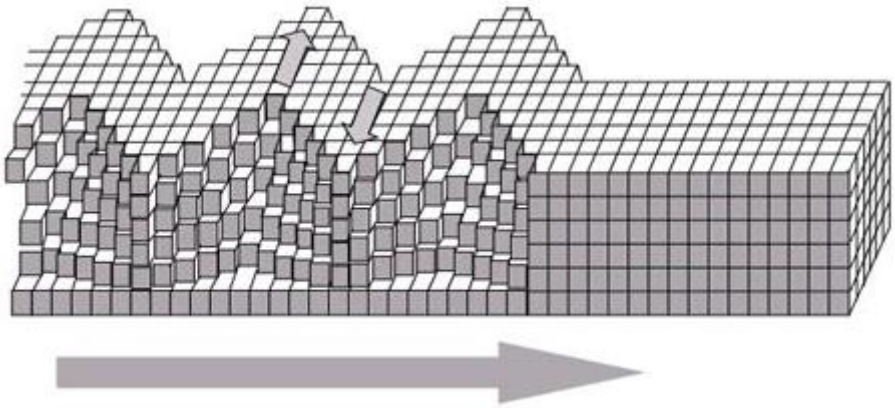

Figure 2-9. Love wave schematic (USGS).

2.3.4 Lamb Waves

Lamb waves were first theorized in 1917 by Horace Lamb. He stated that in plate structures quasi-longitudinal waves, bending waves, and Rayleigh waves could be modeled as one wave (Lamb 1917). This composite wave is now termed free Lamb wave. An example Lamb wave is presented in Figure 2-10.

Figure 2-10. Example of Lamb wave particle motion (Ryden et al., 2004).

These waves are possible only at certain combinations of phase velocities and frequencies. These combinations are given in Equations 3-5, which is termed Lamb's dispersion equation.

$$\frac{\tan\left(\beta\frac{h}{2}\right)}{\tan\left(\alpha\frac{h}{2}\right)} = -\left[\frac{4\alpha\beta k^2}{(k^2-\beta^2)^2}\right]^{\mp 1} \quad (3)$$

$$\alpha = \left(\frac{\omega^2}{V_p^2} - k^2\right)^{0.5} \quad (4)$$

$$\beta = \left(\frac{\omega^2}{V_S^2} - k^2\right)^{0.5} \quad (5)$$

Where h is the thickness of the plate, k is the wave number, c is the phase velocity, and ω is the angular frequency. The ± sign in Equation 3 represents symmetric and antisymmetric wave propagation along the neutral axis of the plate (see Figure 2-11 for an illustration). In traditional SASW, the antisymmetric mode (A0 in Figure 2-11) was most often measured because of inherent limitations in the SASW method (Ryden et al 2004). Although Lamb waves were predicted for plate structures only, research (Martincek 1994) indicates that Lamb waves exist at wavelengths six to seven times the top layer thickness. The implications of this is that for surface wave testing performed on pavements, a traditional Rayleigh wave type inversion is not applicable. Current inversion methods are time consuming and not precise but a crude inversion may be performed on the top layer to obtain the thickness and Rayleigh wave velocity. The Rayleigh wave velocity is the velocity at which the symmetric and antisymmetric modes converge (15-20 kHz).

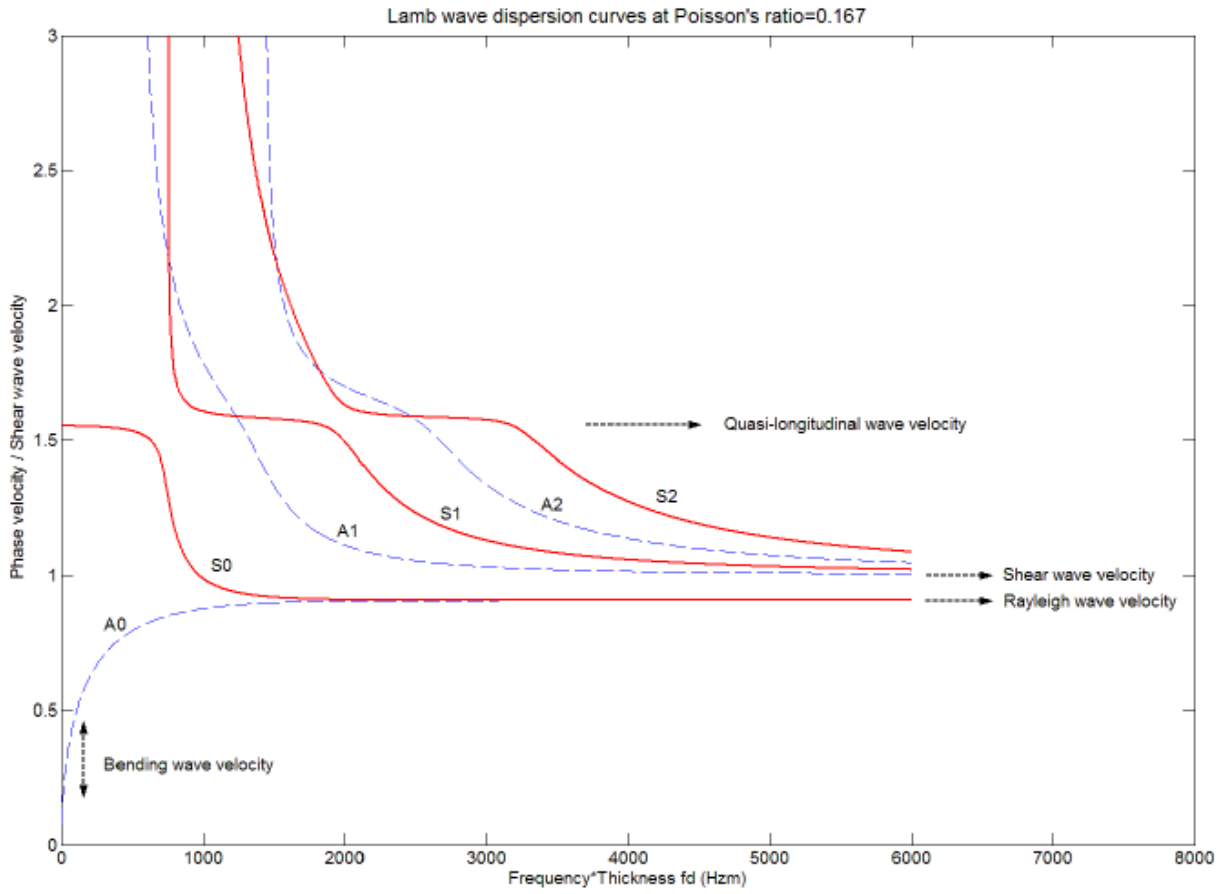

Figure 2-11. Typical Lamb wave dispersion for the first, second, and third modes of symmetric (S) and antisymmetric (A) (Ryden et al., 2004).

2.4 Seismic Wave Testing Methods

Seismic methods offer a unique advantage over other NDTs because seismic NDTs measure the physical properties (e.g., thickness, shear modulus, and Poisson's ratio) of a material rather than empirically correlating results with certain material properties. The following sections will outline the most prevalent seismic tests: steady-state Rayleigh wave method, ultrasonic pulse velocity (UPV), impact echo (IE), spectral analysis of surface waves (SASW), surface wave transmission (SWT), multichannel analysis of surface waves (MASW), and multichannel simulation with one receiver (MSOR).

2.4.1 Steady-State Rayleigh Wave Method

The steady-state Rayleigh wave method was developed by Jones (1958, 1962) and is considered the precursor to modern day surface wave methods. It is a relatively simple test (see Figure 2-12) where a sinusoidal wave with a given frequency is input into the material and two accelerometers are placed in a straight line. The second receiver is then moved until it is in phase with the first. The distance between the two receivers is the wavelength, λ, of the wave. The Rayleigh wave velocity, V_R, is then calculated by Equation 6. The frequency, f, is assumed to be the input frequency.

$$V_R = f\lambda \tag{6}$$

The process is repeated multiple times with different input frequencies and eventually will produce enough data points, creating a dispersion curve. Herein lies the primary disadvantage with the steady-state Rayleigh wave method. It is very time consuming to repeat this test many different times in a trial and error fashion. Additionally, the method does not perform well in stiff-over-soft sites (Foti 2000).

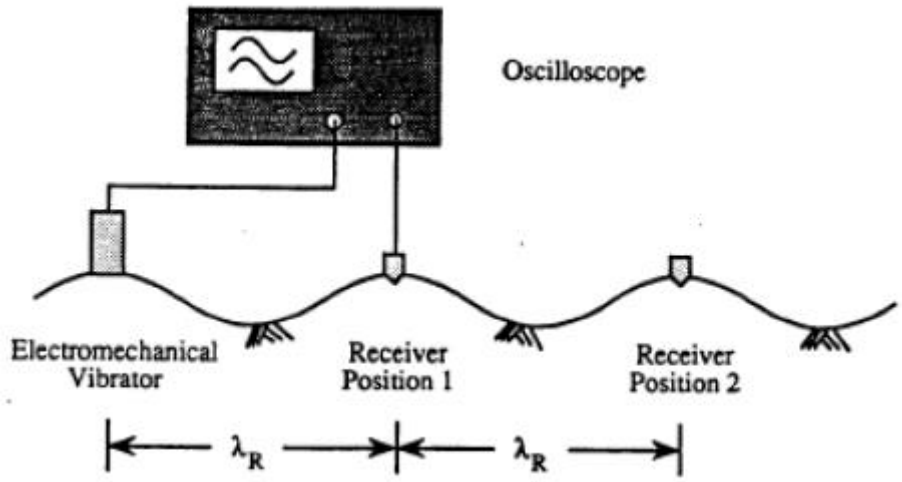

Figure 2-12. Basic steady state Rayleigh wave test method (Foti 2000).

2.4.2 Ultrasonic Pulse Velocity (UPV)

UPV is a simple test method that was first developed in the 1960's and is now standardized by ASTM C597. The test is illustrated in Figure 2-13. The method uses an ultrasonic transmitter to emit a pulse over a known distance to a receiver. The distance divided by the arrival time is the pulse velocity. Any cracking present in the specimen will force the pulse to take a longer path around the cracks (Pessiki 2003). The method is only viable when two opposite sides of a material are unobstructed and can have a transducer or receiver placed on them (e.g. beam or wall).

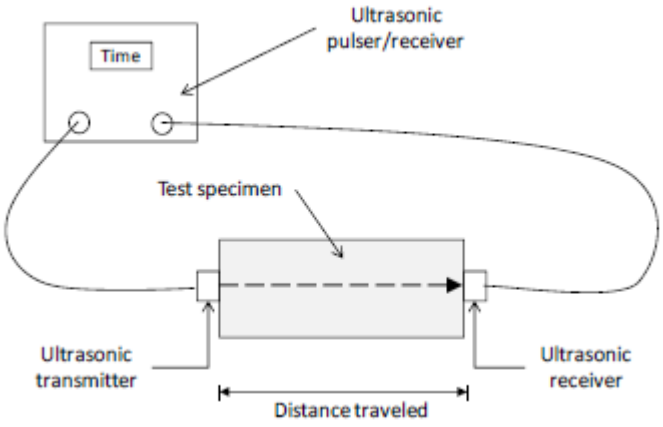

Figure 2-13. Schematic of ultrasonic pulse velocity (UPV) method (Kreitman 2011).

2.4.3 Impact Echo

Impact Echo (IE) was developed throughout the 1980's and was adopted as ASTM 1383 in 1998. The method is based on the principle that p-waves will reflect when there is a difference in acoustic impedance, Z. Acoustic impedance is a function of the material's density. Air has a Z value of 0.4 $\frac{\text{kg}}{\text{m}^2\text{s}}$ while concrete has a Z value of 7x10^6 $\frac{\text{kg}}{\text{m}^2\text{s}}$. This contrast in Z values often results in a full stress wave reflection making results easy to interpret (Carino 2001). The method is not valid for heterogeneous materials (ASTM 1383).

The method is relatively simple to perform; however, there are two separate procedures to determine the p-wave velocity and the thickness. The test is performed by affixing an accelerometer to a surface then an impact is created with a spherical or spherically tipped impactor. The type of impactor is critical because the impact must only last 30μs ±10. It also must be struck within a distance of 0.4*thickness of the accelerometer. The material being tested must have the dimensions of a bar (i.e. the lateral dimensions must be six times the thickness). A fast Fourier transform (FFT) is performed on the accelerometer data and is transformed from the voltage-time domain to the amplitude-frequency domain. The frequency with the largest amplitude is termed the fundamental mode. The p-wave velocity (V_p) is then calculated using Equation 7 and S-wave velocity (V_s) using Equation 8.

$$V_p = \frac{2Tf}{0.96} \tag{7}$$

Where:

V_p =P-wave velocity

f= Fundamental frequency [Hz]

T=Depth to reflecting interface

$$V_s = \frac{0.5 - \mu}{1 - \mu} V_p^2 \tag{8}$$

Where:

Vs= S-wave velocity

μ= Poisson's Ratio

The method is promising in detecting voids and determining the thickness of a slab but it does not obtain a representative measurement of the material as the only area tested is directly beneath the accelerometer.

2.4.4 Spectral Analysis of Surface Waves (SASW)

SASW was primarily developed by Heisey et al. (1982) and Nazarian and Stokoe (1984). The method is capable of determining the thickness and elastic properties of a material. It typically uses two accelerometers or geophones to measure the propagation of Rayleigh waves across a material. An example schematic is presented in Figure 2-14. The test is typically performed where the spacing from the source to receiver one is the same as the spacing from receiver one to receiver two. Typical spacing for pavements range from 0.075 – 2 m. The receiver converts vertical acceleration into an electrical signal that is processed by the data acquisition system (DAQ). The next step is to create a dispersion curve by "unwrapping" the data. This unwrapping process calculates the phase shift between receivers. The phase shift is used to develop an experimental dispersion curve. Unwrapping is the major disadvantage of SASW because it requires a highly trained user and is often time intensive. Because SASW only uses two receivers, it cannot separate higher mode Rayleigh waves from fundamental mode Rayleigh waves. Therefore, if higher modes exist in the wave field, SASW measures a superposition of modes (i.e. the summation of the fundamental and all higher modes). Once the dispersion curve is created, an inversion program is then used to develop a theoretical dispersion curve that matches the experimental dispersion curve. To correctly solve the inverse problem for SASW, the inversion process must model the superposition of all Rayleigh wave modes rather than just the fundamental mode of propagation. When only high frequency waves are of interest, the method is typically termed the ultrasonic surface wave (USW) method.

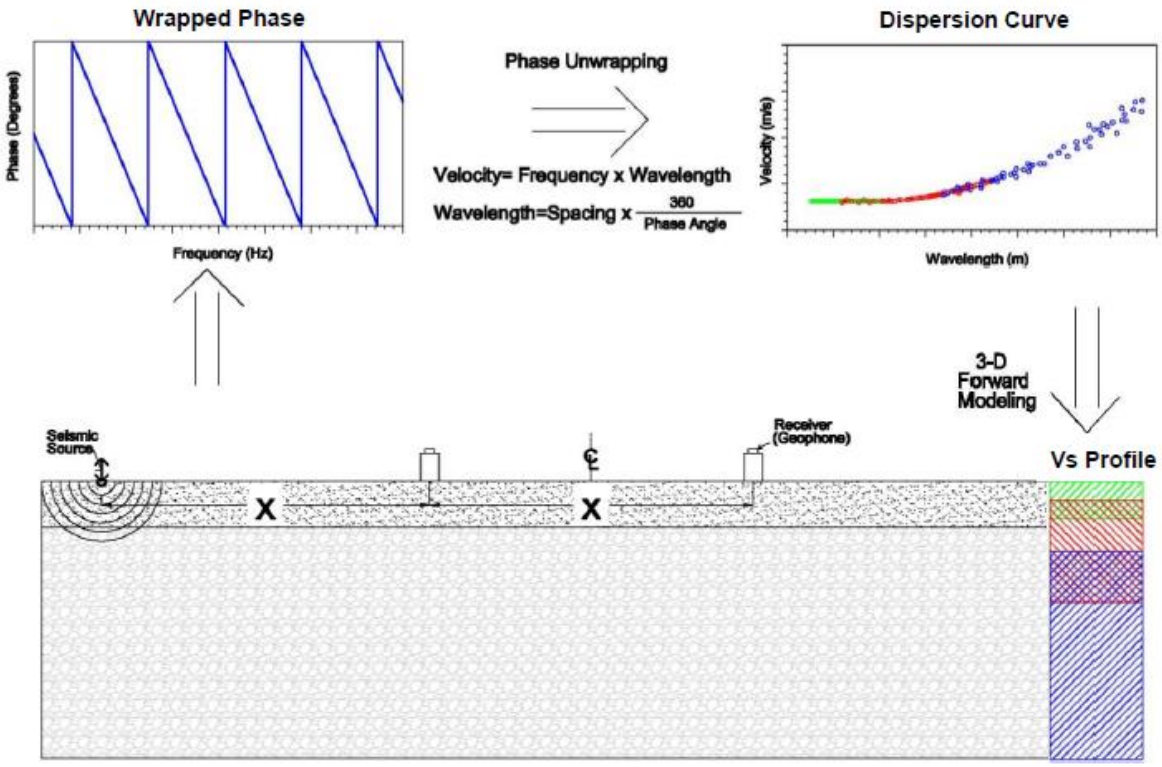

Figure 2-14. Basic SASW testing configuration.

2.4.5 Multichannel Analysis of Surface Waves (MASW)

MASW was first developed by the Kansas Geological Survey (Park et al. 1999) using SASW as a base to build upon. A schematic of the procedure is presented in Figure 2-15. It offers many advantages over SASW because the data processing is less subjective (i.e., operator skill is often lower for MASW than SASW) and significantly faster, outputs robust data, near-field effects as well as noise is mitigated, and has the potential to differentiate modes. An often cited disadvantage of MASW is the cost associated with a DAQ and accelerometers but highway departments place little value in the cost of an NDT when deciding on the implementation of NDT methods (Gucunski 2013). The testing method is similar to SASW in that a seismic source generates surface waves and accelerometers measure the propagation of that wave. It differs in that it is a multichannel method (i.e. 24 receivers) that records data in the space-time domain. A

typical sampling depth for active MASW for dynamic site characterization is 0-30 meters depending on the source and array configuration. Active MASW means that the surface waves are created by a source controlled by the operator (e.g. sledgehammer or Vibroseis). The results of MASW are then inverted to obtain a V_s profile.

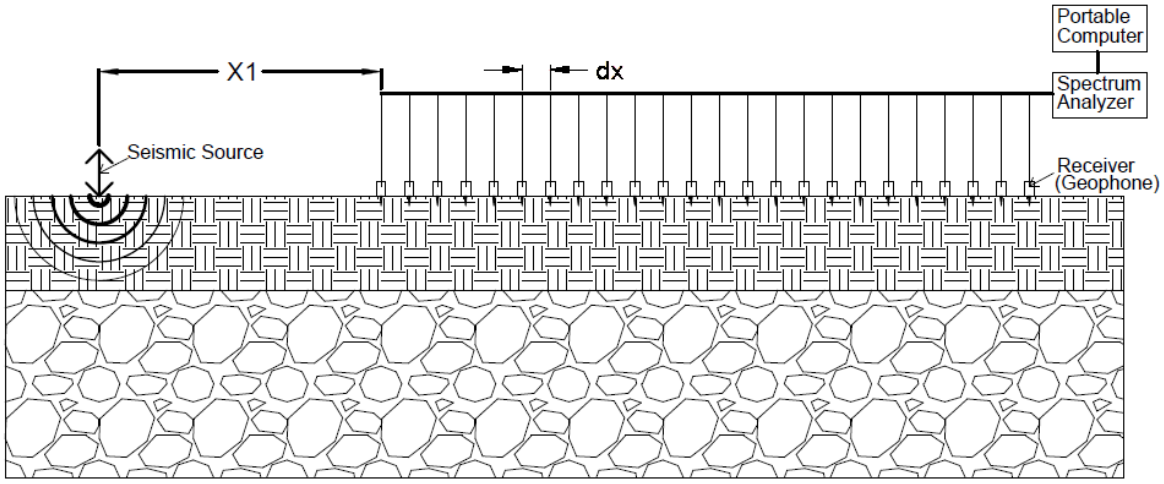

Figure 2-15. Basic MASW testing procedure.

2.4.6 Multichannel Simulation with One Receiver (MSOR)

MSOR was first introduced by Ryden and Ulriksen (2001) shortly after MASW was developed is a close variation of MASW. The two differ in that MSOR only uses one receiver and multiple source offsets to simulate multiple receivers. It is often used when an appropriate signal analyzer capable of recording 24 channels and a large number of accelerometers cannot be obtained. MSOR however produces more uncertainty and is not capable of measuring as high of frequencies as MASW (Lin and Ashlock. 2014).

2.5 MASW

There has been a substantial amount of research done on MASW testing ranging from the effectiveness of different source types to data analysis methods. The proceeding sections will attempt to outline these advances.

2.5.1 Geotechnical Site Characterization

Perhaps the largest use for MASW is for geotechnical site characterization. Typically MASW is used to obtain an average shear wave velocity of the top 30 meters (V_{s30}) to determine the site's ASCE 7 site classification. The results can be used to determine the likelihood of a soil liquefying (Foti 2000).

2.5.2 Pavement Testing

Testing pavements presents a unique challenge because of the stiff over soft site profile compared to the typically normally dispersive profile present when testing soils. The large contrast in seismic wave velocities create interference from higher modes and body wave reflection and refraction. Such difficulties were predicted theoretically (Jones 1962) and seen in SASW results (Sheu et al. 1988; Stokoe et al. 1994). Interference from higher modes may be remedied by examining data at high frequencies (>15 kHz) as the fundamental symmetric and antisymmetric modes converge to the fundamental Rayleigh wave velocity (Park et al. 2001). Much work has been done in recent years in this field and the majority of it is outlined in Section 2.3.4. The current state of practice for MASW testing on pavements allows for the determination of shear wave velocity and thickness of the top layer and as well as crude material properties for layers beyond that. The inversion process is detailed in Section 2.5.9. MASW has also been noted to become less accurate as temperatures rise above 26°C (Alzate-Diaz and Popovics 2009).

2.5.3 Equipment- Source Type

Two categories of sources exist, impulse and harmonic. An example of an impulse source is a hammer, while an ultrasonic transducer is an example of a harmonic source. In determining which style of source to use, the depth of interest must be identified. A harmonic source is useful in testing the very top of the pavement; however, it provides too little energy to overcome environmental noise (Ryden et al. 2001). The area at which high frequency waves lose energy is termed the far-field. Far-field effects can be mitigated by using a source that outputs high frequency energy or by moving the source closer to the receivers (Park et al. 1999). If the one to two meters of depth is of interest, a 230g metal tipped hammer would provide an adequate frequency input. Deeper depths of interest could merit a sledge hammer or Vibroseis.

2.5.4 Equipment- Receivers

In traditional MASW testing on soils, an array of geophones is used. A geophone is simple in theory. A mass wrapped in wire is suspended by a spring and surrounded by a magnet. When the mass moves, it creates voltage in the wire which is proportional to the speed of the mass and is easily interpreted. Geophones are designed to measure frequencies between <1 and 600 Hz depending on the model. This is not practical for MASW testing on pavements as the frequencies of interest are typically well above 600 Hz (Park et al. 2001).

In order to measure these high frequencies, accelerometers must be used in place of the geophones. An accelerometer functions fundamentally different than a geophone. Designs vary but the predominant design uses piezoelectric crystals. When the crystals are stressed by an acceleration, they create a small amount of voltage. This style is termed low impedance integrated circuit piezoelectric (ICP). The voltage is proportional to the acceleration and can be interpreted easily. A typical accelerometer has a frequency range of 5-50000 Hz. This upper limit

is termed the resonant frequency. Ryden et al. (2001) tested the responses of 30 kHz and 54 kHz accelerometers and determined that while the 54 kHz accelerometer had a wider range of frequency response, it was less sensitive to amplitude. Thus Ryden recommends an accelerometer with a resonant frequency of 30 kHz.

There are three main disadvantages to accelerometers. The first is that they require input electricity, which is a disadvantage when recording for long periods of time in a remote (i.e. without electricity) location. The second is that they can be five times as expensive as geophones. Finally, accelerometers are not nearly as robust as geophones. Despite these disadvantages, accelerometers are often the most practical transducers for surface wave testing of pavements.

An important aspect of the receivers used in MASW is the method used to couple the receivers to the pavement. The resonant frequency of the coupling system can be much lower than the resonant frequency of the accelerometer thus creating a low-pass filter. Ryden et al. (2001) studied a variety of coupling systems (glue, weight, threaded stud, gravity, and grease) and determined that grease provided the best results. However, PCB, an accelerometer manufacturer, published Figure 2-16 and recommends using an adhesive rather than a grease when measuring very high frequencies.

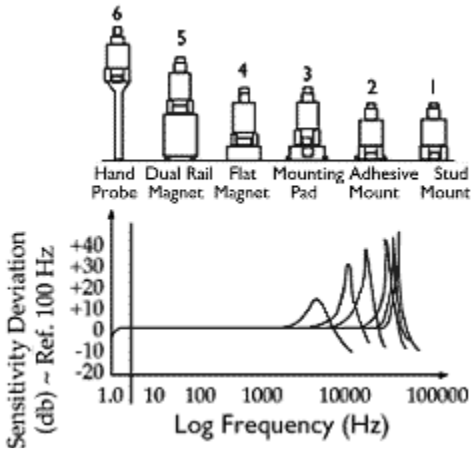

Figure 2-16. Change in accelerometer resonance due to coupling method (www.pcb.com).

2.5.5 Near-field effects

In SASW and MASW testing, it is assumed that only planar Rayleigh waves are being measured by the receivers. This assumption is not valid when the source gets too close to the receiver array. When the source is too close, the wave field is polluted with body waves and cylindrical Rayleigh waves. This region is termed the near-field. Near-field effects typically cause the phase velocity of waves to be underestimated 10-15%. Yoon and Rix (2009) recommend using a mean center array distance of at least two in order to mitigate near-field effects on soil. Array center distance is defined by Equation 9.

$$\text{Mean Center Array Distance} = \frac{\frac{1}{m}\left(\sum_{m=1}^{m} x_m\right)f}{V_R} \qquad (9)$$

Where m is the total number of receivers, x is the receiver distance from the source, f is frequency, and V_R is Rayleigh wave phase velocity.

2.5.6 Equipment- Data Acquisition System (DAQ)

A critical component of MASW is the DAQ. The first and most important component of the DAQ is how many channels it can record simultaneously. The number of channels typically range from 16 to 64 for DAQs used for MASW. Other important features of the DAQ include the rate at which data is sampled and the frequency bandwidth. Ryden et al. (2002) recommend using a DAQ with at least 16 bits of resolution, but 24 bit acquisition systems are often preferred. The number of bits determine the amplitude resolution of the recorded waves (e.g. 16 bits of resolution means that there are 2^{16} (65,536) bins which the measured wave amplitude can be placed in. Therefore given a measurement range of -10 to 10 volts a 16 bit acquisition system would have a resolution limit of 0.3 millivolts). The DAQ must sample at a rate that is twice as fast as the highest frequency of interest to avoid spatial aliasing. Spatial aliasing is defined as the misrepresentation of a measured signal. (Park et al. 1999). For pavements, the higher the frequency, the better (typically 30 kHz or higher).

2.5.7 Acquisition

In traditional MASW testing, 12 to 48 receivers are placed at a fixed spacing to obtain a multichannel data record. Multiple source signals are then input into the surface via a seismic source (impulse or harmonic). A trigger located on or near the source triggers the recording of the data through the DAQ. Typically three or more tests are performed for an average in order to eliminate noise.

2.5.8 Data Processing

Once testing is completed, the data are analyzed using what is called a frequency-wavenumber spectrum approach to create a dispersion curve. The approach uses a 2-D Fourier transformation to convert the data from the space-time domain to the frequency-wavenumber

domain. Once transformed, the power of each f-k pair is calculated by multiplying the steering vector by the spatiospectral correlation matrix then summing over the entire array. This power calculation is then used to create a dispersion curve by determining the maximum power at each frequency then calculating the Rayleigh phase velocity with Equation 6. The resulting frequency-velocity pairs are plotted to create a dispersion curve. A more in depth explanation may be found in Zywicki (1999). This f-k transformation is what provides many of MASW's advantages over SASW. The f-k transform allows for multiple modes of propagation to be identified whereas in SASW data all modes are superimposed on each other. The other distinct advantage it offers is that it significantly speeds up and takes the subjectivity out of data processing. The method used in SASW data processing, phase unwrapping, is often time consuming and iterative.

There are several methods to process the data using an f-k transform. Tran and Hiltunen (2008) found that the cylindrical beamformer method as developed by Zywicki (1999) provides the most resolution among different f-k transformation methods. The other methods (traditional f-k transform, f-p transform, and the Park et al (1998) transform) all treat the wave field as planar. The method outlined by Zywicki assumes a cylindrical wave field and thus uses cylindrical wave equations in the data processing. This method however is not in agreement with the basic assumption of MASW testing, that all waves being measured are planar Rayleigh waves. This is called model incompatibility. Research by Zywicki and Rix (2005) has attempted to address this issue but more work is needed.

2.5.9 Inversion

The inversion process in any surface wave testing method is quite similar. In the data acquisition and processing stages, an experimental dispersion curve (EDC) is created. In the inversion stage, a theoretical dispersion curve (TDC) is estimated using an iterative process that

involves creating a system of horizontal layers where each layer is assigned a thickness, Poisson's ratio or P-wave velocity, shear wave velocity, and mass density. A wave front is then simulated propagating through the layered system and the resulting TDC is obtained. The layered system properties are updated until the TDC approximately matches the EDC. The end result is a shear wave velocity profile for the test site.

The inversion method for geotechnical applications is readily available while the inversion method for pavements remains either crude or complicated. Ryden and Park (2006) developed a method using a global search algorithm called fast simulated annealing inversion (FSA). The method is less user subjective and more unique than existing neighborhood algorithm methods but much more computationally demanding. Lin (2014) improved on the FSA inversion by combining it with a genetic algorithm and terming it genetic simulated annealing (GSA) method. GSA has proved to reduce uncertainty as well as increase efficiency. A crude inversion is possible for the top layer of pavement that allows for a thickness estimation of ± 1 cm (Du Tertre 2010). The Rayleigh wave velocity may also be assumed to be the velocity present at high frequencies (>15 kHz) on the EDC. The Rayleigh wave velocity may then be substituted into Equation 2 to determine the shear wave velocity.

2.5.10 Comparison of MASW Tests

Some research has been done on testing pavements with MASW but there is no published literature on the optimum receiver spacing and source offset. Table 2-1 presents the methods used by selected authors.

Table 2-1. Summary of previous research in MASW on pavements.

Author	Source Type	Number of Recievers (Real or Simulated)	Reciever to Pavement Coupling	Receiver Spacing	Source Offset	MASW or MSOR
Terte (2010)	Ultrasonic Transmitter	12	250g weight	4cm	4cm	MASW
Ryden et al (2004)	225g Hammer w/ Steel Spike	80	Sticky Grease	2.5cm	2.5cm-200cm	MSOR
Shin and Ashlock (2014)	225g Hammer	9	Plumber's Putty	4cm	x	MASW
Shin and Ashlock (2014)	225g Hammer	9	Plumber's Putty	4cm	8cm-40cm	MSOR
Ryden et al (2002)	500g Hammer	24	Sticky Grease	2.5cm	10cm-70cm	MSOR
Alzate-Diaz and Popovics (2009)	8mm Steel Ball	33	x	3cm	3cm-99cm	MSOR
Ryden et al (2002)	x	40	x	5cm	5cm-200cm	MSOR
Park et al. (2001)	225g Hammer	40 Geophones	Conical Base Plates w/ 108kg on array	9cm	x	MASW

2.6 Alkali-Silica Reaction (ASR)

Alkali-Silica Reaction (ASR) was first researched by Stanton (1940). ASR is the resulting reaction between alkalis (NaO, KO, and CaO) and silicic acid (H_4SiO_4) in concrete. Alkalis are typically present in the cement while silicic acids are present in either the fine or coarse aggregate. The rate of reaction not only depends on the concentration of alkalis and silicic acids but also on the temperature and relative humidity. The reaction produces a gel which will absorb water and swell to induce macro and micro cracking (Figure 2-17). This cracking is often

compounded by freeze-thaw cracking. Hobbs (1988) provides a much more detailed description of ASR and its causes.

a) b)

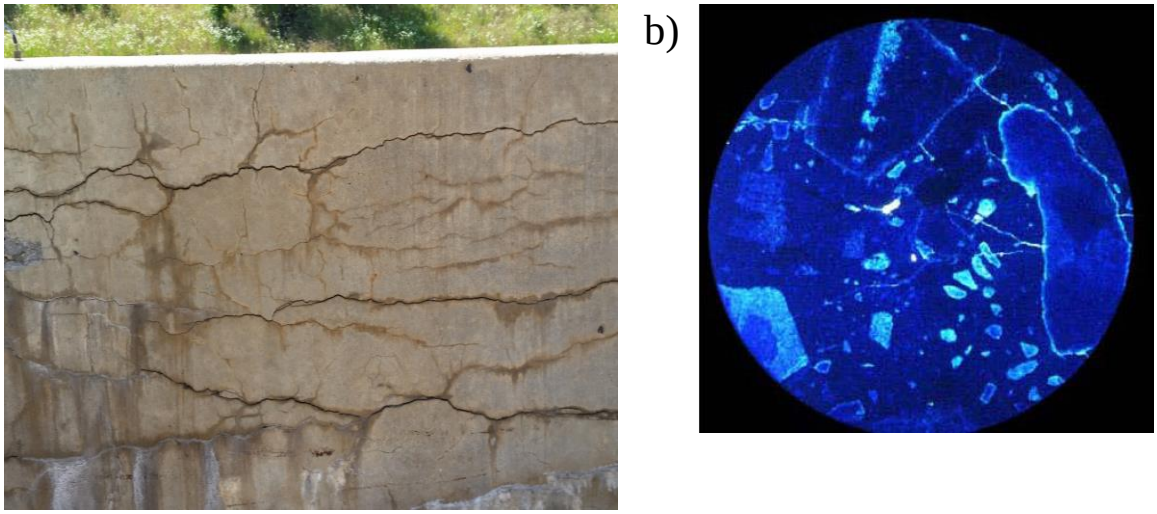

Figure 2-17. a) Macro cracking due to ASR among other causes and b) Microcracking due to ASR (Used with permission from USGS).

ASR is prevalent in concrete infrastructure largely due to the economics of making concrete. If a region only has access to reactive aggregates, then it will use said aggregate and try to mitigate the effects. It simply is not feasible to ship in large quantities of unreactive aggregate. Aggregates are typically tested to determine the level of reactivity with a certain cement using ASTM 1567 (is commonly termed the accelerated mortar bar test or AMBT) and ASTM C1293. Both tests measure the expansion of a rectangular prism over time. AMBT can obtain results concerning the reactivity of an aggregate cement mix within 28 days while ASTM C1293 can take a year or more.

2.6.1 Efforts in Nondestructive Testing of ASR

There is a strong need to develop NDT methods for concrete pavements and structures in order to monitor the effects of ASR and other deleterious reactions in these pavements and structures. If a deleterious reaction is taking place within concrete, no NDT has been developed

to identify the specific reaction. However, there are several NDTs that can measure the extent of damage present in the concrete. Due to the heterogeneous nature of an ASR affected structure, NDTs are not suitable to describe structural behavior (Kreitman et al. 2012). Commonly researched NDTs include impact echo (IE), ultrasonic pulse velocity (UPV), dynamic modulus of elasticity (ASTM C215), surface wave transmission (SWT), and spectral analysis of surface waves (SASW).

Initial research on the effect of ASR on the engineering properties of concrete was first done by Swamy and Al-Asali (1988). Their research used resonant frequency testing to determine that at 0.1% expansion the loss in dynamic modulus was around 20% and at 0.6% it was 60%. Since 1988 other methods such as UPV, IE, SWT, and SASW have come into practice. Kreitman et al. (2012) determined that UPV and IE produce good results for expansions less than 0.1%. After 0.1% the accuracy and effectiveness of these methods quickly deteriorate. In contrast to this, Sargolzahi et al. (2010) suggest that UPV is not sensitive to the degradation of concrete. No research could be found using MASW as a method for monitoring ASR damage although Kreitman et al. (2012) determined that SASW produced similar results to IE and UPV but was much more time consuming and more uncertain. This uncertainty was probably due to the microcracking causing a significant amount of noise in the seismic wave signal (Kreitman et al. 2012). Additionally, Azari et al. (2014) determined that SWT correlated with some uncertainty to the amount of expansion present in concrete blocks. Research indicates that p and s-wave velocities are equally sensitive to damage in concrete (Rivard and Saint-Pierre 2009).

2.7 Conclusions

The methods available to nondestructively test pavement vary from simple (hammer sounding and chain dragging) to complex (MASW). This wide range in NDTs offers a wide

range of results that must be examined beforehand to obtain results that fit the scope of investigation. The multi-channel methods (MASW and MSOR) offer representative engineering properties (thickness and shear modulus) that other NDT methods do not. MASW and MSOR sample over a large area and provide robust results due to the redundant nature of multichannel methods. The methods require limited training to perform and process the data. In addition, an inversion of the top layer can be done with minimal calculations.

Current efforts in the nondestructive characterization of damage in concrete pavements and structures suggest that IE is best qualified to identify degradation. However little to no research has been conducted on the ability of MASW to detect a reduction in shear wave velocity.

3 Methods and Materials

3.1 Introduction

This section presents the methods used to conduct MASW in the field and lab as well as the procedures followed to determine shear wave velocity and expansion of ASR affected prisms.

3.2 MASW

In the following section, the methods for three different parameters for MASW testing are outlined. The three parameters are source type, source offset and receiver spacing. Each parameter was tested on five different materials at the Engineering Research Center (ENRC, see Figure 3-1), which is owned by the University of Arkansas. Pictures of each site are presented in Figure 3-2a-e. The materials tested were soil ("CTTP Soil"), hot mix asphalt pavement ("CTTP Asphalt", and "ENRC Asphalt"), and concrete pavement ("ENRC West Concrete" and "ENRC East Concrete"). Descriptions of each site is presented in Table 3-1. All five sites were chosen in order to minimize traffic flow disturbance, signal noise, and proximity to the researcher's office. Both the asphalt and concrete sites were flat while the soil site had slight undulations. Additional research to determine the effect of horizontal variability on Rayleigh wave propagation was performed on a site known herein as "Soil Box". A picture and schematic of Soil Box are presented in Figure 3-3.

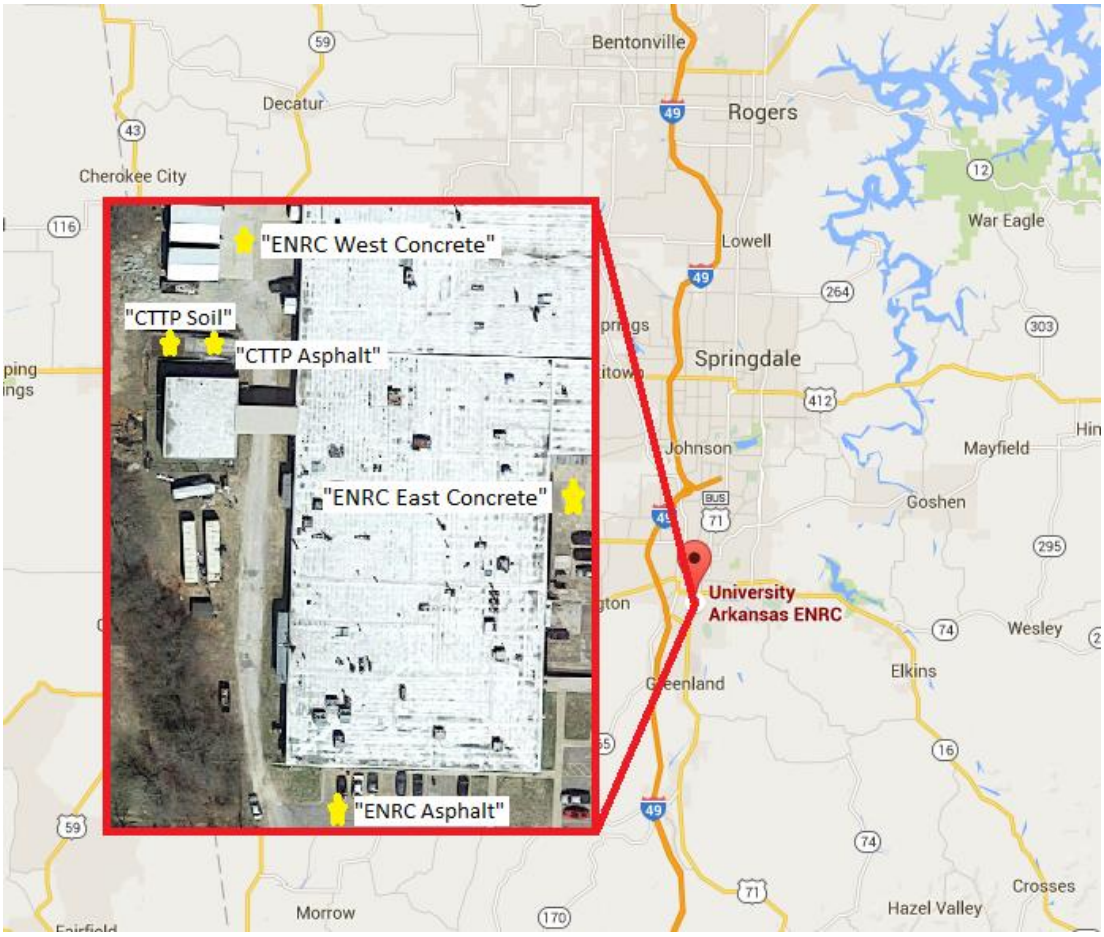

Figure 3-1. Location of MASW testing sites: "ENRC West Concrete", "CTTP Soil", "CTTP Asphalt", "ENRC Asphalt", and "ENRC East Concrete" ("Fayetteville, Arkansas").

a) 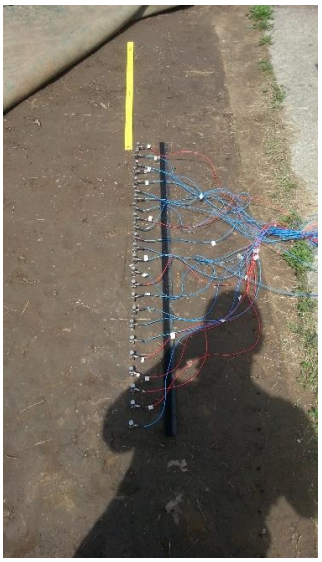 b)  c) 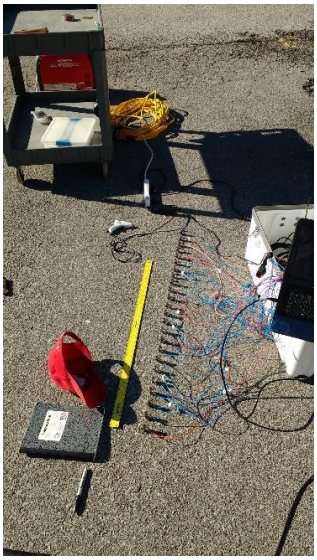

d) 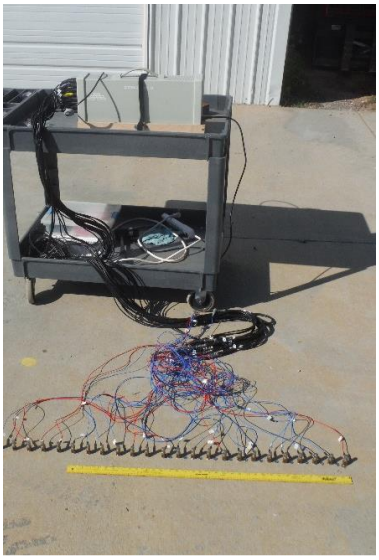 e) 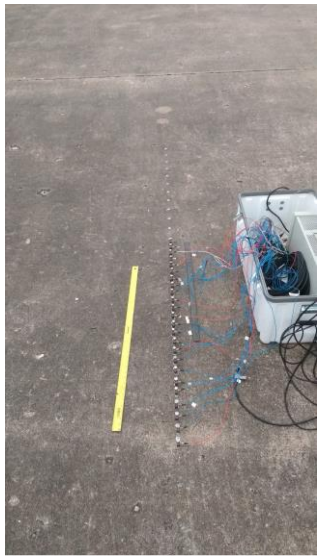

Figure 3-2. Site pictures of: a) "CTTP Soil", b) "CTTP Asphalt", c) "ENRC Asphalt", d) "ENRC West Concrete", and e) "ENRC East Concrete."

a)  b) 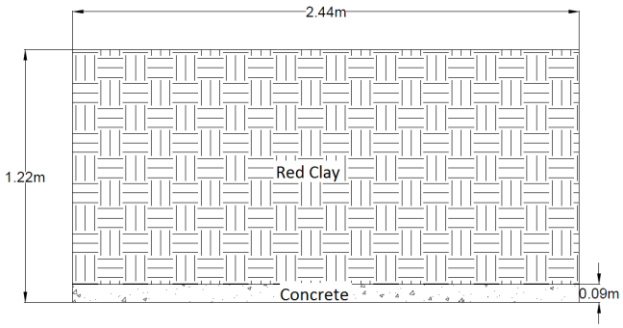

Figure 3-3. a) Picture of "Soil Box" and b) Schematic of "Soil Box."

Table 3-1. Descriptions of sites used in testing.

Name	Top Layer	Second Layer
CTTP Soil	30cm of Brown Silt	Rocky brown clay
Soil Box	120cm Red Clay	Concrete
CTTP Asphalt	10cm HMA	Base Course
ENRC Asphalt	10cm HMA	Base Course
CTTP Concrete	10cm Concrete	Base Course
CTTP Asphalt	18cm Concrete	Base Course

3.2.1 Equipment

The receivers used to collect MASW consisted of 24 Wilcoxon Research 736 high frequency accelerometers. The accelerometers had a resonant frequency of 60 kHz and a sensitivity of 100 mv/g. The accelerometers were attached to 1.3cm x 1.3cm x 1.3cm steel cubes with threaded holes on all six sides. The cube provided the capability to orient the accelerometer either vertically or horizontally. A vertical orientation would measure Rayleigh wave propagation while a horizontal orientation would measure Love wave propagation (Figure 3-4).

a) 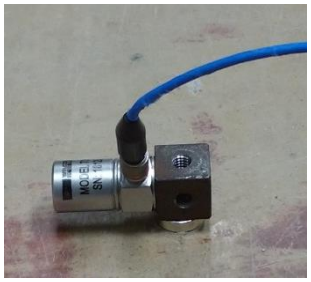 b) 

Figure 3-4. a) Love wave orientation of accelerometer and b) Rayleigh wave orientation of accelerometer.

The accelerometers were connected to the data acquisition system using individual cables. The data acquisition system was a full-function dynamic signal analyzer manufactured by Data Physics Corporation. The mobylizer system is a 32- input channel, 2 –output channel dynamic signal analyzer with 105 kHz simultaneous sampling rate, 120 Gb internal hard drive, 24 bit ADC, 120 Db dynamic range, and 110 Db anti-alias filters. It is controlled with a windows based software package produced by Data Physics (Signal Calc 730) that has measurement capabilities in both the time and frequency domain. Software modules are available for auto-power spectrum, transfer function, synchronous average, auto and cross correlation, histogram analysis, throughput to disk with event capture, zoom analysis, stepped sine, and active X communication (Wood 2009).

3.2.2 Testing

For each site a clear, continuous area was chosen for testing. The receiver spacing (2.5 cm, 5 cm, or 10 cm) was then marked on the material surface using a permanent marker and metric measuring tape. Washers with a diameter of 1.44 cm were affixed to the asphalt and concrete surfaces using superglue or hot glue. Superglue was primarily used but in some cases the surface was too cold or too irregular and the superglue would not cure. On soil, a masonry nail with a head diameter of 1.3 cm and shank length of 3.2 cm was driven into the ground at the

given receiver spacing interval. To ensure spacing uniformity on soil between tests, a template was constructed from 19 mm plywood. To construct the template, a strip of plywood approximately 1.3 m long by 5 cm wide was cut longitudinally in half. The two halves were then held together by c-clamps and 24, 4.75 mm holes were drilled every 5 cm. The template is presented in Figure 3-5. Accelerometers were then attached to the washers or nails using 1.3 cm diameter donut shaped magnets. Donut shaped magnets and oversized washers were used in order to prevent the polarity of the magnet from moving it off center. After the accelerometers were affixed to the pavement, source offset distances of 12.5 cm, 25 cm, 50 cm, 75 cm, 100 cm, and 150 cm were marked on the material surface. Data was collected for all offsets and receiver distances using a 230 gram hammer as well as an 1160 gram hammer. Both hammers are presented in Figure 3-6. This process was repeated on all materials. Each individual test (e.g. 2.5 cm receiver spacing, 12.5 cm source offset, and 230 gram hammer), was repeated five times for average. A summary of these tests is presented in Table 3-2.

Figure 3-5. Template for placing masonry nails in soil.

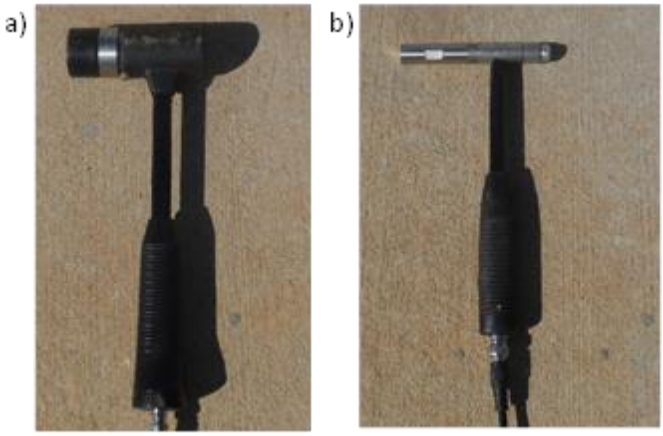

Figure 3-6. Sources used in investigation: a) 1160 gram hammer and b) 230 gram hammer.

Table 3-2. Summary of MASW testing procedure.

MASW Variable Parameter			
Location	Source Type (1160 gram and 230 gram hammers)	Source Offset (12.5cm, 25cm, 50cm, 75cm, 100cm, and 150cm)	Reciever Spacing (2.5cm, 5cm, 10cm)
Soil Box	x	x	
CTTP Soil	x	x	x
CTTP Asphalt	x	x	x
ENRC Asphalt	x	x	x
ENRC West Concrete	x	x	x
ENRC East Concrete	x	x	x

3.2.3 Data Acquisition using SignalCalc 730 and Analysis

SignalCalc 730 allows for a multitude of outputs and the setup used in this testing utilized the transfer function, cross power spectrum, the coherence function between every receiver and the source in MATLAB format along with the auto power spectrum for each channel. The outputs were then analyzed using MATLAB scripts titled "UofA_MASW" and "PlotAndCutPoints". UofA_MASW performs a frequency domain beamformer calculation (Zywicki 1999) that calculates the maximum power at each frequency then calculates phase velocity. These frequency-velocity pairs are then used to create a raw dispersion curve. An example of the dispersion curve produced is presented in Figure 3-7a. PlotAndCutPoints allows the user to delete data points that are obvious outliers or inconsistent with the trend of the curve. The resultant dispersion curve is much easier to analyze and outputs into an inversion program. An example dispersion curve outputted by PlotAndCutPoints is presented in Figure 3-7b.

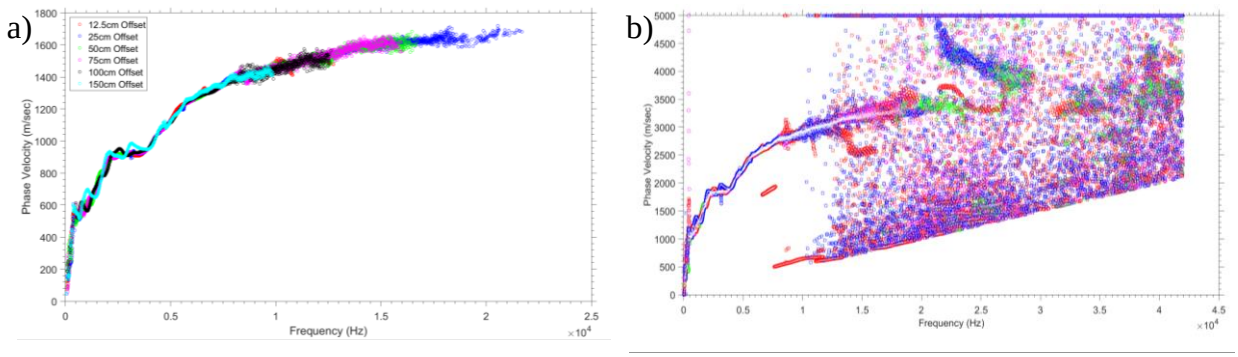

Figure 3-7. a) Edited dispersion curve using the MATLAB script "PlotAndCutPoints" and b) Unedited dispersion curve developed using the MATLAB script "UofA_MASW."

3.2.4 MASW- ASR

Field testing of MASW on ASR affected concrete barrier walls was performed at three sites on Interstate 49 south of Fayetteville, Arkansas. A map and coordinates of the sites are presented in Figure 3-8 and Table 3-3 while a cross sectional view of the wall is presented in Figure 3-9a. A visual inspection performed in 2013 by Richard Deschenes of the University of Arkansas assigned Site C-1 (Figure 3-9b) as being minimally damaged, Site C-2 (Figure 3-9c) as being moderately damaged, and Site C-3 (Figure 3-9d) as being severely damaged. In addition to ASR damage, the barrier walls were significantly damaged by the freeze thaw cycle. Richard was tasked by the Arkansas Highway and Transportation Department (AHTD) to monitor the strain for each site in 2013 but the first noted presence of ASR in the barrier wall was in 2005. Optimum MASW testing parameters were determined before testing at the sites began. The testing parameters are as followed:

5 cm receiver spacing

230 gram hammer

Source offsets of 12.5 cm, 25 cm, 50 cm, and 75 cm

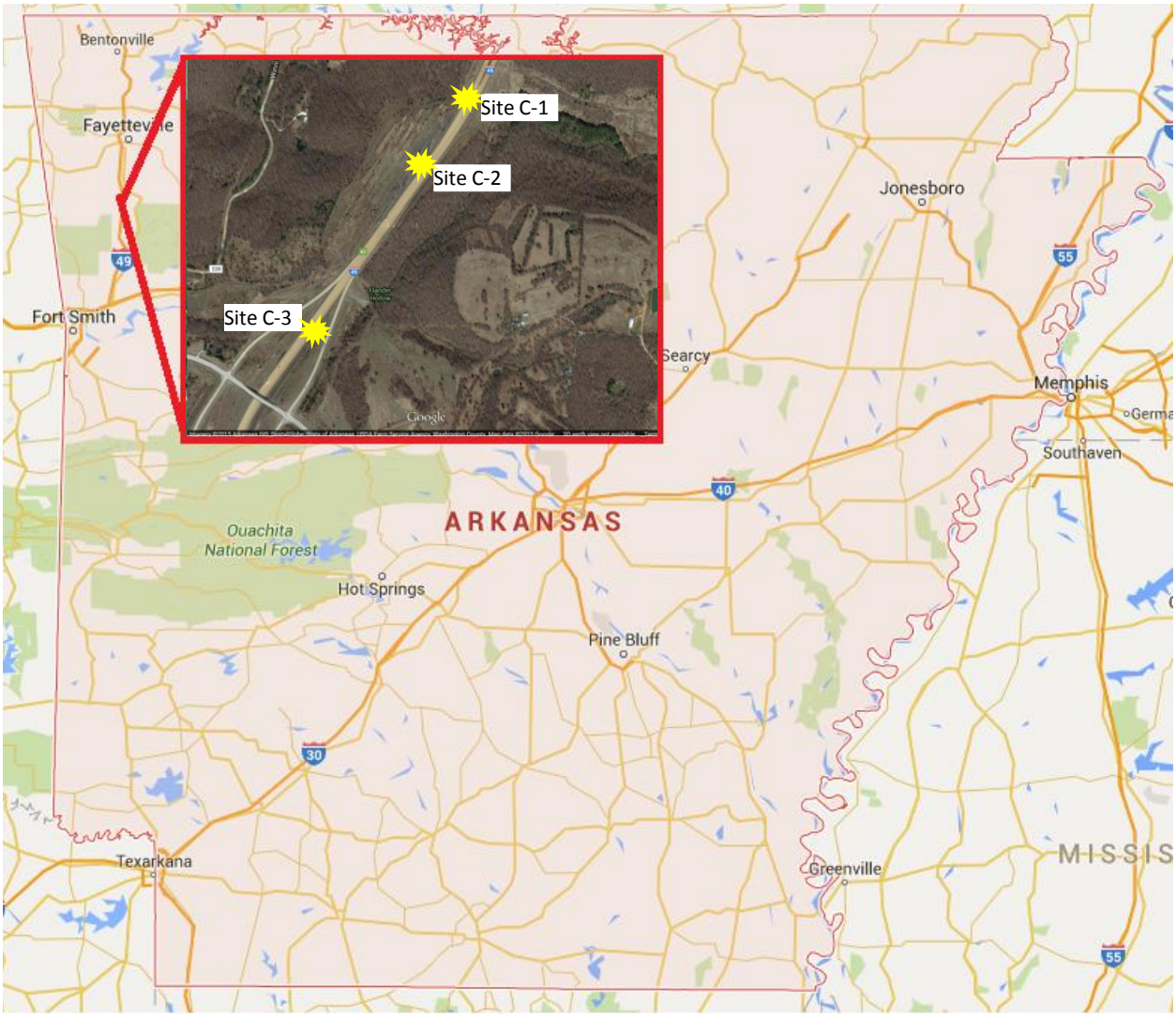

Figure 3-8. Location of MASW tested ASR affected sites on 1-49 ("Arkansas").

Table 3-3. Coordinates of ASR affected barrier wall sites tested by MASW.

Site	Coordinates
C-1	35.82759N 94.18386W
C-2	35.82567N 94.18546W
C-3	35.82111N 94.18964W

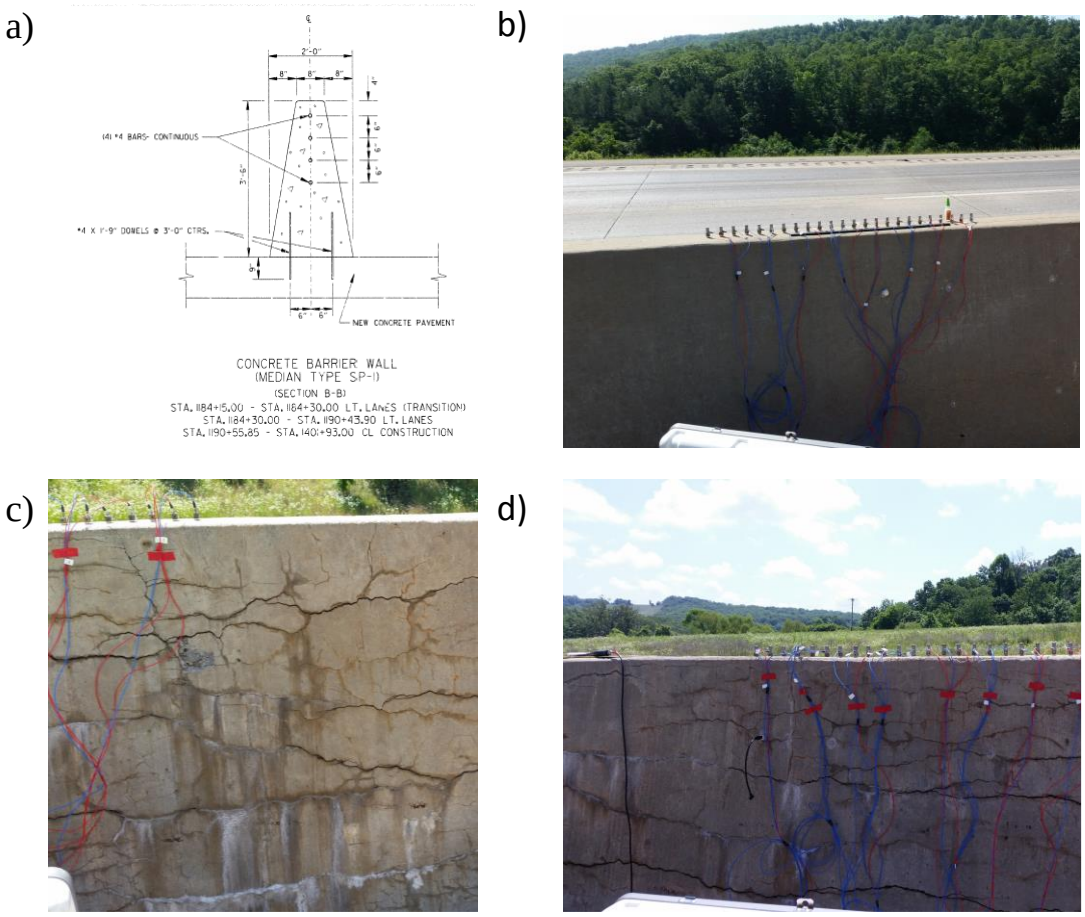

Figure 3-9. a) Schematic of barrier wall tested on I-49 near Exit 45, b) Site C-1 visually classified as having "minimal" ASR damage, c) Site C-2 visually classified as having "moderate" ASR damage, and d) Site C-3 visually classified as having "severe" ASR damage.

3.3 Torsional Resonant Frequency Testing of ASR Affected Concrete Prisms

In order to monitor the effects of expansion on shear wave velocity, concrete prisms were cast in accordance with ASTM C1293 with dimensions of 7.6 cm x 7.6 cm x 27.9 cm. The prisms also meet the requirements of ASTM C215. The prisms' expansion and shear wave velocity were then measured weekly and monthly. The following section outlines the procedure used to cast and test the specimens.

Three different mix designs were used and three specimens were cast for each mix design for a total of 9 prisms. Each mix design used a cement with an alkali content of 0.9%. The mix

designs varied by changing the amount of two materials, Jobe sand and sodium hydroxide (NaOH) pellets. The sodium hydroxide pellets raised the alkali content from 0.9% to 1.25% which ensured a surplus of alkalis to react with the silicic acid in the Jobe sand. The control group (known herein as "0C") had no Jobe sand, one reactive group had an unreactive sand to Jobe sand ratio of 8:2 (known herein as "20R"), and the final reactive group had an unreactive sand to Jobe sand ratio of 6:4 (known herein as "40R"). Phillips et al. (2015) concluded prisms with 40% Jobe sand proved to have a moderate ASR rate compared to 100% Jobe sand (see Figure 3-10). A granite aggregate was used due to convenience and lack of reactivity. The mix designs are presented in Table 3-4.

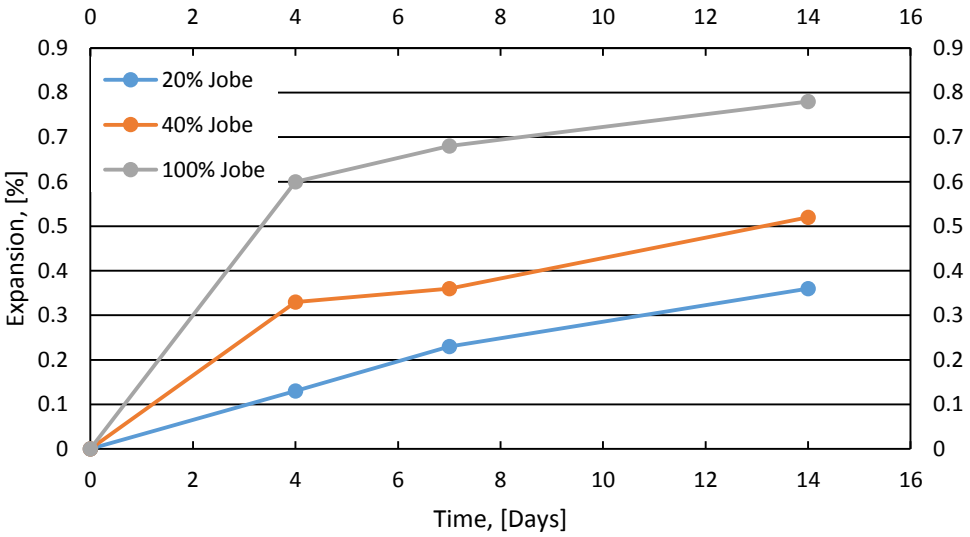

Figure 3-10. 14 day expansion of prisms with unreactive sand to Jobe sand ratios of 8:2, 6:4, and 10:0 (Phillips et al. 2015).

Table 3-4. Mix designs for 0C, 20R, and 40R.

	Mix Design					
Material	**0C**		**20R**		**40R**	
Cement	6.56	lb	6.56	lb	6.56	lb
Coarse Aggregate	16.50	lb	16.50	lb	16.50	lb
Jobe Sand	0.00	lb	2.13	lb	4.37	lb
Van Buren Sand	10.67	lb	8.54	lb	6.40	lb
Water	3.06	lb	3.06	lb	3.06	lb
NaOH	0.00	g	13.82	g	13.82	g

3.3.1 Prism Expansion- ASTM C1293

The mix designs were cast from 6/24/15 to 7/30/15. Molds (Humboldt MFG H3254) were provided by Dr. Micah Hale of the University of Arkansas. The molds had a threaded hole on either end which allowed for small metal studs to be embedded in the prisms which were used to measure strain. An example of the casting process is presented in Figure 3-11. Once cast, the prisms were cured in a 23.5°C curing room for 24 hours then demolded. After demolding, the prisms were placed in a five gallon bucket detailed in Figure 3-12. The bucket was then placed in a hot water bath (37.8°C) and tested as specified in ASTM C1293. The hot water bath consisted of a 0.61m x 1.82m x0.61m (0.64m^3) galvanized metal stock tank, temperature variable switch with plug-in, immersion water heater, 0.5 $\frac{m^3}{hr}$ pump, and foam lid. The temperature variable switch and heater kept the water between 36.7 and 38.9°C. The water heater was suspended in the water by a 10cm x 10cm x 7.5cm cube of blue insulation foam. A picture of the water bath is pictured in Figure 3-13.

a)  b) 

Figure 3-11. a) Casting of prisms and b) cured prisms.

a)  b) 

Figure 3-12. Five gallon bucket for accelerated ASR prisms.

a) b)

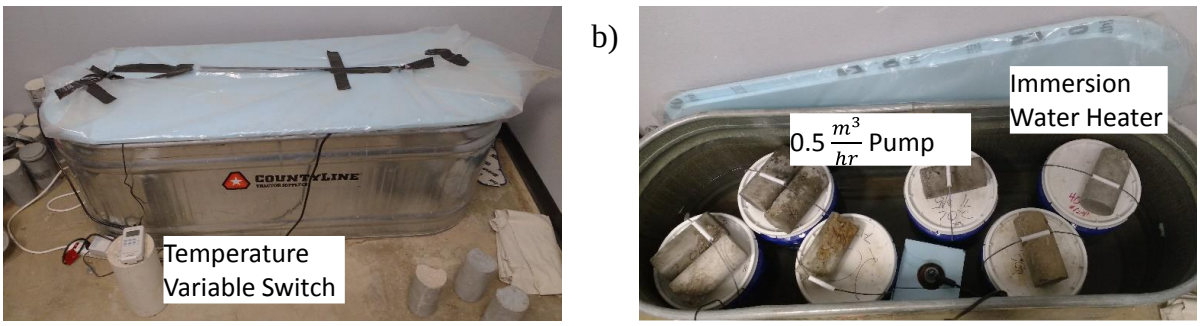

Figure 3-13. Water bath for accelerated ASR prisms illustrating a) temperature variable switch and b) the immersion heater and 0.5 m^3/hr. pump.

The prisms were tested for expansion and shear wave velocity at 24 hours, 3 days, 7 days, 14 days, 28 days, and subsequent monthly intervals. An example of the strain guage used to measure expansion is presented in Figure 3-14.

Figure 3-14. ASR prism being tested for expansion.

3.3.2 Shear Wave Velocity- ASTM C215

The shear wave velocity of each prism was determined by following the procedures outlined in ASTM C215. The ASTM specifies how to measure the fundamental transverse,

longitudinal, and torsional frequencies of a concrete prism. For this study, the torsional frequency was of interest because it is a function of the material's shear wave velocity.

The test is performed by supporting the prism at its longitudinal midpoint by a foam strip. An accelerometer is then placed 1.3 cm from the top surface and 6.6 cm from one end. The prism is then struck with a 230 gram hammer 1.3 cm from the bottom and 3.6 cm from the opposite end five times for average. A schematic of the accelerometer placement and strike point is presented in Figure 3-15.

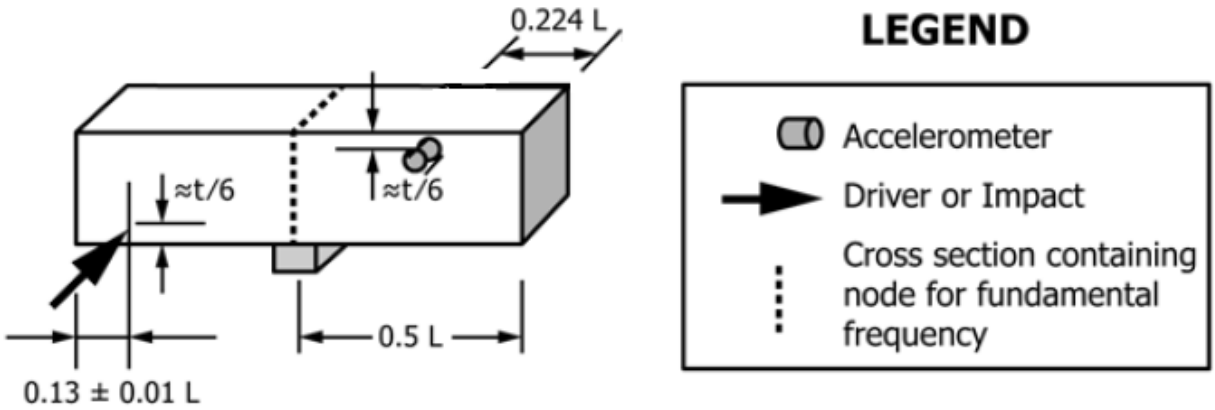

Figure 3-15. Schematic of accelerometer placement and strike point (ASTM C215).

The data from the accelerometer is collected by a SignalCalc Ace DAQ. The Ace has four input channels, two output channels, one tachometer channel, 94 kHz standard real time rate, and a dynamic range of over 120 dB. It uses SignalCalc 240 software. The software is set up to sample at a rate 80 kHz of and have 12800 points of the waveform which resulted in a frequency resolution of 6.25 Hz. The test was repeated five times for average to reduce uncertainty and would not be recorded if the source produced more than 10 volts. An example output of the average auto power spectrum is presented in Figure 3-16. The figure is used to pick the peak frequency. The test was conducted at the same time as the expansion testing. After testing was

completed, each specimen was weighed and measured. The shear wave velocity was then determined in accordance with ASTM C215.

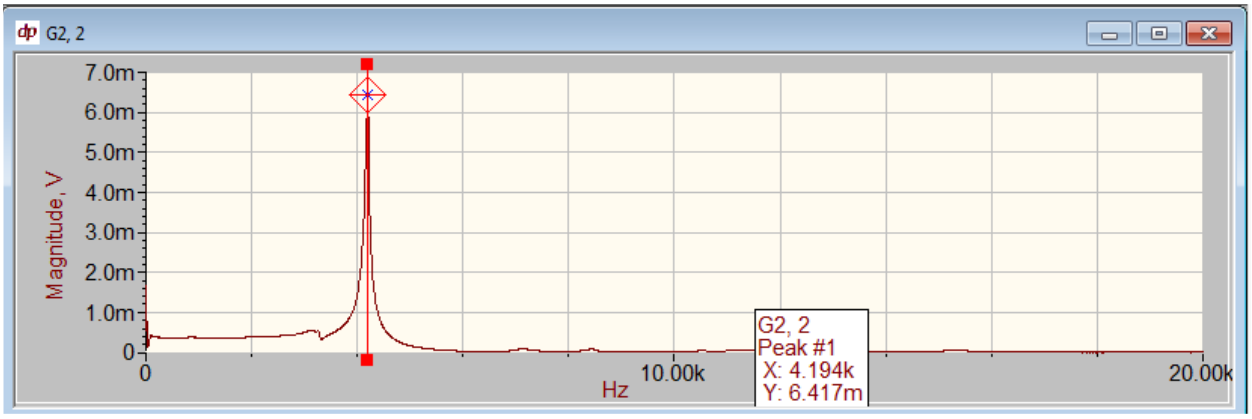

Figure 3-16. Example output of SignalCalc 240 with the fundamental frequency highlighted.

3.4 Conclusions

There were five sites used for determining optimum MASW testing parameters. The sites included two asphalt (CTTP Asphalt and ENRC Asphalt), two concrete (ENRC East Concrete and ENRC West Concrete), and one soil (CTTP Soil). All of the sites were located at the University of Arkansas Engineering Research Center in Fayetteville, Arkansas. The data from these tests were analyzed using a cylindrical beamformer technique developed by Zywicki (1999).

To test the sensitivity of surface wave testing to damage in concrete, two phases of tests were implemented. The first involved casting three groups of three concrete prisms (one control and two with varying levels of damage) in accordance with ASTM C1293. The expansion and shear wave velocity were recorded for each prism for one year. The second phase of testing was to perform MASW on three concrete barrier wall sections located on I-49 south of Fayetteville, Arkansas. The three sections had varying degrees of damage (minimal, moderate, and severe).

4 Analysis of MASW Testing Procedure on Pavement and Soil

4.1 Overview

In determining the optimum field testing parameters for MASW, four testing parameters were investigated: source type, accelerometer spacing, source offset, and number of receivers. A schematic of the parameters is presented in Figure 4-1. The three materials types were tested: asphalt, concrete, and soil. In addition to these materials, which are used in transportation infrastructure, soil was also evaluated in order to conduct tests on soil as discussed in Section 4.6. The parameters were evaluated by comparing the coefficient of variation (COV) (which quantifies the amount of scatter in the data) and examining if the parameter produced far-field or near-field effects. To compare COVs between parameters, the COV was averaged over the entire frequency range. The typical average COV is below 0.02 which is considered acceptable. In light of this, COV was used as a secondary evaluation tool behind the frequency range measured. Far-field effects for MASW occur when the source is located too far from the receiver array resulting in high frequency waves damping out before they reach the array. High frequency stress waves damp out before low frequency stress waves because the number of cycles is directly related to the amount of energy expended (i.e., a 2000 Hz wave will use more energy in one second than a 200 Hz wave). Far-field effects are manifested in the dispersion curve as a loss of coherence at high frequencies. It is critical for MASW that high frequency (~20 kHz) data exists as that is when the waves behave like Rayleigh waves in pavement systems. Rayleigh waves are important because they can be directly related to shear wave velocity by Equation 2. Near-field effects are when the waves being measured are assumed to be plane Rayleigh waves but are contaminated with body waves because the source is too close. The result is an underestimation (~10%) of Rayleigh wave velocity. Another important frequency range is below 500 Hz. This range

contains “leaky modes” and is critical when fully inverting the data to develop a shear wave velocity profile for the testing area. However, the full inversion of the dispersion data is beyond the scope of this research and therefore will not be discussed further.

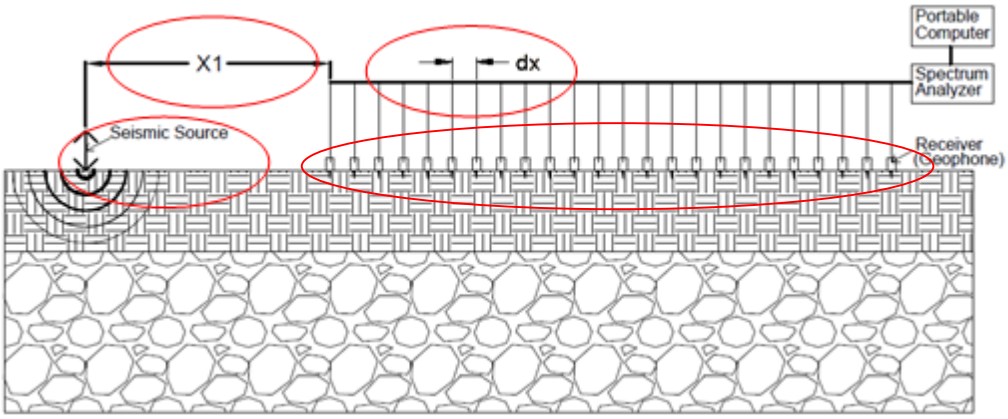

Figure 4-1. Schematic of MASW parameters evaluated.

4.2 Source Type

In the following section, two source types were investigated. The first source was an 1160 gram, rubber-tipped, instrumented hammer displayed in Figure 4-2a, while the second source was a 230 gram, metal-tipped, instrumented hammer displayed in Figure 4-2b. Literature (Ryden et al., 2001) suggests that the 1160 gram hammer would produce more energy at low frequencies while the 230 gram hammer would produce more energy at high frequencies. To test this hypothesis, both hammers were used to conduct MASW testing using arrays with 24 receivers and a receiver spacing of either 2.5 cm or 5 cm on three materials types: (1) asphalt (CTTP Asphalt, ENRC Asphalt), (2) concrete (ENRC East Concrete, ENRC West Concrete), and (3) soil (CTTP Soil). For more information on the test sites, please see Section 3.

a)  b) 

Figure 4-2. Sources used in the investigation: a) 1160g hammer and b) 230g hammer.

4.2.1 Asphalt

A comparison of the dispersion and COV curves for the 230g and 1160g hammers for ENRC Asphalt is presented in Figure 4-3. The arrays utilized 24 receivers and a 2.5 cm receiver spacing. Source offsets of 12.5 cm, 25 cm, and 50 cm were utilized by averaging the results of the three offsets. For the two hammers, the dispersion curves varied slightly but with no clear differences at frequencies less than 5 kHz but the 1160g hammer performed markedly worse (average COV of 150% than that of the 230g hammer) at frequencies between 5 and 10 kHz. The 1160g hammer did not produce any coherent data at frequencies higher than 10 kHz, whereas the 230g hammer produced coherent results to over 20 kHz.

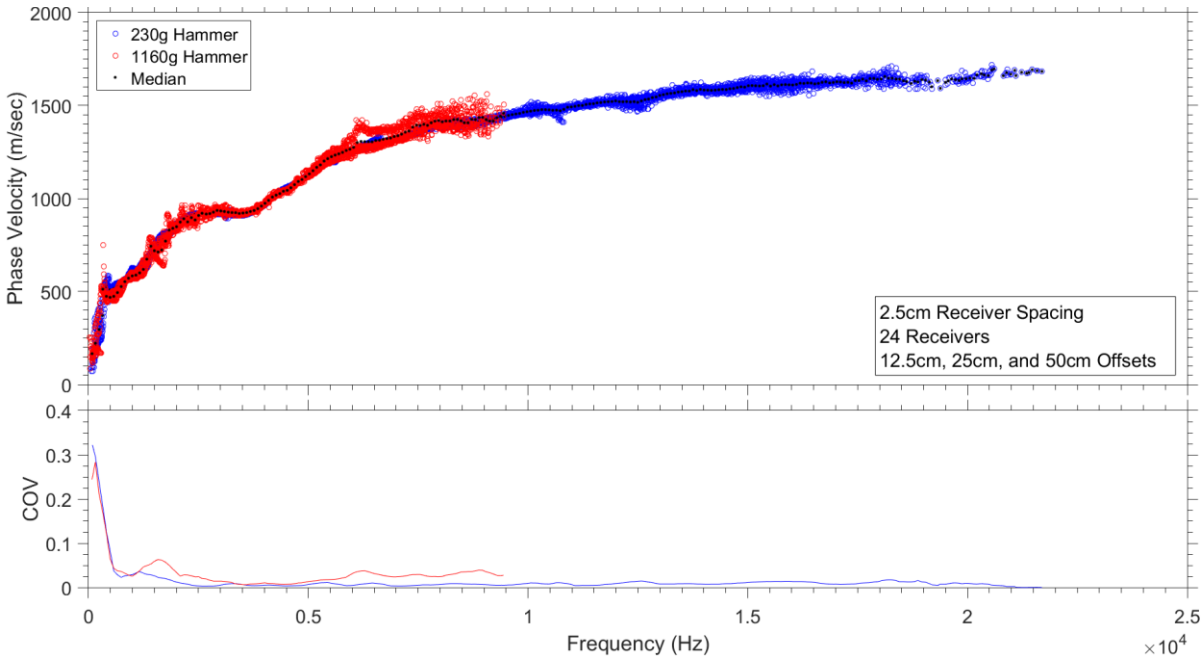

Figure 4-3. Comparison of the dispersion and COV curves for a 230g and 1160g hammer at ENRC Asphalt. A receiver array of 24 receivers with a 2.5 cm receiver spacing and source offsets of 12.5 cm, 25 cm, and 50 cm (averaged together) were used for the comparison.

A comparison of the dispersion and COV curves for the 230g and 1160g hammers for CTTP Asphalt is presented in Figure 4-4. The arrays utilized 24 receivers and a 2.5 cm receiver spacing. Source offsets of 12.5 cm, 25 cm, and 50 cm were utilized by averaging the results of the three offsets. The trends for CTTP Asphalt are, in general, in agreement with the results from ENRC Asphalt. The 1160g hammer fails to produce any coherent data above 10 kHz and has an average COV that is 50% larger than the 230g hammer over the entire frequency range. Yet unlike the ENRC Asphalt results, the 230g hammer does not produce data with a low COV at frequencies above 10 kHz. This may be due to variances in the asphalt pavement itself.

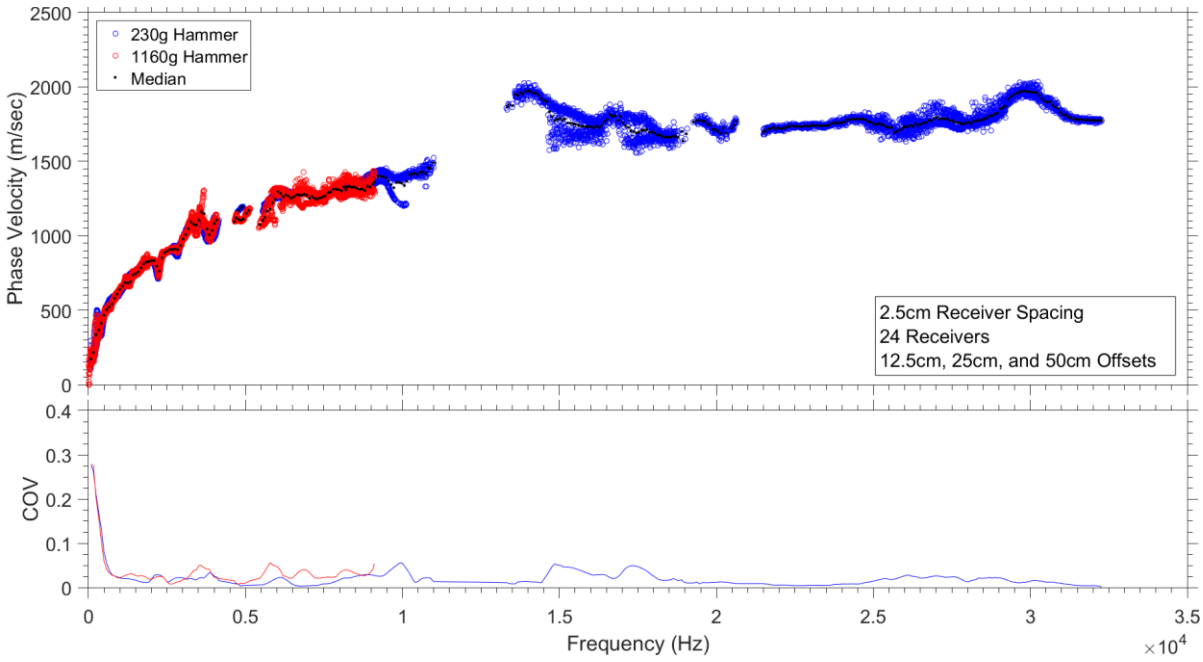

Figure 4-4. Comparison of the dispersion and COV curves for a 230g and 1160g hammer at CTTP Asphalt. A receiver array of 24 receivers with a 2.5 cm receiver spacing and source offsets of 12.5 cm, 25 cm, and 50 cm (averaged together) were used for the comparison.

The influence of the source type when testing asphalt pavements is critical and the correct source must be used to obtain high frequency data. Therefore, for this study the 230g hammer was the most effective when testing asphalt.

4.2.2 Concrete

A comparison of the dispersion and COV curves for the 230g and 1160g hammers for ENRC East Concrete is presented in Figure 4-5. The arrays utilized 24 receivers and a 5 cm receiver spacing. Source offsets of 12.5 cm, 25 cm, 50 cm, and 75 cm were utilized by averaging the results of the four offsets. At most frequencies below 32 kHz, there is little to no discernable difference in the dispersion trends (though the 1160g hammer has an average COV of 20% larger than that of the 230g hammer). However, the 1160g hammer does not produce coherent data from 32 to 42 kHz, while the 230g hammer produces some sparse data with a noticeable trend.

Nonetheless, both dispersion curves have converged to the Rayleigh wave velocity (2500 m/s) by 32 kHz thus the data from 32-42 kHz may be considered superfluous.

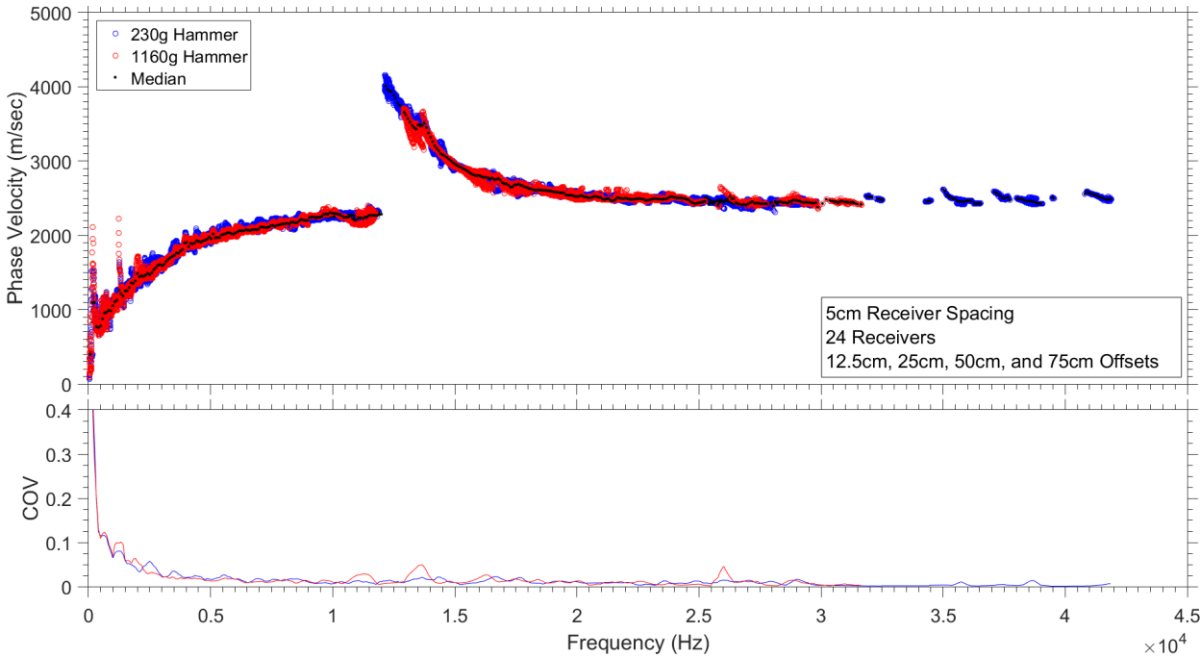

Figure 4-5. Comparison of the dispersion and COV curves for a 230g and 1160g hammer at ENRC East Concrete. A receiver array of 24 receivers with a 5 cm receiver spacing and source offsets of 12.5 cm, 25 cm, 50 cm, and 75 cm (averaged together) were used for the comparison.

A comparison of the dispersion and COV curves for the 230g and 1160g hammers for ENRC West Concrete is presented in Figure 4-6. The arrays utilized 24 receivers and a 5 cm receiver spacing. Source offsets of 12.5 cm, 25 cm, 50 cm, and 75 cm were utilized by averaging the results of the four offsets. For this site, there is no clear trend between the performances of the hammers with the dispersion curves for each hammer being approximately the same (i.e., COVs within 5%). Both hammers produce data to a maximum frequency of 42 kHz. The primary difference between the two dispersion curves is the presence of the symmetric mode in the 230g hammer data between 1.5 and 2.5 kHz. The cause of this is unknown and either mode is acceptable as long as it converges to the Rayleigh wave velocity. Both curves plateau at a

Rayleigh wave velocity of 2200 m/s indicating they provide similar estimates of stiffness for the site.

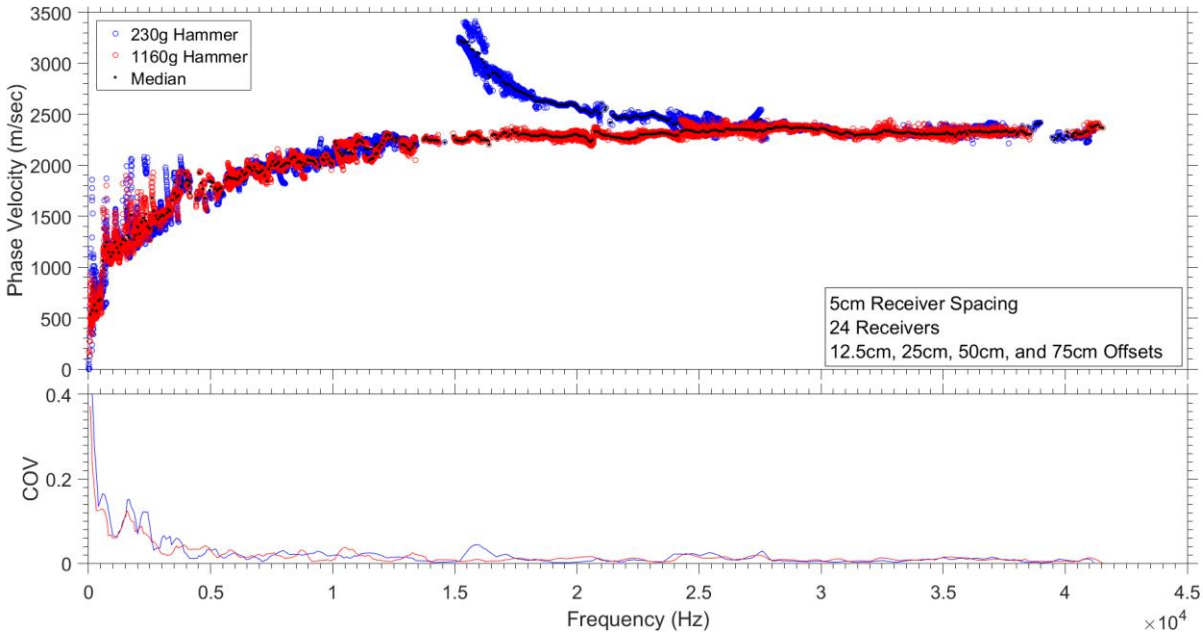

Figure 4-6. Comparison of the dispersion and COV curves for a 230g and 1160g hammer at ENRC West Concrete. A receiver array of 24 receivers with a 5 cm receiver spacing and source offsets of 12.5 cm, 25 cm, 50 cm, and 75 cm (averaged together) were used for the comparison.

For this study, the source type for MASW testing on concrete is not as critical as it is for asphalt. In the cases tested, both source types allowed for a determination of the Rayleigh wave velocity of the top material layer thus the mass of the hammer is not significant.

4.2.3 Soil

A comparison of the dispersion and COV curves for the 230g and 1160g hammers for CTTP Soil is presented in Figure 4-7. The arrays utilized 24 receivers and a 5 cm receiver spacing. Source offsets of 12.5 cm, 25 cm, and 50 cm were utilized by averaging the results of the three offsets. Comparing the dispersion curves, the 1160g hammer has a greater COV at all frequencies sampled (150% larger than that of the 230g hammer) and samples a frequency range

of almost an order of magnitude (150-500 Hz compared to 200-1800 Hz) less that the 230g hammer. Therefore, the 230g hammer clearly performs better when testing soil sites.

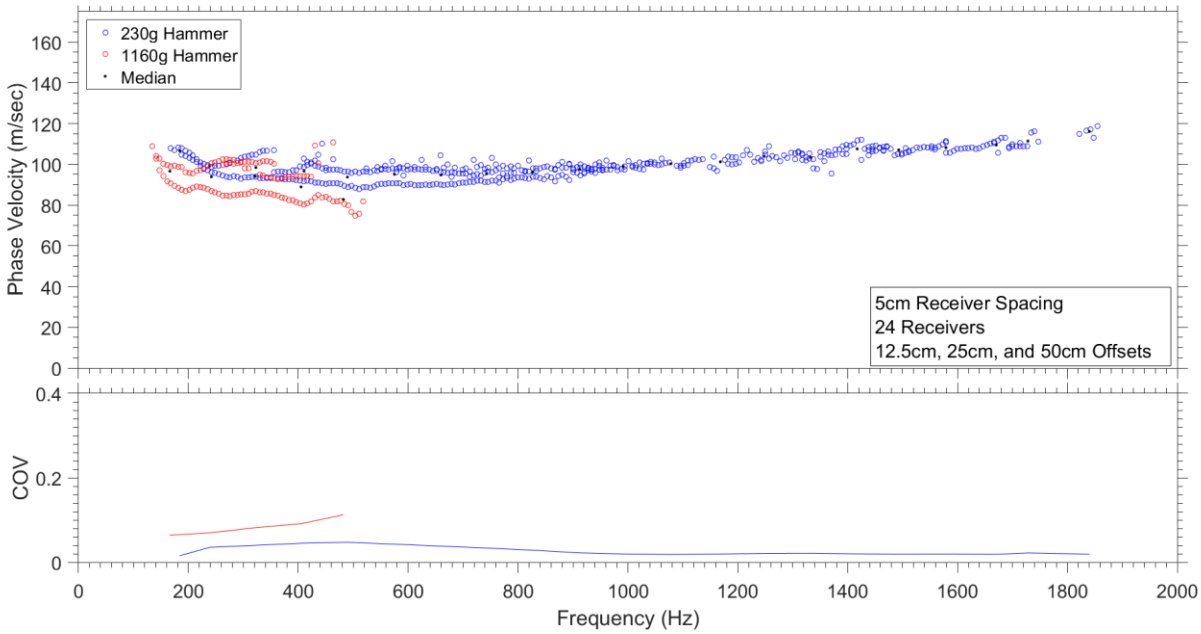

Figure 4-7. Comparison of the dispersion and COV curves for a 230g and 1160g hammer at CTTP Soil. A receiver array of 24 receivers with a 5 cm receiver spacing and source offsets of 12.5 cm, 25 cm, and 50 cm (averaged together) were used for the comparison.

4.3 Receiver Spacing

Three receiver spacings were examined in order to determine which would provide the clearest resolution at both high and low frequencies. The three receiver spacings tested were 2.5 cm (Figure 4-8a), 5 cm (Figure 4-8b), and 10 cm (Figure 4-8c). It was hypothesized that the shorter the spacing, the more apt the array would be to accurately measure high frequency waves and detect small defects in the pavement. Conversely, the longer spacings should more accurately measure low frequencies but struggle to measure high frequencies (due to far-field effects). In addition, longer arrays may not be able to detect small defects in the pavement. In the following subsections, a 230g hammer and multiple source offsets (12.5 cm, 25 cm, 50 cm, and 75 cm) are used for each comparison.

a) b)

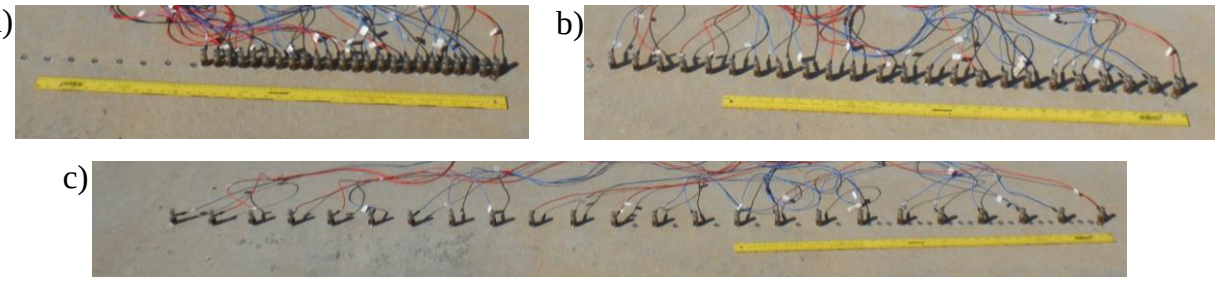

c)

Figure 4-8. MASW array with: a) 2.5 cm spacing, b) 5 cm spacing, and c) 10 cm spacing.

4.3.1 Asphalt

A comparison of the dispersion and COV curves comparing receiver spacings of 2.5 cm, 5 cm, and 10 cm for ENRC Asphalt is presented in Figure 4-9. The arrays utilized 24 receivers and a 230g hammer. Source offsets of 12.5 cm, 25 cm, and 50 cm were utilized by averaging the results of the three offsets. Comparing the dispersion curves from the three receiver spacings, there is little variation between the curves at frequencies above 2 kHz with each receiver spacing having COVs less than 0.01. The 10 cm receiver spacing has an average COV that is about half of the average COV for the 2.5 cm spacing. However, the 10 cm receiver spacing does not produce coherent data above 9 kHz, while the 5 cm receiver spacing stops producing coherent data at 16 kHz and the 2.5 cm spacing stops producing coherent data at 23 kHz. Importantly, the dispersion curve begins to plateau around 16 kHz (1500 m/s), which is only captured by the 2.5 cm receiver spacing.

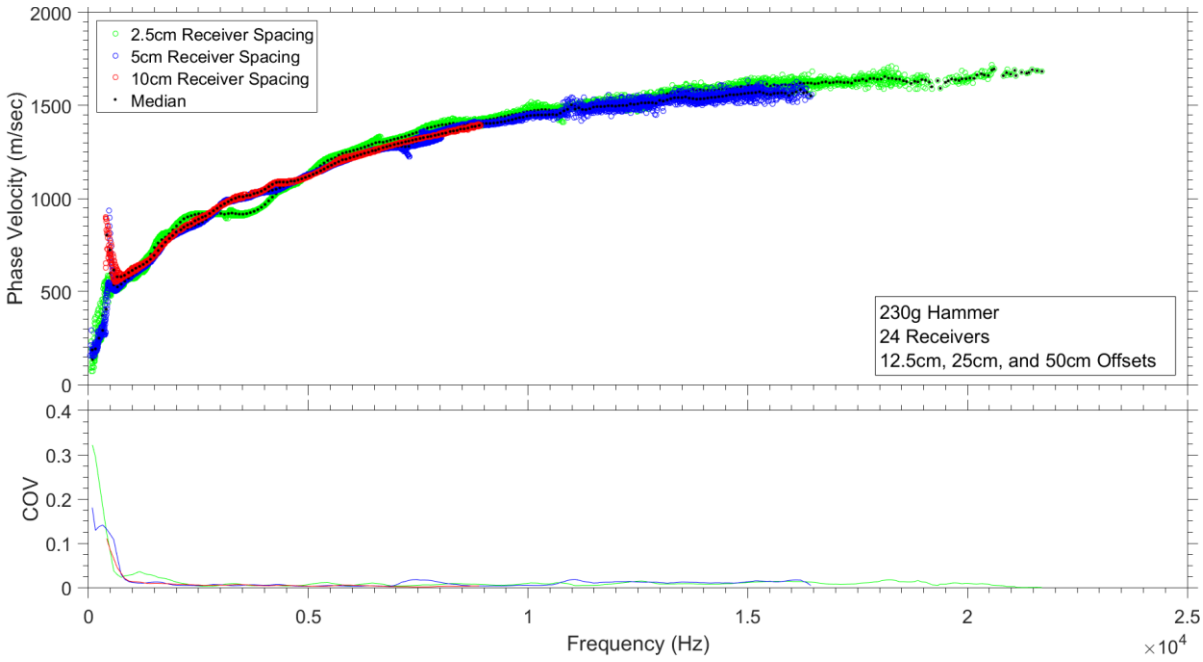

Figure 4-9. Comparison of the dispersion and COV curves for 2.5 cm, 5 cm, and 10 cm receiver spacings at ENRC Asphalt. A receiver array of 24 receivers, a 230g hammer and source offsets of 12.5 cm, 25 cm, and 50 cm (averaged together) were used for the comparison.

A comparison of the dispersion and COV curves comparing receiver spacings of 2.5 cm, 5 cm, and 10 cm for CTTP Asphalt is presented in Figure 4-10. The arrays utilized 24 receivers and a 230g hammer. Source offsets of 12.5 cm, 25 cm, and 50 cm were utilized by averaging the results of the three offsets. The 10 cm spacing dispersion curve has a low COV from 1 kHz to 7.5 kHz. It has an average COV that is 10% less than the 2.5 cm average COV. However, it produces no coherent data beyond 7.5 kHz. The 5 cm spacing has the highest COV from around 5-10 kHz and the highest average COV (25% more than the 2.5 cm spacing's average COV). The symmetric mode appears in the 5 cm spacing dispersion curve around 12 kHz. The curve then plateaus and reaches the near surface Rayleigh wave velocity (1700 m/s) and terminates at 27 kHz. The 2.5 cm receiver spacing curve follows approximately the same trend except the curve terminates around 33 kHz. One notable difference between the 2.5 cm and 5 cm curves is

the undulation present at the end of the 5 cm curve. This increase occurs in the 2.5 cm curve only 4 kHz later.

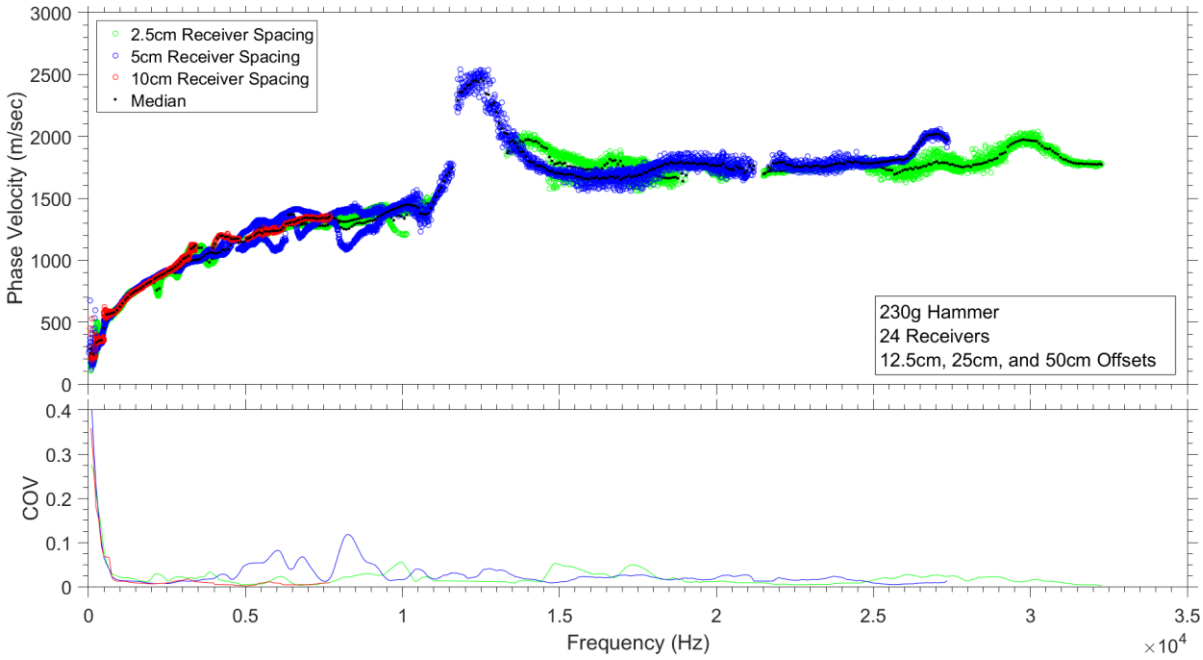

Figure 4-10. Comparison of the dispersion and COV curves for 2.5 cm, 5 cm, and 10 cm receiver spacings at CTTP Asphalt. A receiver array of 24 receivers, a 230g hammer and source offsets of 12.5 cm, 25 cm, and 50 cm (averaged together) were used for the comparison.

The spacing between each receiver is a crucial aspect of MASW testing on asphalt pavements. The sites exhibited similar trends and were in agreement that the 2.5 cm spacing provides the highest frequency data of the three spacings and lowest average COV. Results from CTTP Asphalt show slight undulations that occur at different frequencies for different spacings. The impact of this is that the results of MASW testing on pavement are highly variable and only useful to determine the average Rayleigh wave velocity rather than identifying defects in the pavement. Therefore for this study, the 2.5 cm receiver spacing performed the best for asphalt testing.

4.3.2 Concrete

A comparison of the dispersion and COV curves for receiver spacings of 2.5 cm, 5 cm, and 10 cm for ENRC East Concrete is presented in Figure 4-11. The arrays utilized 24 receivers and a 230g hammer. Source offsets of 12.5 cm, 25 cm, 50 cm, and 75 cm were utilized by averaging the results of the four offsets. The 2.5 cm receiver spacing has the largest variability in the dispersion curve from 0 to 20 kHz and has the highest average COV (100% more than the 5 cm spacing average COV). After 20 kHz, all three spacings have very similar dispersion trends and equivalent COVs. The 2.5 cm spacing stops producing coherent data after 30 kHz but this is after the dispersion curve has plateaued at the Rayleigh wave velocity (20 kHz and 2500 m/s). The 5 cm spacing has a larger COV than the 10 cm spacing from 1 kHz to 7 kHz. However, the COVs are relatively close (within 0.002) at greater frequencies.

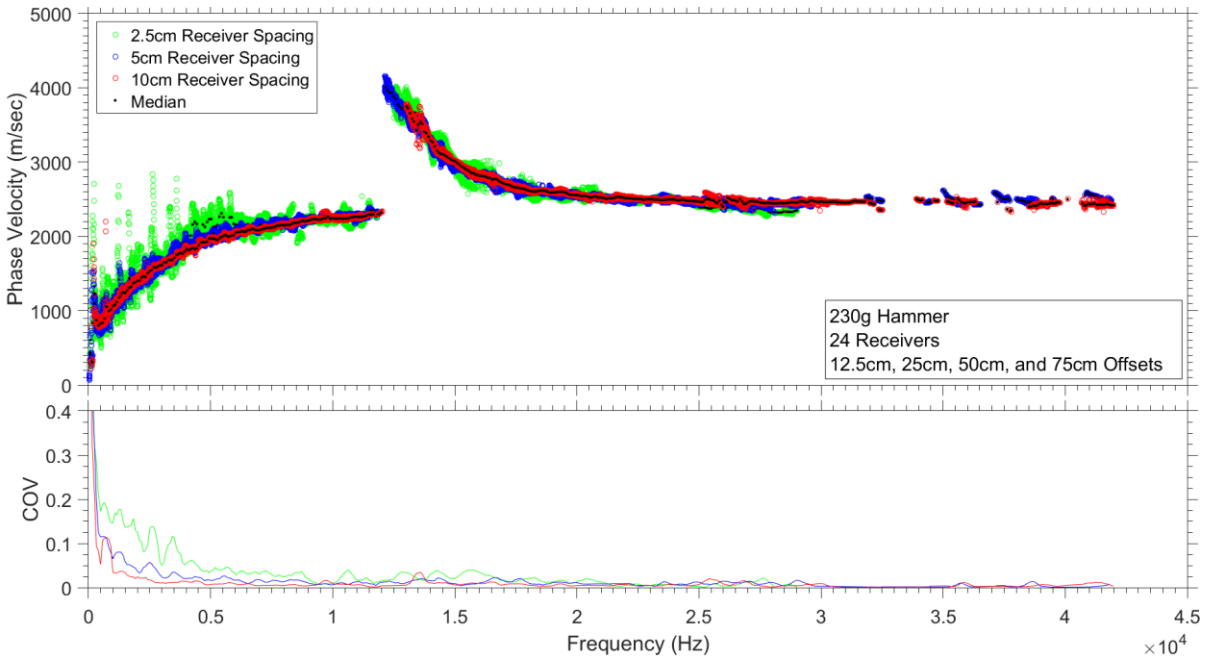

Figure 4-11. Comparison of the dispersion and COV curves for 2.5 cm, 5 cm, and 10 cm receiver spacings at ENRC East Concrete. A receiver array of 24 receivers, a 230g hammer and source offsets of 12.5 cm, 25 cm, 50 cm, and 75 cm (averaged together) were used for the comparison.

A comparison of the dispersion and COV curves comparing receiver spacings of 2.5 cm, 5 cm, and 10 cm for ENRC West Concrete is presented in Figure 4-12. The arrays utilized 24 receivers and a 230g hammer. Source offsets of 12.5 cm, 25 cm, 50 cm, and 75 cm were utilized by averaging the results of the four offsets. Similar to the results at ENRC West Concrete, the 2.5 cm receiver spacing has the highest COV (125% larger than the 5 cm average COV) until the data becomes incoherent at around 30 kHz. The 5 cm spacing has a larger COV than the 10 cm spacing from 2-15 kHz but then has a very similar COV until 42 kHz. The two have essentially the same average COV of ~0.015 across frequencies between 15 and 42 kHz. The symmetric mode appears in the 5 cm spacing data around 15 kHz and converges with the Rayleigh wave velocity at 25 kHz.

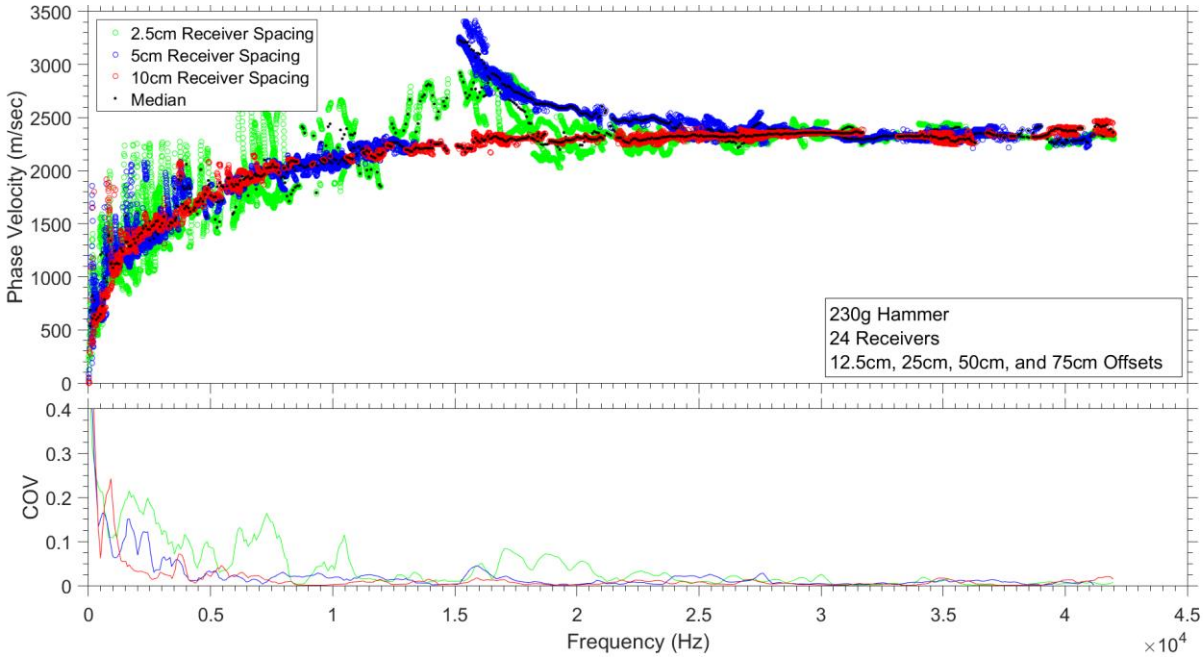

Figure 4-12. Comparison of the dispersion and COV curves for 2.5 cm, 5 cm, and 10 cm receiver spacings at ENRC East Concrete. A receiver array of 24 receivers, a 230g hammer and source offsets of 12.5 cm, 25 cm, 50 cm, and 75 cm (averaged together) were used for the comparison.

For this study, the receiver spacing proved to be an important but not vital aspect of MASW testing on concrete. Unlike asphalt, the optimum receiver spacing for concrete is not 2.5

cm. In contrast, the 10 cm is the optimum spacing, yet it is only marginally better than the 5 cm spacing and was difficult to construct in the field because it was three meters long and barely fit between relief cuts in the concrete. For reasons of practicality, it is recommended that a 5 cm spacing is used.

4.3.3 Soil

A comparison of the dispersion and COV curves comparing receiver spacings of 5 cm and 10 cm for CTTP Soil is presented in Figure 4-13. A 2.5 cm spacing was not tested due to the difficulty associated with construction. The arrays utilized 24 receivers and a 230g hammer. Source offsets of 12.5 cm, 25 cm, and 50 cm were utilized by averaging the results of the three offsets. The dispersion curve for the 10 cm spacing exhibits far-field effects at approximately 900 Hz and loses coherency. Therefore, no data exists for the 10 cm spacing beyond 900 Hz. The 10 cm receiver spacing dispersion curve also has an average COV of 25% greater than that of the 5 cm receiver spacing average COV. The 5 cm curve remains at a low COV until 1900 Hz when far-field effects damp out the higher frequency waves.

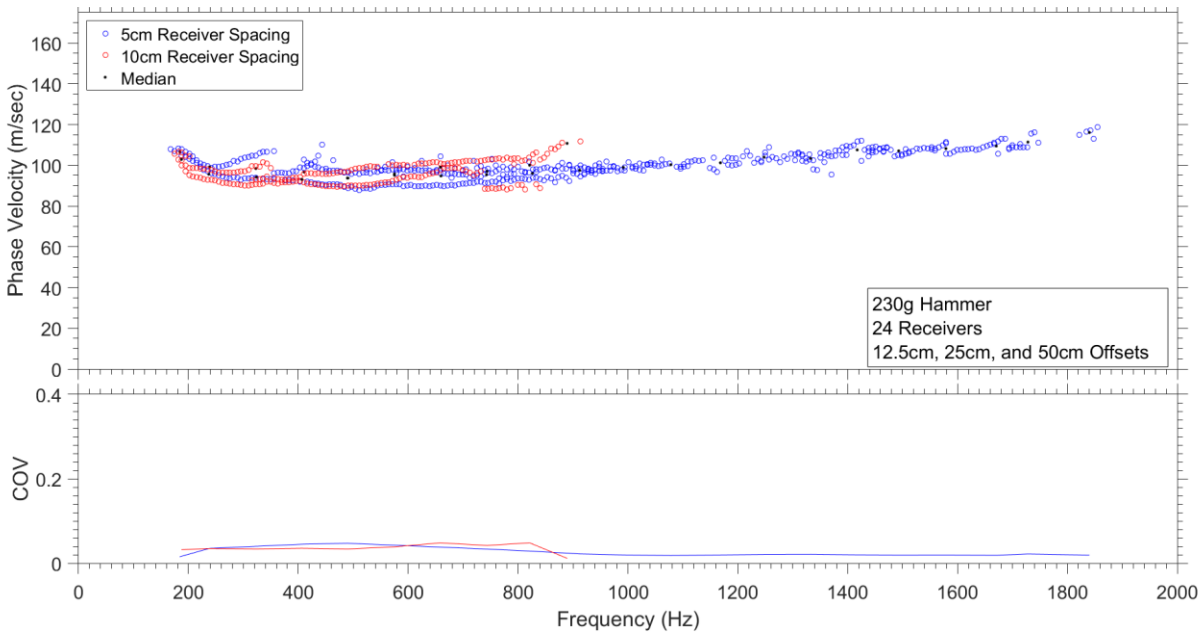

Figure 4-13. Comparison of the dispersion and COV curves for 2.5 cm, 5 cm, and 10 cm receiver spacings at CTTP Soil. A receiver array of 24 receivers, a 230g hammer and source offsets of 12.5 cm, 25 cm, and 50 cm (averaged together) were used for the comparison.

4.3.4 Conclusions

The receiver spacing for the MASW tests performed proved to be of high importance because of far-field effects and data scatter when testing on asphalt and soil. For asphalt pavements, it was determined that a 2.5 cm spacing offers the highest frequency resolution while for concrete pavements a 5 cm or 10 cm spacing provides the highest frequency resolution with a low COV. This author recommends a 5 cm spacing due to the 10 cm spacing producing an array that is about three meters long which can be challenging to set up and find space for. For near surface soil MASW testing, a receiver spacing of 5 cm is recommended as the 10 cm spacing dispersion curve displayed large far-field effects.

4.4 Source Offset

Six source offsets were investigated in order to understand the influence of near and far-field effects on the measured dispersion data. The source offset is defined as the distance between the source and the first receiver in the MASW array as illustrated in Figure 4-14. Source

offsets of 12.5 cm, 25 cm, 50 cm, 75 cm, 100 cm, and 150 cm were investigated. The corresponding dispersion and COV curves will be examined to determine the optimum offset. The COV curves have been enlarged to examine the large number of lines in detail.

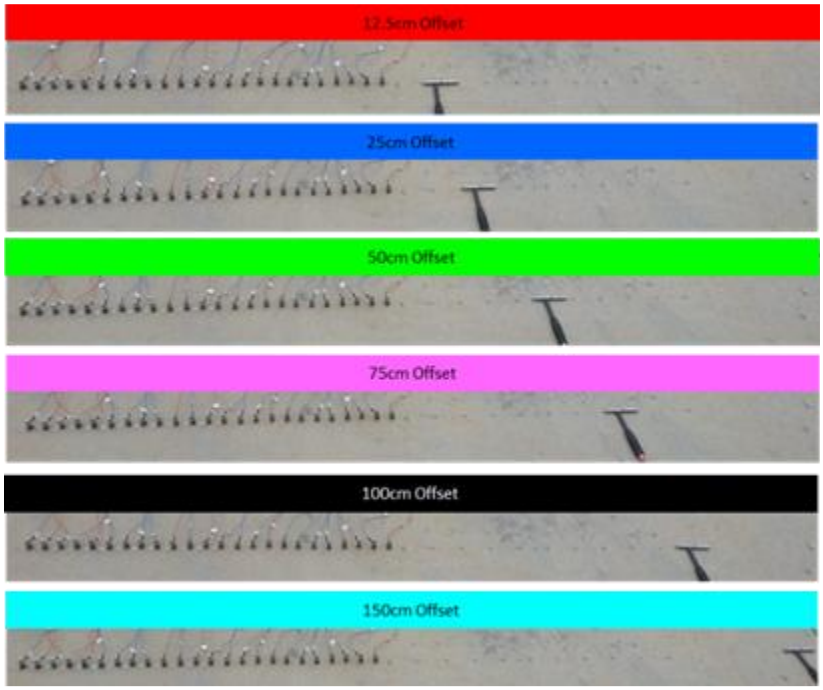

Figure 4-14. Source offsets of 12.5 cm (red), 25 cm (blue), 50 cm (green), 75 cm (magenta), 100 cm (black), and 150 cm (cyan) for MASW testing shown with a 5 cm receiver spacing and 24 receivers.

4.4.1 Asphalt

A comparison of the dispersion and COV curves for source offsets of 12.5 cm, 25 cm, 50 cm, 75 cm, 100 cm and 150 cm for ENRC Asphalt is summarized in Table 4-1 and presented in Figure 4-15a-b. The arrays utilized 24 receivers, a 230g hammer, and a 2.5 cm receiver spacing. All of the offsets perform similarly from approximately 0-10 kHz. At 7.5 kHz, the 150 cm (average COV=0.019) and 100 cm (average COV=0.012) offset dispersion curves display an increase in scatter and COV and cease to produce coherent data at 10 and 13 kHz, respectively. Likewise, the 75 cm (average COV=0.17) and 50 cm (average COV=0.013) offset dispersion

curves show an increase in COV around 7.5 kHz but continue to produce far-field effect free results until 16 kHz. The 25 cm offset produces the best data (average COV=0.008) and terminates at 22 kHz. The 25 cm, 50 cm, and 75 cm are the only offsets that produce frequencies above 15 kHz which is when the waves behave like Rayleigh waves. Surprisingly, the 12.5 cm offset does not produce good data (average COV=0.013) as it terminates around 13 kHz similar to the 100 cm offset. This is a good example of the need for redundant offsets because the test does not always act as predicted.

Table 4-1. Summary of frequency ranges and average COVs for various offsets for ENRC Asphalt. A 230g hammer and a receiver array of 24 receivers with a 2.5 cm receiver spacing were used in the summary.

ENRC Asphalt		
Offset	Frequency Range [kHz]	Average COV
12.5cm	0-6.6, 10-11	0.013
25cm	0-21	0.008
50cm	0-17	0.013
75cm	0-16	0.017
100cm	0-12	0.012
150cm	0-10	0.019

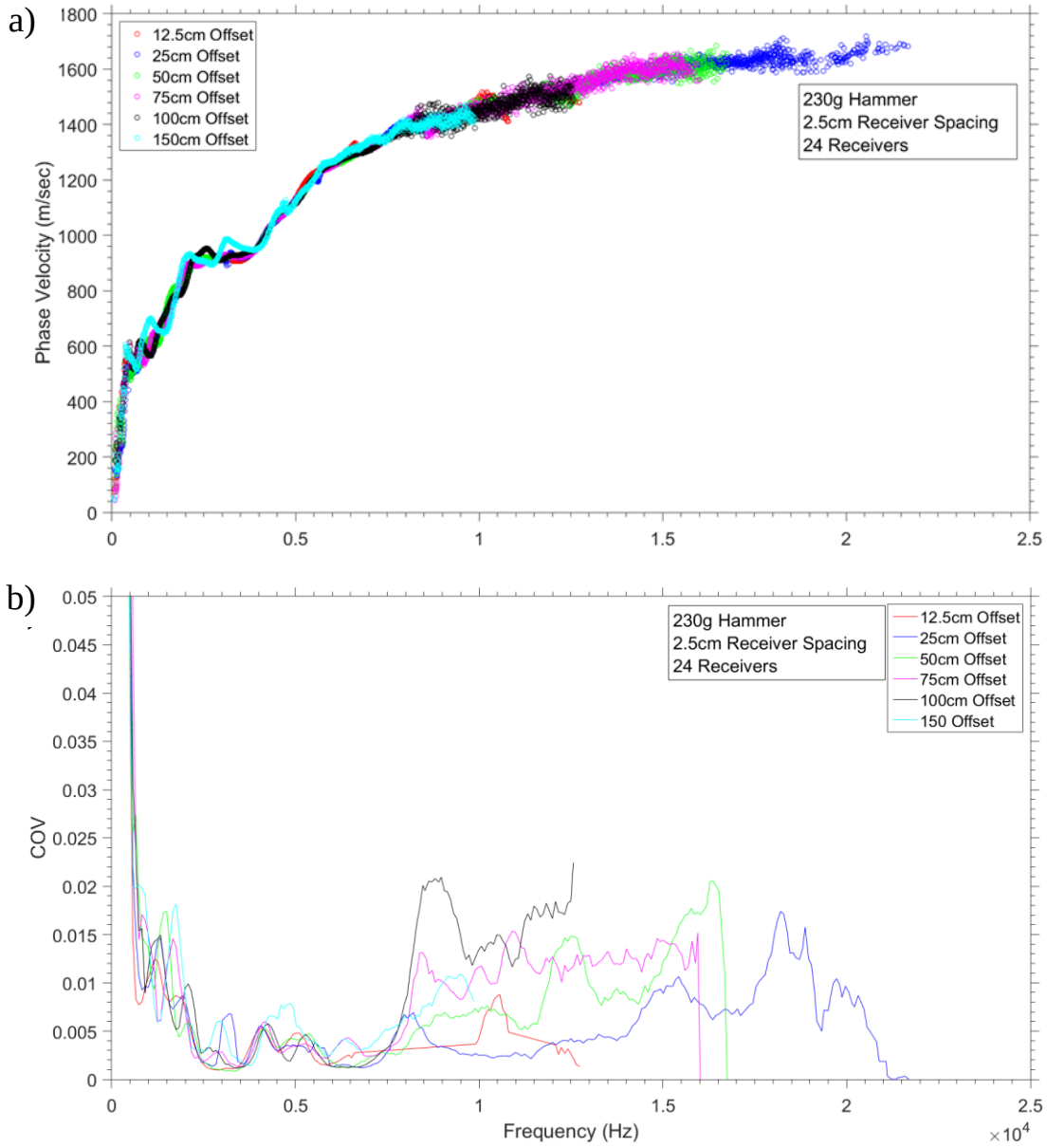

Figure 4-15. Comparison of the dispersion and COV curves for source offsets of 12.5 cm, 25 cm, 50 cm, 75 cm, 100 cm, and 150 cm at ENRC Asphalt. A 230g hammer and a receiver array of 24 receivers with a 2.5 cm receiver spacing were used for the comparison.

A comparison of the dispersion and COV curves for source offsets of 12.5 cm, 25 cm, 50 cm, 75 cm, 100 cm and 150 cm for CTTP Asphalt is summarized in Table 4-2 and presented in Figure 4-16a-b. The arrays utilized 24 receivers, a 230g hammer, and a 2.5 cm receiver spacing. The 150 cm, 100 cm, and 50 cm offsets had varying average COVs (0.029, 0.032, and 0.019

respectively), but had very similar frequency ranges as they all terminated around 4 kHz. The 75 cm offset performed slightly better by terminating at 8 kHz and posting an average COV of .020. Only the 12.5 cm and 25 cm produce data at Rayleigh wave frequencies (above 15 kHz) although the 25cm produces data with twice as large a COV (0.015 compared to 0.009) as the 12.5 cm offset.

Table 4-2. Summary of frequency ranges and average COVs for various offsets for CTTP Asphalt. A 230g hammer and a receiver array of 24 receivers with a 2.5 cm receiver spacing were used in the summary.

CTTP Asphalt		
Offset	Frequency Range [kHz]	Average COV
12.5cm	0-11,13-32	0.009
25cm	0-11, 14-19, 25-30	0.015
50cm	0-4.1	0.019
75cm	0-7.4	0.020
100cm	0-5.1	0.032
150cm	0-4.3	0.029

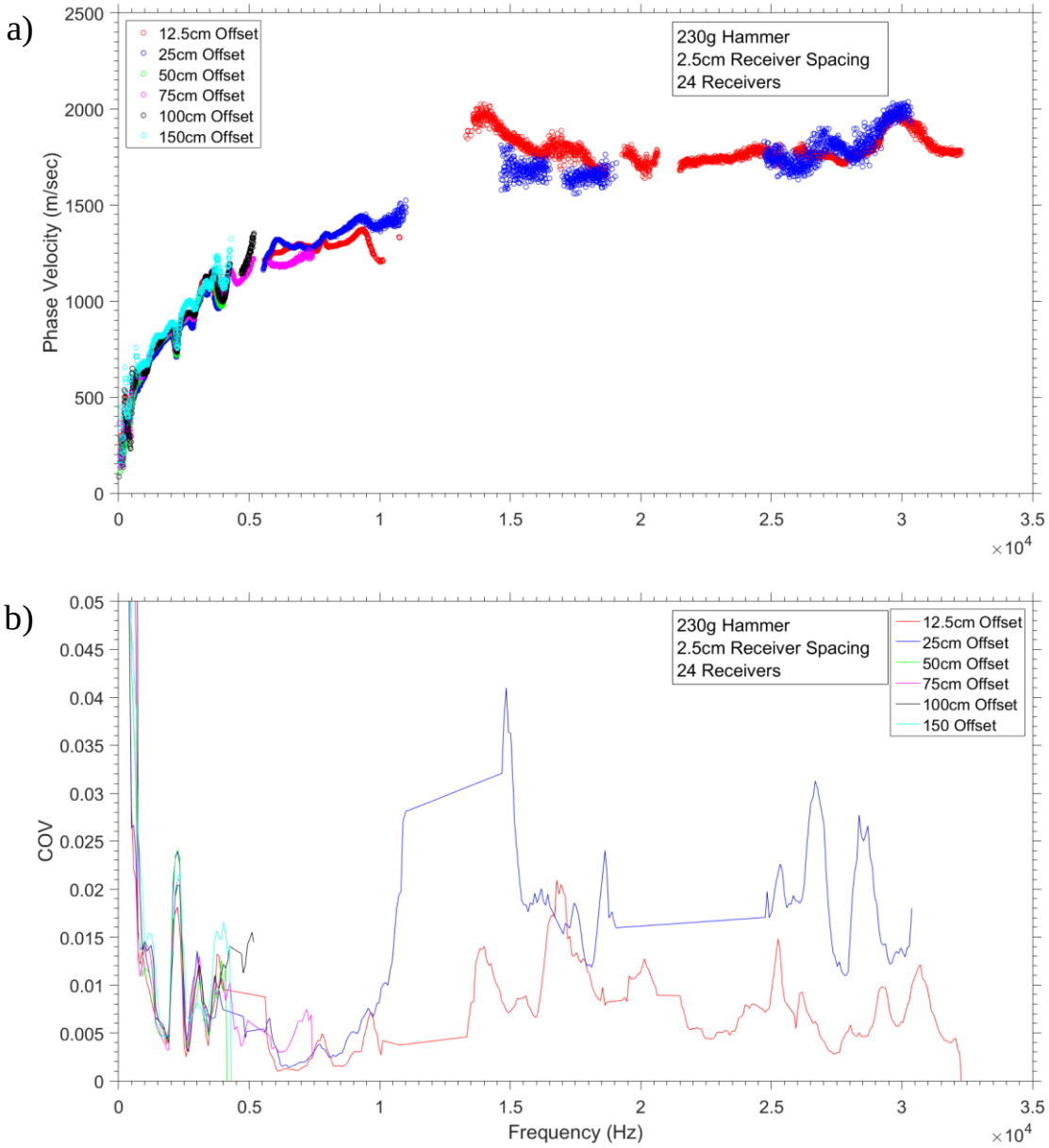

Figure 4-16. Comparison of the dispersion and COV curves for source offsets of 12.5 cm, 25 cm, 50 cm, 75 cm, 100 cm, and 150 cm at CTTP Asphalt. A 230g hammer and a receiver array of 24 receivers with a 2.5 cm receiver spacing were used for the comparison.

Based on the data available, the recommended source offsets are 12.5 cm, 25 cm, and 50 cm for testing on asphalt. COV typically increases with distance thus closer offsets are more applicable as the longer offsets have significant far-field effects. It is possible for only one offset to be used during testing, but additional offsets take very little time compared to array setup

times. Since results from some offsets can be unpredictable, multiple offsets add redundancy to the data that will help achieve acceptable results under multiple conditions.

4.4.2 Concrete

A comparison of the dispersion and COV curves for source offsets of 12.5 cm, 25 cm, 50 cm, 75 cm, 100 cm and 150 cm for ENRC East Concrete is summarized in Table 4-3 and presented in Figure 4-17a-b. The arrays utilized 24 receivers, a 230g hammer, and a 5 cm receiver spacing. All the offsets performed similarly as all of them produced data up to a maximum frequency of 42 kHz. However, the 150 cm and 100 cm offsets do produce a larger average COV (0.012 and 0.014 respectively) from 10- 20 kHz and from 35-42 kHz. This data suggests that the source offset does not significantly impact the quality of data at this site. The 12.5 cm offset produces the lowest average COV (0.009). However, it only produces data out to a maximum frequency of 37 kHz. The 25 cm and 50 cm offsets produce data for similar frequency ranges and have similar average COVs (~0.01).

Table 4-3. Summary of frequency ranges and average COVs for various offsets for ENRC East Concrete. A 230g hammer and a receiver array of 24 receivers with a 5 cm receiver spacing were used in the summary.

ENRC East Concrete		
Offset	Frequency Range [kHz]	Average COV
12.5cm	0-28, 35-42	0.009
25cm	0-29	0.010
50cm	0-29, 31-42	0.010
75cm	0-29	0.010
100cm	0-26, 37-42	0.014
150cm	0-27, 38-42	0.012

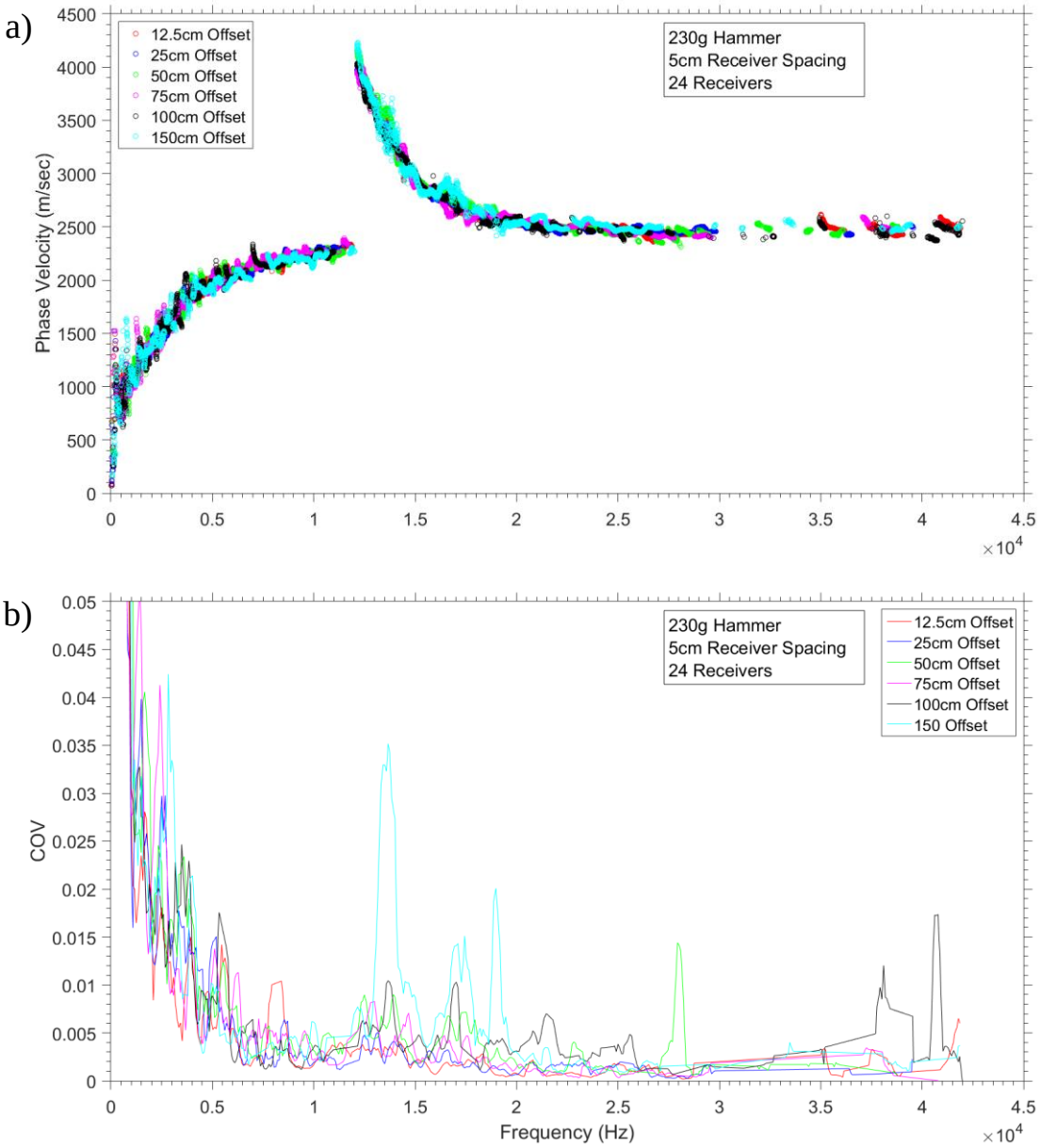

Figure 4-17. Comparison of the dispersion and COV curves for source offsets of 12.5 cm, 25 cm, 50 cm, 75 cm, 100 cm, and 150 cm at ENRC East Concrete. A 230g hammer and a receiver array of 24 receivers with a 5 cm receiver spacing were used for the comparison.

A comparison of the dispersion and COV curves comparing source offsets of 12.5 cm, 25 cm, 50 cm, 75 cm, 100 cm and 150 cm for ENRC West Concrete is summarized in Table 4-4 and presented in Figure 4-18a-b. The arrays utilized 24 receivers, a 230g hammer, and a 5 cm receiver spacing. The 150 cm and 100 cm offsets performed the worst as they do not produce

data at all frequencies and have high average COVs. The 25 cm and 75 cm offsets produce large COV values at 15 kHz, 25 kHz, and 35 kHz but low COV at all other frequencies. Each offset produces good data at varying frequency ranges and thus multiple offsets are needed to create a complete and robust dispersion curve. These dispersion curves also suggests that source offset is not a controlling factor in the quality of dispersion data in concrete.

Table 4-4. Summary of frequency ranges and average COVs for various offsets for ENRC West Concrete. A 230g hammer and a receiver array of 24 receivers with a 5 cm receiver spacing were used in the summary.

ENRC West Concrete		
Offset	Frequency Range [kHz]	Average COV
12.5cm	0-37	0.009
25cm	0-3.2, 7.3-13, 16-18, 24-27, 29-42	0.011
50cm	0-3.2, 3.7-14, 24-28, 32-42	0.010
75cm	0-3.2, 3.7-14, 24-38	0.013
100cm	0-3.6, 6.8-14, 24-39	0.013
150cm	0-3.6, 6.8-14,24-27	0.017

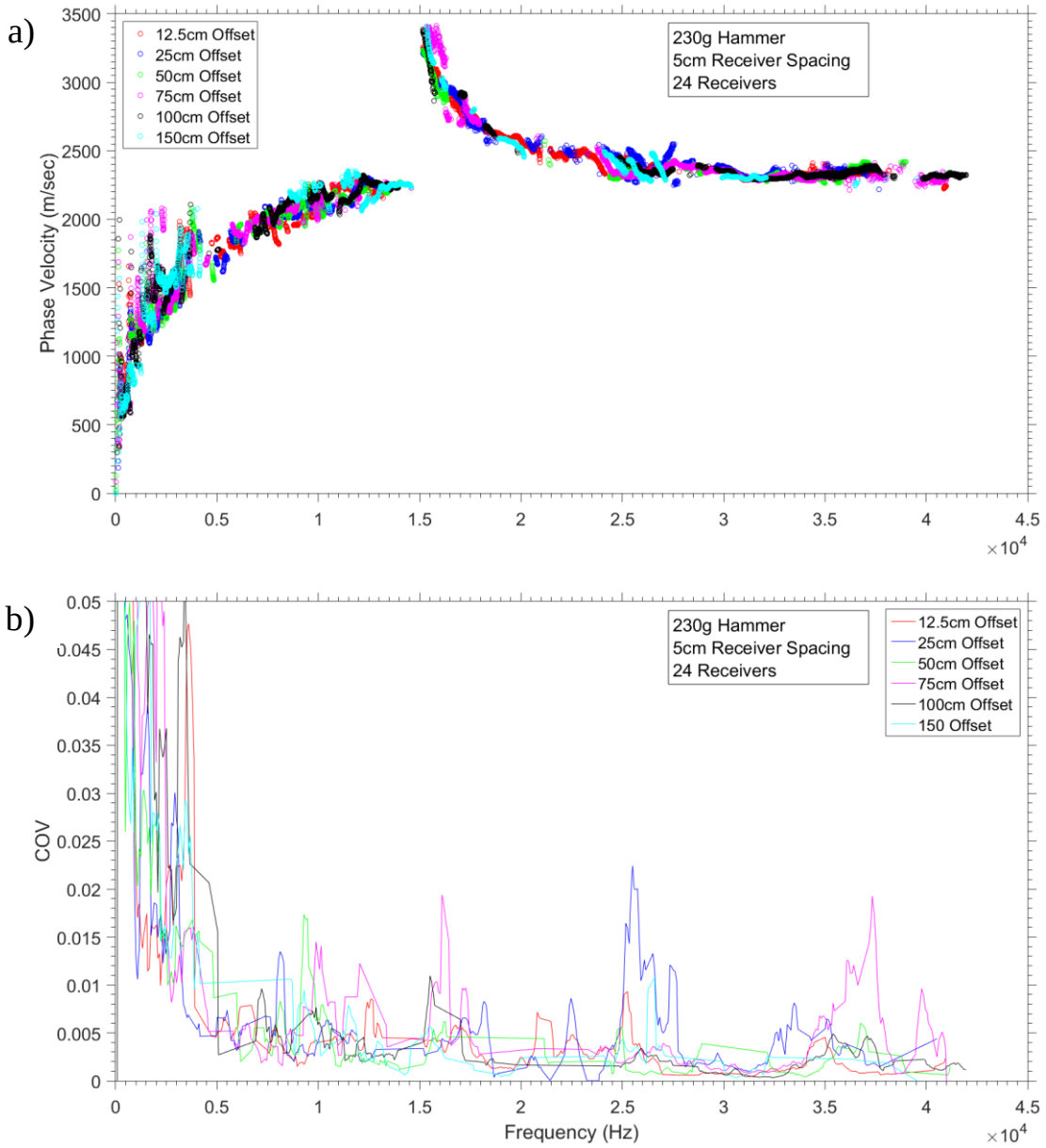

Figure 4-18. Comparison of the dispersion and COV curves for source offsets of 12.5 cm, 25 cm, 50 cm, 75 cm, 100 cm, and 150 cm at ENRC West Concrete. A 230g hammer and a receiver array of 24 receivers with a 5 cm receiver spacing were used for the comparison.

All offsets in this study performed similarly and it can be concluded that concrete is not as susceptible to changes in the quality of data from different source offsets as asphalt. All the offsets produce data out to a maximum frequency of 42 kHz. Based on this data, it is recommended that offset of 12.5 cm, 25 cm, 50 cm, and 75 cm are used in conducting MASW

testing on concrete pavements. Using multiple offsets allows for a dispersion curve that is robust and has data at all frequencies and each offset only takes approximately one minute to perform in the field.

4.4.3 Soil

A comparison of the dispersion and COV curves for source offsets of 12.5 cm, 25 cm, 50 cm, 75 cm, 100 cm and 150 cm for CTTP Soil is summarized in Table 4-5 and presented in Figure 4-19a-b. The arrays utilized 24 receivers, a 230g hammer, and a 5 cm receiver spacing. The 150 cm and 100 cm offset dispersion curves display significant far-field effects as they only produced data only in the 0.2-0.4 kHz range. The 75 cm offset dispersion curve also displays significant far-field effects as it only produces data out to 0.6 kHz. The 12.5 cm, 25 cm and 50 cm offsets all produce data until ~1.7 kHz Thus it is recommend for near surface MASW testing on soil that source offsets of 12.5 cm, 25 cm, and 50 cm are used.

Table 4-5. Summary of frequency ranges and average COVs for various offsets for CTTP Soil. A 230g hammer and a receiver array of 24 receivers with a 5 cm receiver spacing were used in the summary.

CTTP Soil		
Offset	Frequency Range [kHz]	Average COV
12.5cm	0.18-1.85	0.008
25cm	0.18-1.7	0.010
50cm	0.18-1.7	0.013
75cm	0.23-0.6	0.017
100cm	0.21-0.45	0.012
150cm	0.23-.295	0.019

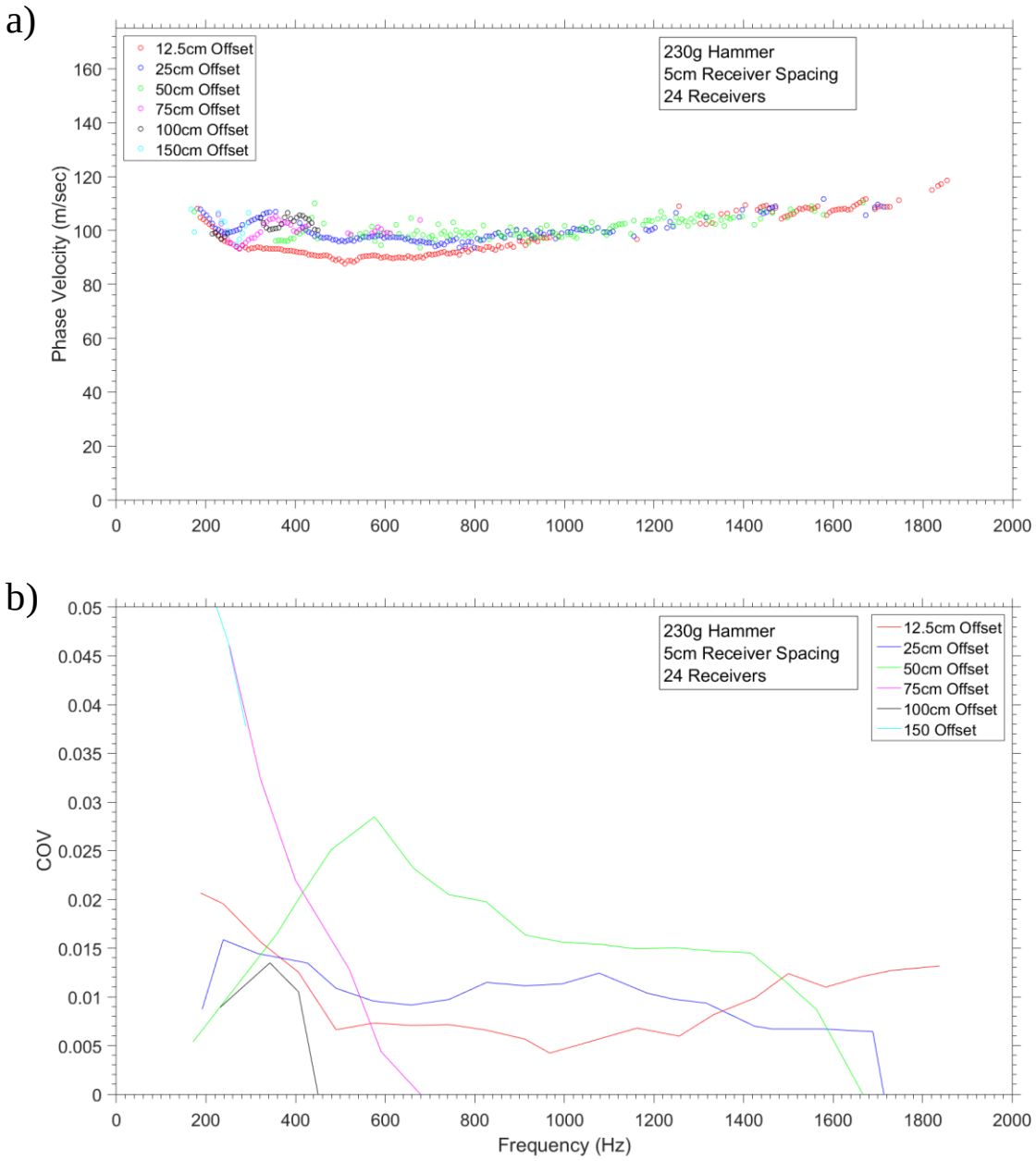

Figure 4-19. Comparison of the dispersion and COV curves for source offsets of 12.5 cm, 25 cm, 50 cm, 75 cm, 100 cm, and 150 cm at CTTP Soil. A 230g hammer and a receiver array of 24 receivers with a 5 cm receiver spacing were used for the comparison.

4.4.4 Conclusions

Given the data presented, the source offset is a critical parameter of MASW of asphalt pavements. The waves in asphalt have significant far-field effects and thus the offsets need to be close to the receiver array. Source offsets of 12.5 cm, 25 cm and 50 cm are recommended.

Although for concrete, the source offset was not as vital as far-field effects were not present. Source offsets of 12.5 cm, 25 cm, 50 cm, and 75 cm are recommended in order to produce a robust and complete dispersion curve. For soils, source offsets of 12.5 cm, 25 cm, and 50 cm are recommended as the other offset dispersion curves display significant far-field effects. In any of the three materials, more offsets in addition to the author's recommendation can be used as they take approximately one minute to perform but little extra data should be expected.

4.5 Number of Receivers

The number of receivers in a MASW array was investigated to maximize frequency range and data clarity. The more receivers in the array, the more robust and precise the data sets should be. An illustration of arrays with 12, 18, and 24 receivers is presented in Figure 4-20a-c. The following sections will examine arrays on asphalt, concrete, and soil.

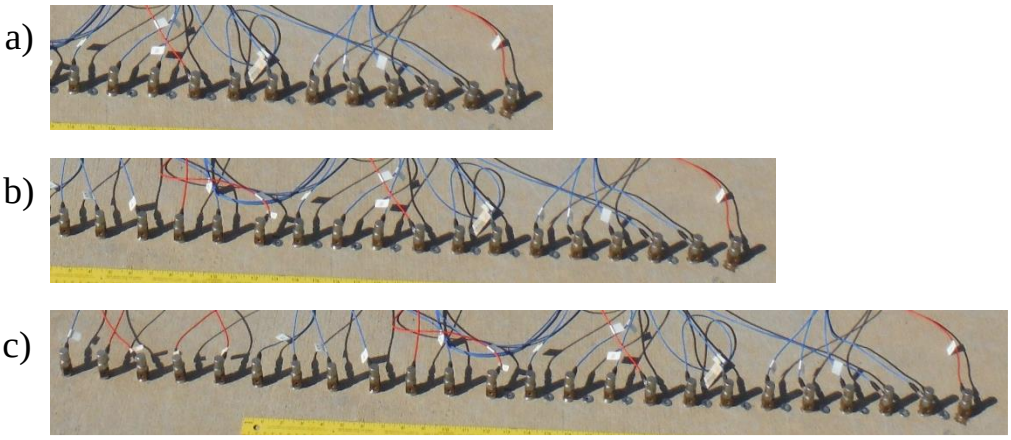

Figure 4-20a-c. A) MASW array with 12 receivers, B) MASW array with 18 receivers, and C) MASW array with 24 receivers.

4.5.1 Asphalt

A comparison of the dispersion and COV curves for arrays with 12, 18 and 24 receivers for ENRC Asphalt is presented in Figure 4-21. The arrays utilized a 230g hammer, a 2.5 cm receiver spacing. Source offsets of 12.5 cm, 25 cm, and 50 cm were utilized by averaging the results of

the three offsets. The dispersion curve for 12 receiver array loses high frequency coherency at 15 kHz and shows an undulation at 2 kHz not seen in other curves. This loss in frequency range is not expected since the 12 receiver array is closest to all source offsets, which should reduce the effect of far-field effects. The dispersion curve for the 18 receiver array loses coherency at 18 kHz and the dispersion curve for the 24 receiver array loses coherency at 22 kHz. The average COVs decrease as the number of receivers increase (12 receivers= 0.027, 18 receivers= 0.015, and 24 receivers= 0.01) as expected.

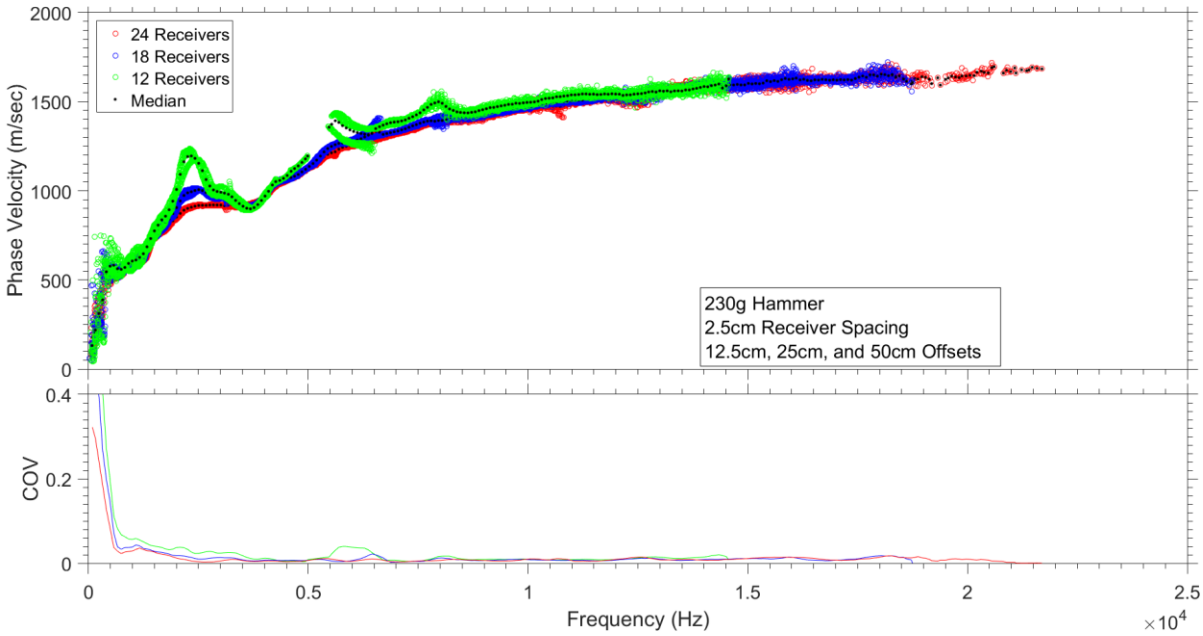

Figure 4-21. Comparison of the dispersion and COV curves for 12, 18 and 24 receivers at ENRC Asphalt. A 2.5 cm receiver spacing and a 230g hammer offset 12.5 cm, 25 cm, and 50 cm (averaged together) were used for the comparison.

A comparison of the dispersion and COV curves for receiver arrays with 12, 18 and 24 receivers for CTTP Asphalt is presented in Figure 4-22. The arrays utilized a 230g hammer, a 2.5 cm receiver spacing. Source offsets of 12.5 cm, 25 cm, and 50 cm were utilized by averaging the results of the three offsets. Unlike the results from ENRC Asphalt, the number of receivers did not affect the frequency range measured. All three arrays were not able to resolve the phase velocity at certain frequencies (e.g. 5 kHz) but a decreasing COV trend was observed similar to

the ENRC Asphalt results (12 receivers= 0.025, 18 receivers= 0.02, and 24 receivers= 0.015). The dispersion curve for the 12 receiver array has undulations at 5 and 9 kHz similar to results observed for ENRC Asphalt.

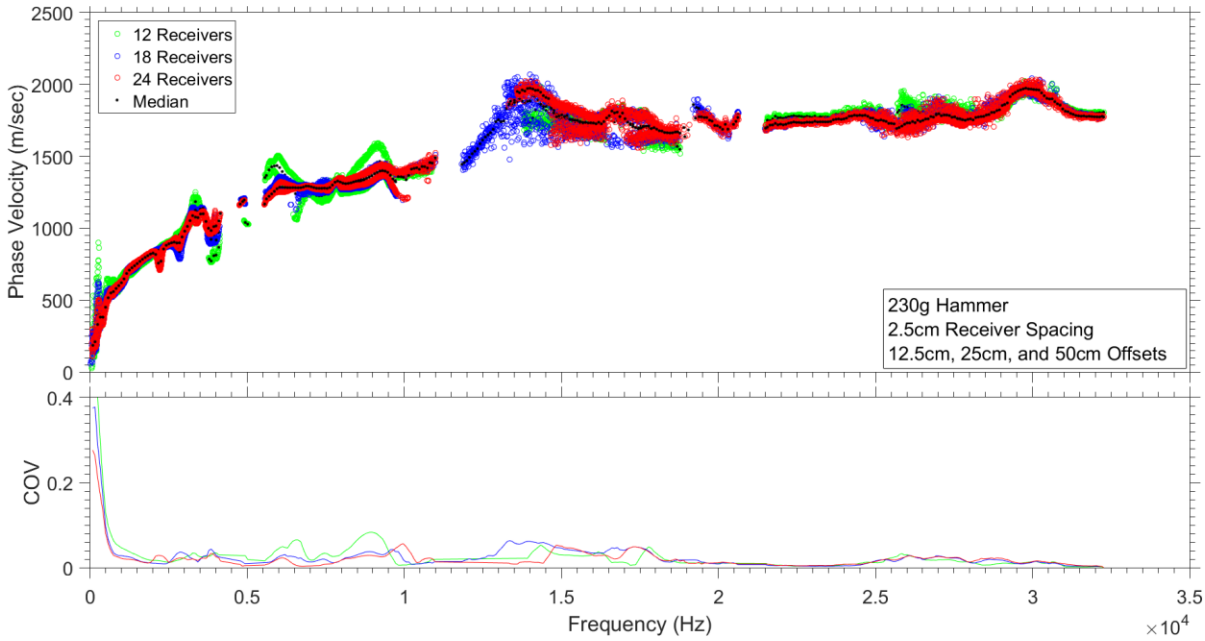

Figure 4-22. Comparison of the dispersion and COV curves for 12, 18 and 24 receivers at CTTP Asphalt. A 2.5 cm receiver spacing and a 230g hammer offset 12.5 cm, 25 cm, and 50 cm (averaged together) were used for the comparison.

Given the data presented, the 24 receiver array produced the lowest COV and most accurate data. However, the 18 receiver array had comparable COVs at high frequencies and may be used in future field testing. The 18 receiver array requires less initial monetary investment as well as a faster setup time. An 18 receiver array can save about six minutes or 20% of the total time needed compared the 24 receiver array. The 12 receiver array did not produce high frequency data at ENRC Asphalt so it cannot be recommended.

4.5.2 Concrete

A comparison of the dispersion and COV curves for arrays with 12, 18 and 24 receivers for ENRC East Concrete is presented in Figure 4-23. The arrays utilized a 230g hammer, a 5 cm

receiver spacing. Source offsets of 12.5 cm, 25 cm, 50 cm, and 75 cm were utilized by averaging the results of the four offsets. Like previous test, the number of receivers in the array did affect both the COV and the frequency range measured. The average COV for the dispersion curve using a 12 receiver array when compared to the dispersion curve using a 24 receiver array increased by 150% (average COV=0.012 for 24 receivers compared to .031 for 12 receivers) while the dispersion curve for the 18 receiver array increased by 50% (average COV=0.018). The 12 receiver array also shows an increase of about 10% in Rayleigh wave velocity at 25 kHz compared to the velocity estimated using the 24 receiver array. The 24 receiver array was the only array to measure frequencies out to 42 kHz. However, the velocity remains constant from 20- 30 kHz so data at 42 kHz is not vital to accurately classifying the Rayleigh wave velocity of the pavement.

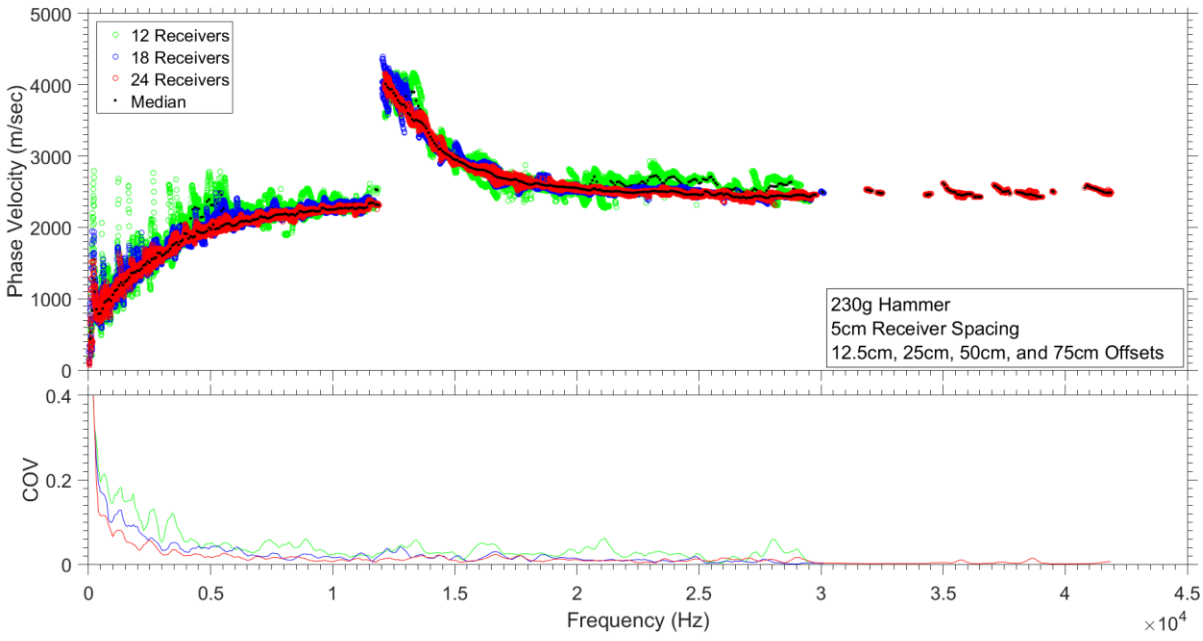

Figure 4-23. Comparison of the dispersion and COV curves for 12, 18 and 24 receivers at ENRC East Concrete. A 5 cm receiver spacing and a 230g hammer offset 12.5 cm, 25 cm, 50 cm, and 75 cm (averaged together) were used for the comparison.

A comparison of the dispersion and COV curves for arrays with 12, 18 and 24 receivers for ENRC West Concrete is presented in Figure 4-24. The arrays utilized a 230g hammer, a 5 cm

receiver spacing. Source offsets of 12.5 cm, 25 cm, 50 cm, and 75 cm were utilized by averaging the results of the four offsets. The 12 receiver array has a large amount of scatter at frequencies less than 10 kHz compared to the dispersion curve using a 24 receiver. The COV for the 12 receiver array dispersion curve increased by 160% while the dispersion curve using an 18 receiver array increased by 90%. While there is a large difference in COV, the arrays produce very similar average Rayleigh wave velocities at frequencies above 25 kHz and the difference in COV may be attributed to frequencies lower than 25 kHz.

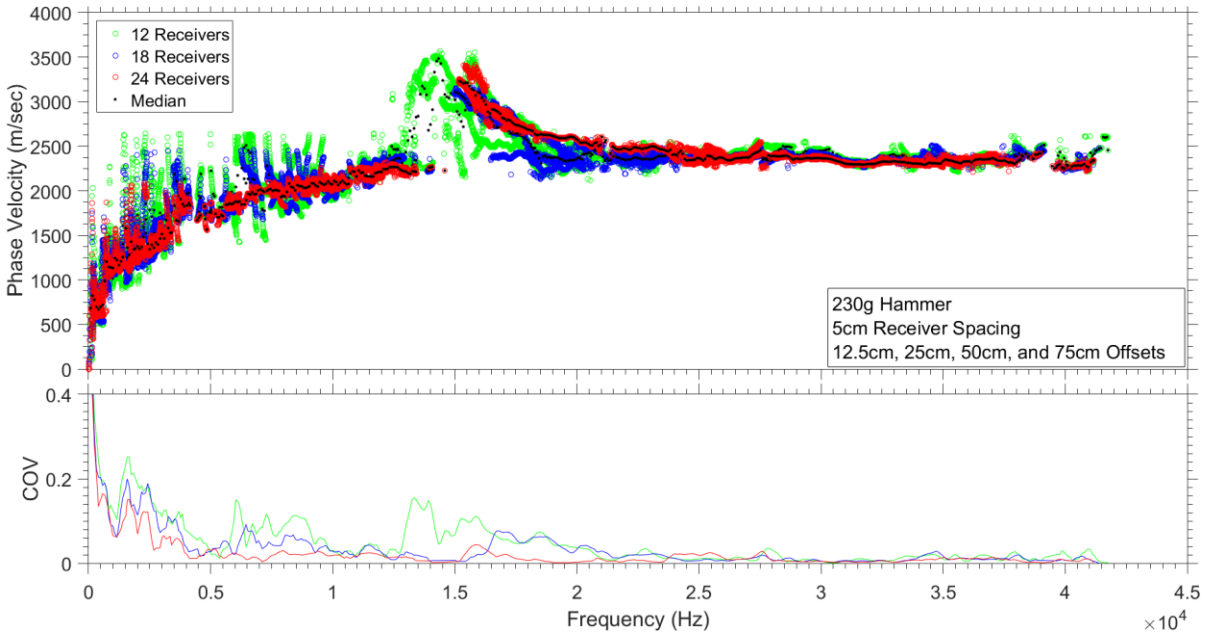

Figure 4-24. Comparison of the dispersion and COV curves for 12, 18 and 24 receivers at ENRC West Concrete. A 5 cm receiver spacing and a 230g hammer offset 12.5 cm, 25 cm, 50 cm, and 75 cm (averaged together) were used for the comparison.

Given the data presented, an array with 24 receivers produces the most precise data. However, if a simple inversion (Rayleigh wave velocity for only the top layer) is all that is needed, then an array with 18 receivers produces results that are in agreement with a 24 receiver

array. A 12 receiver array is not recommended as a 10% error in Rayleigh wave velocity was observed in the ENRC East Concrete dispersion curve.

4.5.3 Soil

A comparison of the dispersion and COV curves for arrays with 12, 18, and 24 receivers for CTTP Soil is presented in Figure 4-25. The arrays utilized a 230g hammer, a 5 cm receiver spacing. Source offsets of 12.5 cm, 25 cm, and 50 cm were utilized by averaging the results of the three offsets. Overall, the results from the three receiver arrays provided similar dispersion curves with similar COVs of less than approximately 5%. Each array was able to measure dispersion data over the same frequency with no improvement in data quality when increasing the number of receivers. The number of receivers in the array is not a critical parameter for near-surface MASW testing on soil. However, any further testing done in this study will utilize 24 receivers.

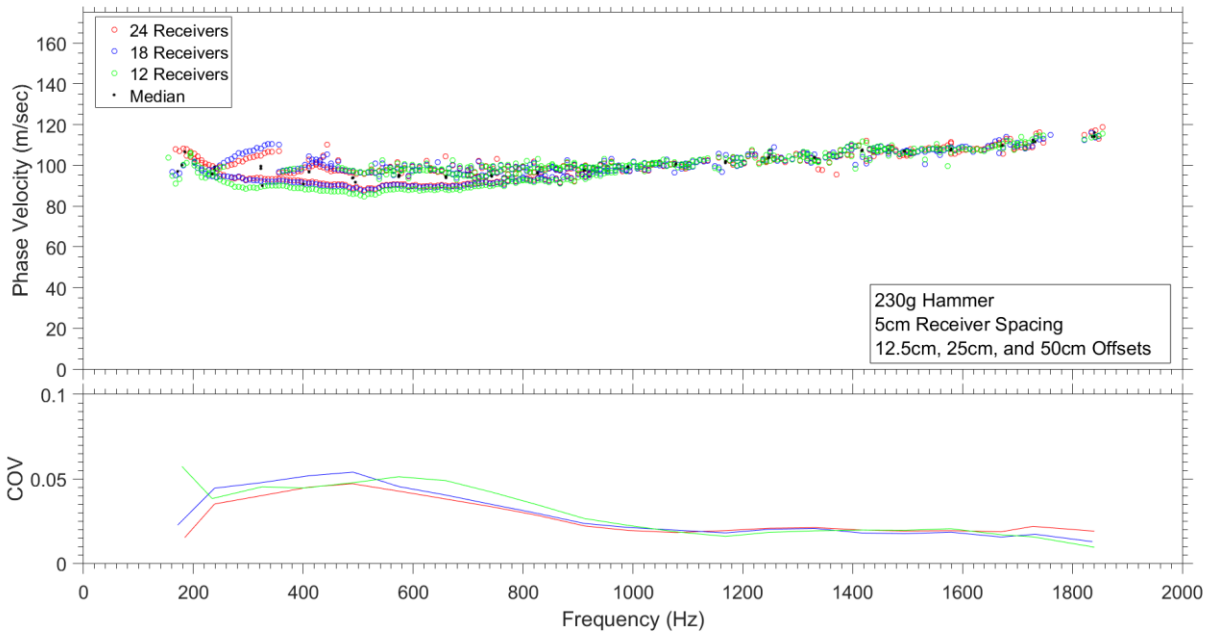

Figure 4-25. Comparison of the dispersion and COV curves for 12, 18 and 24 receivers at CTTP Soil. A 5 cm receiver spacing and a 230g hammer offset 12.5 cm, 25 cm, and 50 cm (averaged together) were used for the comparison.

4.5.4 Conclusions

Out of the three materials tested, soil proved to be the least affected by the number of receivers in the array because the frequency range did not change and the 12 and 18 receiver arrays had COVs that increased by 20% and 5% respectively when compared to a 24 receiver array. These increases in COV are not significant thus a 12 receiver array is recommended based on this data. No near-field effects were observed when only 12 receivers were used. However, further testing done in this study will utilize a 24 receiver array. The concrete was the second least affected data set by the number of receivers. The 12 receiver array consistently had a 150% increase in COV and had variations in high frequency Rayleigh wave velocity while the 18 receiver array average COV was 65% more than the 24 receiver array but displayed similar high frequency Rayleigh wave velocities. For the purposes of this research, arrays with 24 receivers will be used to collect data but other practitioners may find an array with 18 receivers to be sufficient. Additionally, an 18 receiver array can save about six minutes which is about 20% of the time needed to conduct the test. Asphalt pavement proved to be the most volatile and dependent on the number of receivers in the array. The 12 and 18 receiver arrays did not measure the same frequency range and had larger COVs than the 24 receiver array. Based on the data collected, the 24 receiver array is recommended for all future MASW testing on asphalt pavement.

4.6 Lateral influence of Rayleigh wave propagation

As stated in Section 4.1, the recommended soil testing parameters were determined and will be used to determine the lateral influence of Rayleigh wave propagation. In the current state of practice, the effect of lateral variability in soil on MASW dispersion results is not known. To test the lateral variability, a wooden box with dimensions of 1.2 m by 2.4 m by 1.2 m was

constructed and is presented in more detail in Section 3. A concrete wall was placed on the near side of the box shown in Figure 4-26 and then sand was placed in the box as presented in Figure 4-26a. The sand proved to be troublesome so it was removed and a homogenous red clay (Figure 4-26b) was placed in the box. The testing procedure was identical for both soils as MASW arrays were placed at the 1/8 (15cm), 1/4 (30cm), 1/2 (60cm), and 3/4 (90cm) widths of the box away from the concrete wall as presented in Figure 4-27. Testing was then conducted but both materials produced incoherent dispersion curves and will not be discussed thoroughly.

a) b)

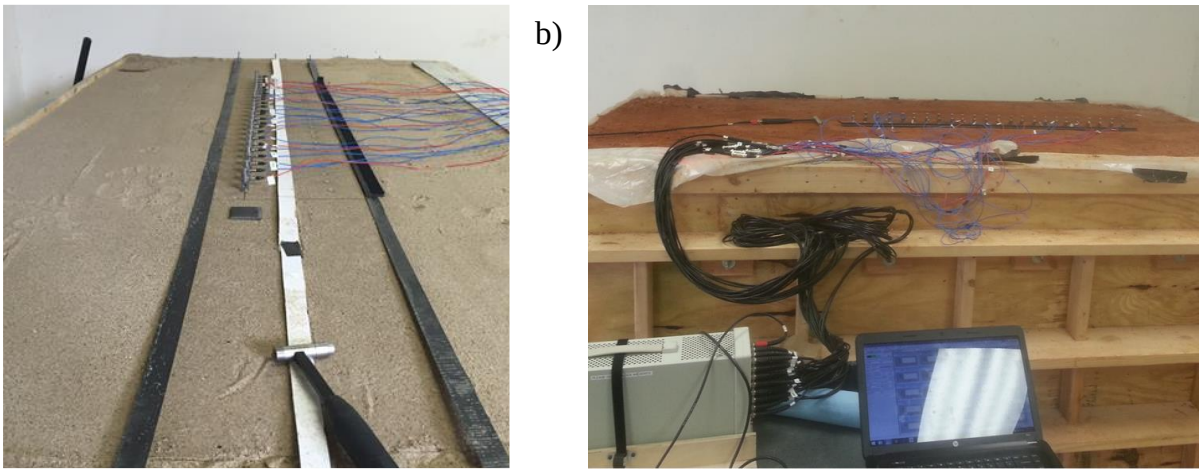

Figure 4-26a-b. Laboratory testing environment for evaluating the horizontal resolution of Rayleigh waves using: a) sand and b) homogenous red clay.

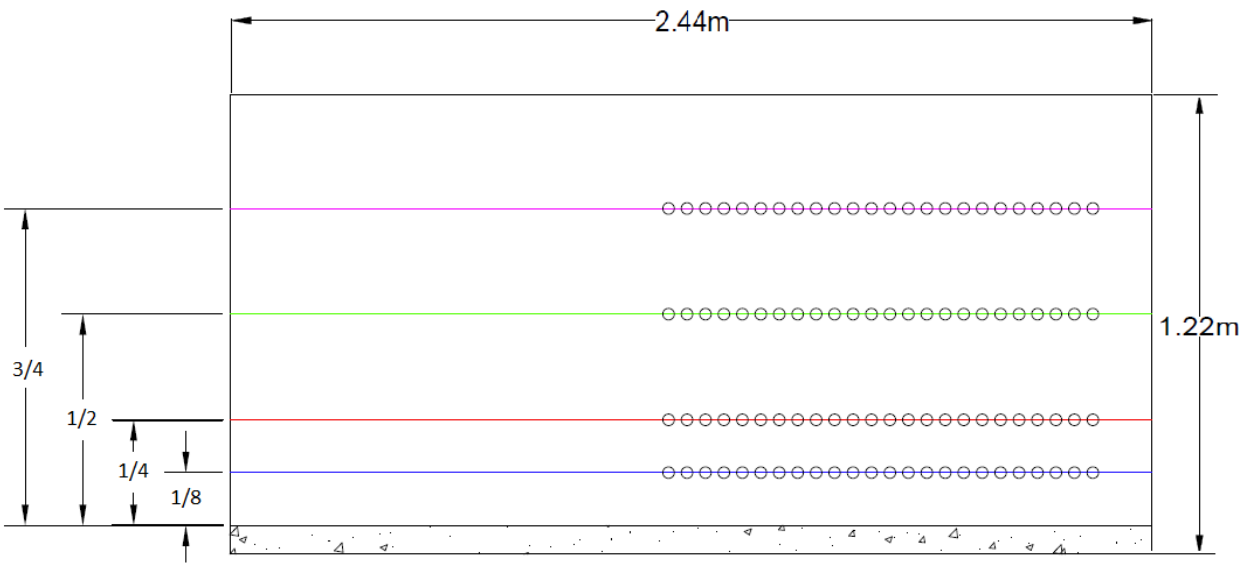

Figure 4-27. Array configuration for determining the horizontal resolution of Rayleigh waves (Blue=Offset 1, Red=Offset 2, Green=Offset 3, Magenta=Offset 4).

4.6.1 Sand

The dispersion curves for MASW testing on sand are presented in Figure 4-28. The test utilized 24 receivers, a 230g hammer, and a source offset of 25 cm. There appears to be no relationship between array offset and a change in dispersion values. The 1st and 3rd offset behave in a similar manner particularly at 400 Hz. Offset 2 and 4 behave in an unpredictable manner that is likely due to inconsistencies in the density of the sand. No meaningful conclusions were drawn from these results thus a new fill material (clay) was chosen.

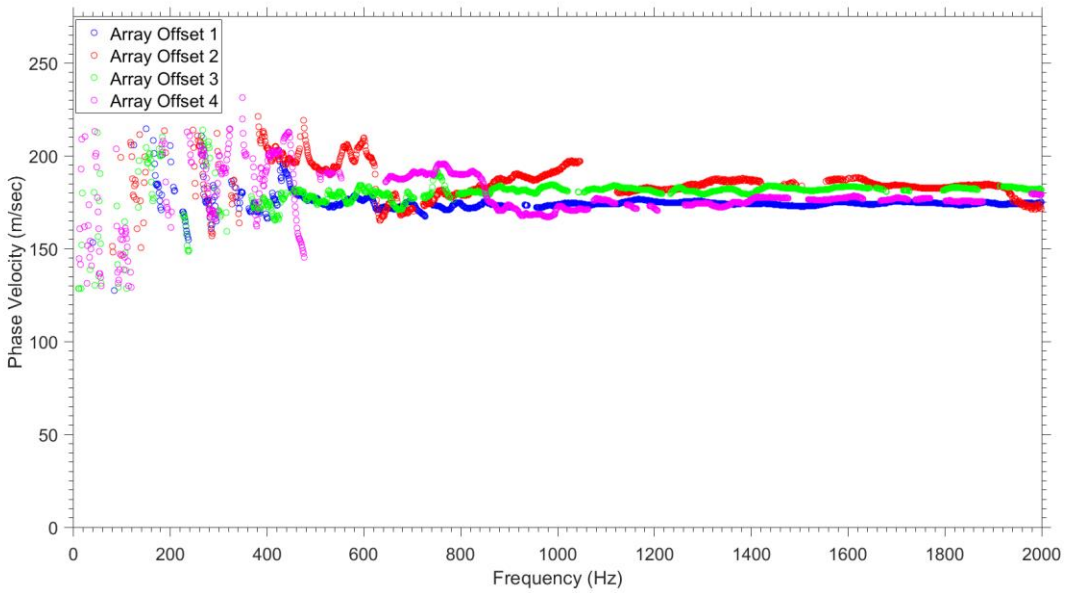

Figure 4-28. Dispersion curves displaying arrays on sand with horizontal offsets of 1/8 (Offset 1), 1/4 (Offset 2), 1/2 (Offset 3), and 3/4 (Offset 4) of the box width away from the concrete wall.

4.6.2 Clay

Additional MASW testing was performed on clay but the dispersion curves did not provide coherent results. A possible cause for the problematic data could be the manner in which the soil was compacted. The soil was compacted with a plate compactor that ultimately bowed out the sides of the box producing a non-uniform compaction within the box.

The initial results from testing the effect of lateral variability on Rayleigh wave propagation indicate that there is no systematic difference as the array is moved closer to the wall. Further testing is required to definitively determine the effect of horizontal variability on MASW data.

4.7 Overall Conclusions

The proper testing procedure for performing MASW on asphalt pavement and soil is critical as the results proved to be much more dependent on the testing parameters than concrete

pavement results. The findings of this section are summarized below and in Table 4-6. The recommended testing procedure for MASW on asphalt includes a source with a mass of approximately 230g with a metal tip, a receiver spacing of 2.5 cm, 24 receiver array, source offsets of 12.5 cm, 25 cm, and 50 cm. Concrete, as mentioned above, was much more resilient in that the testing methods did not dramatically affect the data collected. The recommended testing procedure for MASW testing on concrete includes a source with a mass of approximately 230g with a metal tip, a receiver spacing of 5 cm, 24 receiver array, and source offsets of 12.5 cm, 25 cm, 50 cm, and 75 cm. If needed, the amount of receivers may be reduced to 18 if only high frequency data is of interest. Like asphalt, soil proved to be very dependent on the method used to collect the data. The recommend testing procedure for MASW testing on soil includes a source with a mass of approximately 230g with a metal tip, a receiver spacing of 5 cm, 12 receiver array, source offsets of 12.5 cm, 25 cm, and 50 cm.

Table 4-6. Recommended MASW testing procedure for asphalt, concrete, and soil.

Recommended Asphalt Testing Procedure		Recommended Concrete Testing Procedure		Recommended Soil Testing Procedure	
Source Type	230g Metal tipped hammer	Source Type	230g Metal tipped hammer	Source Type	230g Metal tipped hammer
Reciever Spacing	2.5cm	Reciever Spacing	5cm	Reciever Spacing	5cm
Source Offsets	12.5cm, 25cm, 50cm	Source Offsets	12.5cm, 25cm, 50cm, 75cm	Source Offsets	12.5cm, 25cm, 50cm
Minimum Number of Receivers	24	Minimum Number of Receivers	18	Minimum Number of Receivers	12

5 Relationship between ASR Expansion and Shear Wave Velocity in Concrete

5.1 Overview

In determining if MASW has the capability to detect damage from common pavement defects, two phases of testing were implemented. The first phase, Section 5.2, is to examine the relationship between an increase in material damage and shear wave velocity. The second phase will consist of MASW field tests done on highly damaged concrete barrier walls located south of Fayetteville, Arkansas on Interstate 49.

For the following results, alkali-silica reaction (ASR) was examined because it causes a large increase in strain due to micro and macro cracking. For this purpose, three groups of three prisms were constructed with varying amounts of Jobe sand, which changed the degree of ASR reactivity of each prism set. The two reactive groups, 40R and 20R, contained 40% and 20% Jobe sand, respectively, while the control group (0C) contained no Jobe sand. Jobe sand was used because of its high silica content and it is known to be highly reactive (Phillips et al. 2015). To further ensure ASR, the prisms were cured in a high heat, high humidity curing chamber. The shear wave velocity was recorded in accordance with ASTM C215. The results are presented and discussed in the following section.

5.2 Discussion

The results presented in Figure 5-2 were corrected in order to objectively examine the shear wave velocity degradation due to ASR. The shear wave velocity was corrected because the concrete was gaining shear wave velocity due to the curing process meanwhile microcracking was causing a reduction. The reactive specimen data was corrected by the increase in velocity of the control group for the same period or $\sum_{t=1}^{7} V_{s(t)}$. An example is provided in Figure 5-1.

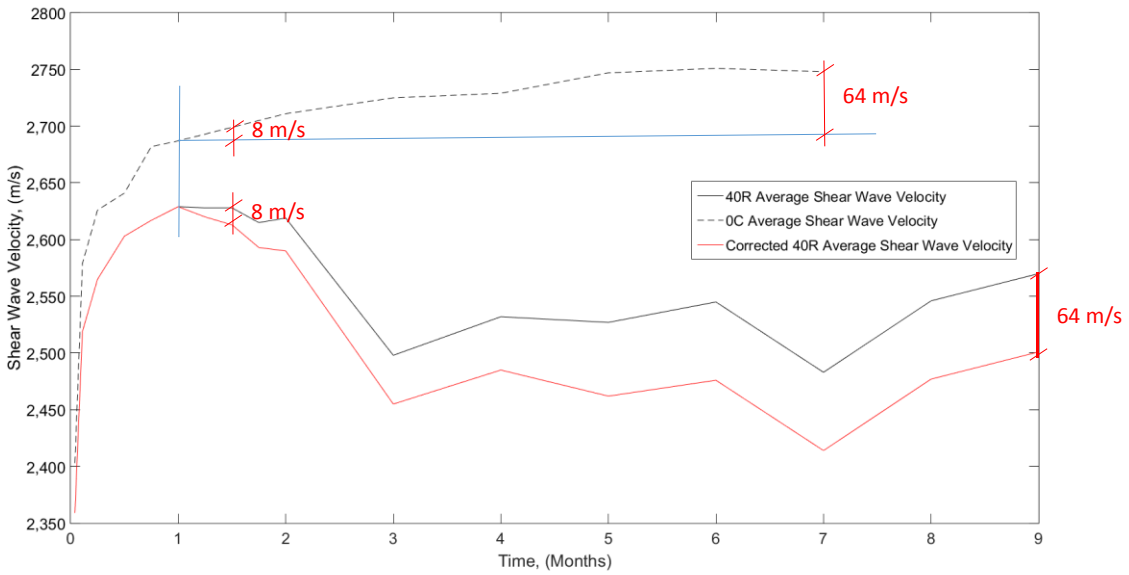

Figure 5-1. Example reduction of shear wave velocity.

The results from the resonant frequency testing on prisms with 40% Jobe sand (40R), 20% Jobe sand (20R), and 0% Jobe sand (0C) are presented in Figure 5-2. Additionally, pictures detailing the typical exterior condition of each set of prisms is presented in Figure 5-3a-c.

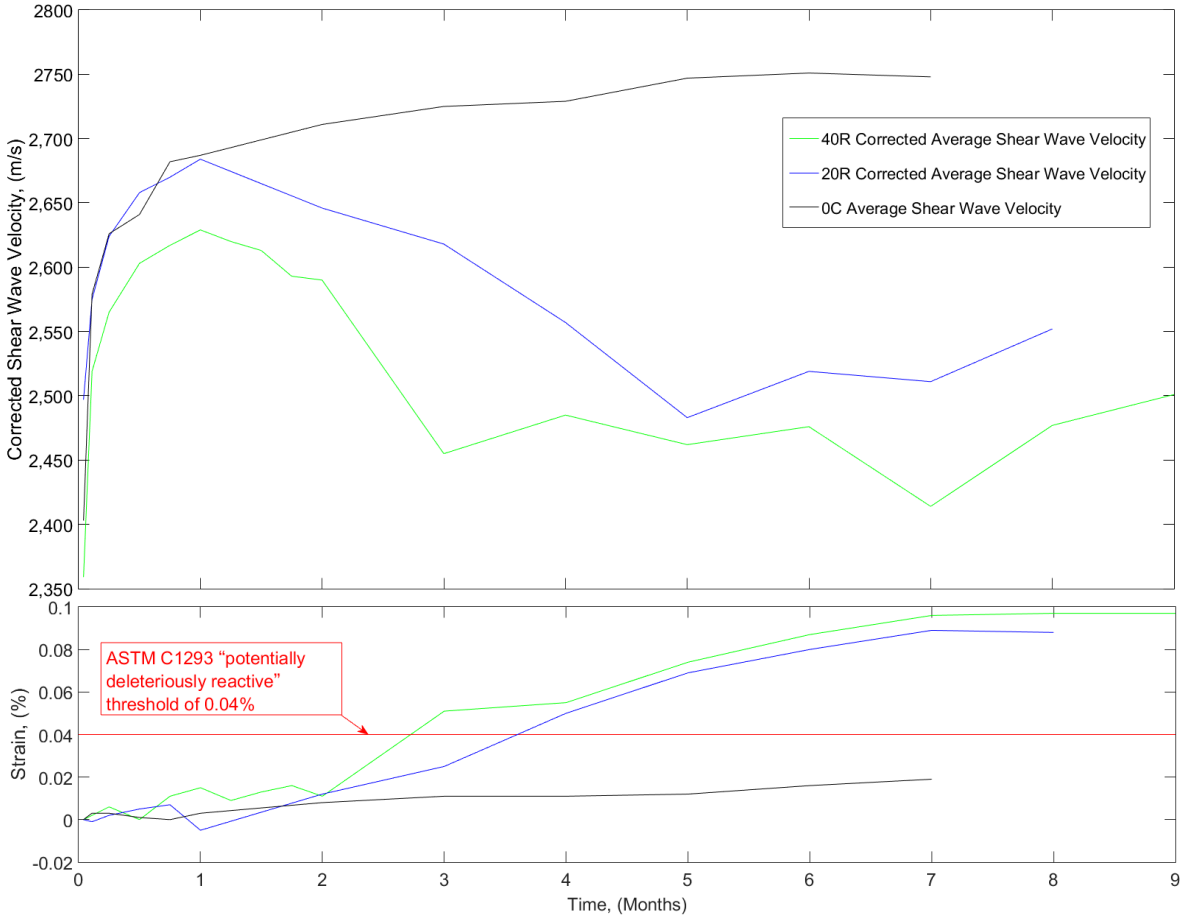

Figure 5-2. Shear wave velocity and strain results for prism groups 40R, 20R, and 0C. Trends are shown as the average of the three specimens in each group.

a)

b)

c)

Figure 5-3a-c. Typical cracking from ASR in: a) 40R, b) 20R, and c) 0C.

The shear wave velocity for both reactive groups (20R and 40R) begins to decrease as strain increases around one month. The 20R group had roughly an 8% decrease from the corresponding 0C velocity while increasing in strain by a difference of 0.07%, which produced longitudinal cracking (Figure 5-3b). Likewise the 40R group had approximately a 10% decrease in velocity and a difference in strain of 0.077%, which also produced longitudinal cracking (Figure 5-3a). The control group exhibited no cracking (Figure 5-3c). For the strain levels measured in this study, shear wave velocity can be correlated to strain increases caused by ASR damage.

5.3 MASW Case Study Overview

The second phase of research focuses on MASW field testing on a concrete barrier wall with known ASR damage along Interstate 49. Three locations were chosen with varying amounts of damage. Site C-1, which is pictured in Figure 5-4a, was visually classified as having "minimal" ASR damage. Site C-2, which is pictured in Figure 5-4b, was visually classified as having "moderate" ASR damage. Site C-3, which is pictured in Figure 5-4c, was visually classified as having "severe" ASR damage. The pictures are colored coded to relate to the dispersion curves in Figure 5-5.

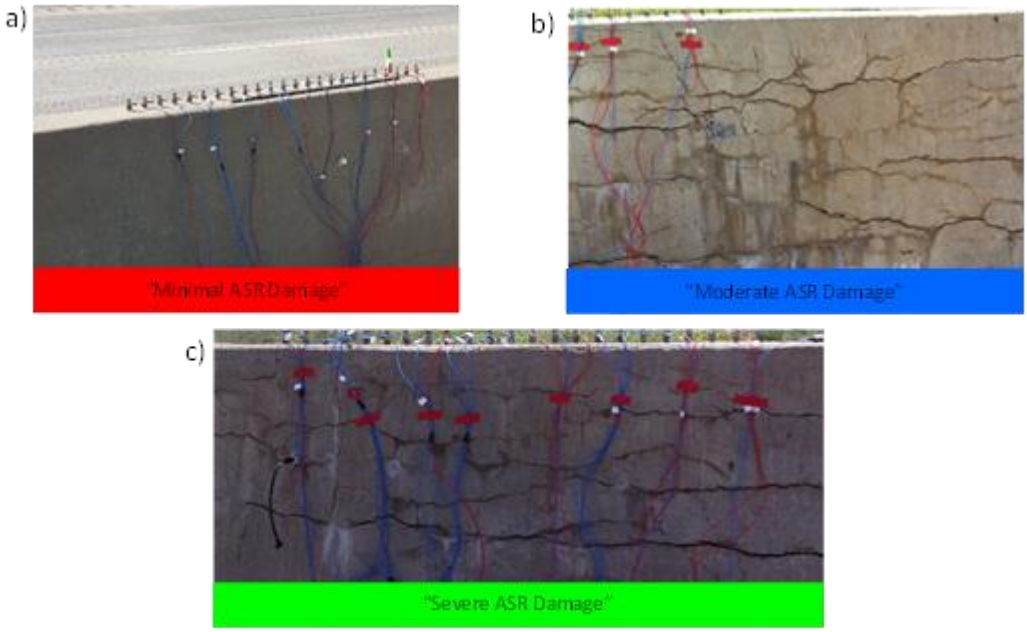

Figure 5-4. Three barrier wall sites with varying levels of damage located near Exit 45 on Interstate 45 south of Fayetteville, Arkansas. a) Site C-1 visually classified "minimal" ASR damage, b) Site C-2 visually classified "moderate" ASR damage, c) Site C-3 visually classified "severe" ASR damage.

5.4 Discussion

The dispersion curves for testing done in June 2015 and March 2016 at each site are presented in Figure 5-5. The strain levels associated with each site and date are presented in

Table 5-1. Unlike MASW testing performed on pavement, MASW testing on a barrier wall does not produce Lamb waves because a barrier wall is not a plate-like structure.

For the two dispersion curves measured at Site C-1, which are approximately 9 months apart, the March 2016 dispersion curve has a slightly larger Rayleigh wave phase velocity (~2.5%) and a lower percent strain. This is likely due to the wall shrinking because of temperature effects. The two dispersion curves for Site C-2 are also in general agreement until 18 kHz when the June 2015 phase velocity increases to approximately 2500 m/s, while the March 2016 velocity decreases to 2200 m/s. This could be interpreted as an increase in material damage close to the surface that occurred over the 9 month period. For the two dispersion curves for Site C-3, an average decrease in velocity of 50-100 m/s between the June 2015 and March 2016 data is observed. Therefore, for site C-3 damage seems to be occurring at all depths, while additional damage at site C-2 is constrained to the top portion of the barrier wall.

When simply comparing the results from Sites C-2 and C-3 for both testing dates, similar Rayleigh wave velocities (ranging from 0-10% difference) were observed but vastly different strain levels were measured for the two sites (i.e., Site C-3 has a measured strain roughly 250% greater than that of Site C-2). This negligible difference in Rayleigh wave velocity but vast difference in strain can be attributed to two different reasons. The first is that strain measures external conditions while Rayleigh waves propagate throughout the entire specimen. The second reason is that the strains for sites C-2 and C-3 could be similar because the reported strain levels are not absolute (i.e., ASR was first noted in these walls in 2005 but strain monitoring did not begin until 2013). Sites C-2 and C-3 compare favorably to Site C-1 in that they have approximately a 20% difference in measured Rayleigh wave velocity. Therefore, using MASW, it is possible to classify the damage when evaluating samples with less than approximately

0.09% strain. Beyond 0.09% strain or where significant damage has occurred, it appears to be less sensitive to additional damage and it is difficult to differentiate between moderately and severely damaged sections. It is important to note that MASW, like all stress wave NDTs, cannot identify ASR directly, but can only measure the damage associated with ASR.

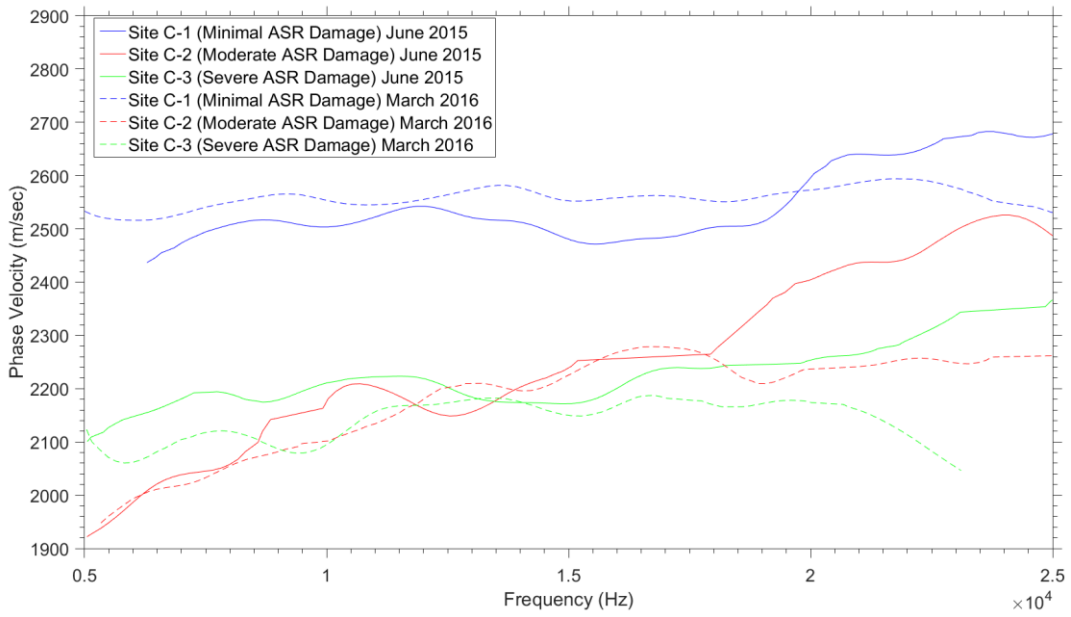

Figure 5-5. Dispersion curves of ASR damaged barrier walls sites C-1, C-2, and C-3 for June 2015 (solid) and March 2016 (dashed).

Table 5-1. Strain associated with three ASR affected barrier wall sites.

	Strain	
Site	June 2015	March 2016
C-1	0.017%	0.009%
C-2	0.088%	0.100%
C-3	0.291%	0.327%

5.5 Conclusions

The reactive prisms (40R and 20R) exhibited a small amount of external macro cracking and strain levels double that of what the ASTM classifies as “potentially deleteriously reactive.” The reactive groups’ (40R and 20R) shear wave velocities at eight months decreased by 10% and

8% and while strains increased by 0.077% and 0.069%, respectively compared to the control group. This indicates that shear wave velocity can be correlated to strain increases caused by ASR damage.

Similar to resonant frequency testing, MASW testing can detect a general degradation of shear wave velocity but MASW may not be capable of reliably correlating strain levels and shear wave velocities in highly damaged concrete. MASW is better suited to evaluate specimens with less than 0.09% strain based on the limited testing done but additional testing is planned to better identify the limits of MASW testing. Additionally, there can be significant variation (30%) in Rayleigh wave velocity at frequencies ranging from 5 kHz to 25 kHz thereby making it difficult to choose a representative Rayleigh wave velocity to assign to the concrete specimen being tested.

6 Summary and Conclusions

In determining the optimum parameters for performing MASW on pavements, four parameters were evaluated using five different sites. The parameters investigated were source type, source offset, receiver spacing, and total number of receivers in the array. For investigating the optimum source type, two sources were used: a 230g metal-tipped hammer and an 1160g rubber-tipped hammer. Six source offsets were investigated were 12.5 cm, 25 cm, 50 cm, 75 cm, 100 cm, and 150 cm from the first receiver in the array. The receiver spacings tested were 2.5 cm, 5 cm, and 10 cm. The last parameter tested was the number of receivers. For this section, arrays with 12, 18, and 24 receivers were tested. Each one of these parameters was evaluated at five different sites which consisted of three materials common in transportation: asphalt, concrete, and soil. There were two asphalt sites ("CTTP Asphalt" and "ENRC Asphalt"), two concrete sites ("ENRC East Concrete" and "ENRC West Concrete"), and one soil site ("CTTP

Soil"). All of the sites were located at the University of Arkansas Engineering Research Center located in Fayetteville, Arkansas.

The second portion of this research focused on establishing a relationship between a degradation in shear wave velocity and an increase in material damage. This was conducted in two phases. The first phase was to construct three groups of concrete prisms in accordance with ASTM C1293. The three groups (one control and two reactive) each had a varying amount of ASR deleterious reactivity. The prisms' expansion and shear wave velocity were tested on a monthly basis. The second phase of this research was to perform MASW on three ASR damaged barrier walls south of Fayetteville, Arkansas on Interstate 49. These sites were chosen because the strain is currently being monitored by Ricky Deschenes of the University of Arkansas.

Based on testing conducted in this research, the optimum MASW testing parameters are presented below. Although these parameters worked well in this research, results show that obtaining good results at some sites, particular asphalt sites, is more contingent on using the appropriate testing parameters than other sites. Therefore, multiple setups maybe required at some sites to obtain quality data.

For the two source types investigated in this research, the 230g hammer generally performed better on all three surfaces. The 230g hammer performed best on the asphalt and soil sites while the dispersion curve generated using the 1160g hammer had significant far-field effects at these sites. In some cases, the 1160g hammer's maximum measured frequency was 200% lower than the maximum resolved frequency measured when using a 230g hammer as a source. On concrete, the source type did not prove to be of significance in data quality as both hammers produced comparable data at all frequencies.

The distance the source was placed from the receiver array was determined to be an important aspect when testing asphalt and soil. Source offsets of 12.5 cm, 25 cm, and 50 cm were optimal for both sites. Any further offset showed significant far-field effects and produced little high frequency data. Somewhat unpredictably, a 12.5 cm source offset did not produce good high frequency data which highlights the need for redundant testing (i.e., more than one source offset). Each offset takes about one minute to perform so it is easy to mitigate the risk of not having enough dispersion data by performing multiple offsets. For concrete, source offsets of 12.5 cm, 25 cm, 50 cm, and 75 cm were determined to be most appropriate.

The receiver spacing is a critical parameter for all three materials tested. For asphalt, a receiver spacing of 2.5 cm produced data with the highest maximum resolvable frequency. Offsets of 5 cm and 10 cm produced data with maximum frequencies that were 50% to 400% less than the maximum frequency resolved using the 2.5 cm spacing. The 2.5 cm spacing did not perform well on concrete through. The spacing produced a much larger COV compared to the 5 cm and 10 cm receiver spacings. It is recommended that a 5 cm rather than a 10 cm spacing is used for concrete testing because of the ease of constructing the array. On soil, the 10 cm spacing had a 50% smaller frequency range compared to the 5 cm spacing due to far-field effects. It is recommended that a 5 cm spacing is used when testing soil.

For asphalt, 24 receivers were needed to produce the highest quality, high frequency data. The 12 and 18 receiver arrays produced data with a frequency range that was 30-50% less than that of the 24 receiver array. On concrete, the 12 receiver array produced acceptable high frequency data but it had a larger COV compared to either the 18 or 24 receiver array. The 18 receiver array performed very similarly to the 24 receiver array. Therefore, for testing on concrete at least 18 receivers are recommend for MASW testing. Finally, the number of receivers

proved to be of little significance on near surface MASW testing on soil. A 12 receiver array performed nearly identically to the 24 receiver array. A 12 receiver array also did not produce any near-field effects in the data collected. Therefore, at least 12 receivers are recommended for MASW testing on soils. Regardless of the sites tested, the inclusion of more receivers always results in improved data quality. Therefore, using more receivers to collect MASW data is always recommended.

A summary of all recommended MASW testing parameters is presented in Table 6-1. It is important to note that this recommendation is based on materials tested in this study and may not be applicable to all scenarios.

Table 6-1. Recommended MASW testing procedure for asphalt, concrete, and soil.

Recommended Asphalt Testing Procedure		Recommended Concrete Testing Procedure		Recommended Soil Testing Procedure	
Source Type	230g Metal tipped hammer	Source Type	230g Metal tipped hammer	Source Type	230g Metal tipped hammer
Reciever Spacing	2.5cm	Reciever Spacing	5cm	Reciever Spacing	5cm
Source Offsets	12.5cm, 25cm, 50cm	Source Offsets	12.5cm, 25cm, 50cm, 75cm	Source Offsets	12.5cm, 25cm, 50cm
Minimum Number of Receivers	24	Minimum Number of Receivers	18	Minimum Number of Receivers	12

The second section of the research conducted for this thesis studied the relationship between material damage and shear wave velocity. It was determined using the torsional frequency test outlined in ASTM C215, a general trend can be identified that as material damage/strain increases, shear wave velocity will decrease. A reduction in shear wave velocity from the control group to the 40R group of 10% was measured while a strain increase of 0.077% was observed between the two groups. Likewise, there was a reduction in shear wave velocity from the control group to the 20R group of 8% was measured while a stain increase of 0.07% was observed between the two groups. Based on this limited data set, shear wave velocity can be reliably correlated to the strain levels measured in this study.

Additional MASW testing of ASR affected concrete was conducted along sections of a barrier wall on I-49. A definitive decrease in shear wave velocity was observed (15-20%) between a heavily damaged section and a lightly damaged section. However, when comparing two heavily damaged sections (one with 0.09% strain and one with 0.29% strain) there was only a small to negligible change in shear wave velocity. This negligible difference in shear wave velocity could be due to the strain measurements being taken at the exterior of the wall while the Rayleigh waves are propagating through a more interior portion of the wall (i.e., the two tests are measuring two different conditions). Also ASR was first noted in the barrier wall in 2005 but strain was not measured until 2013 thus the strain levels are not absolute. Based on this limited data set, MASW can be recommended to evaluate minimally to moderately damaged concrete (0-0.09% strain) but given the data collected it cannot be determined if MASW can be used to differentiate between concrete sections with strains larger than 0.09% (i.e., sections with heavy damage). More testing is needed on specimens with strain levels ranging from 0-0.3% to develop a definitive relationship between strain and shear wave velocity at those high strain levels in damaged concrete.

7 Future Research

Future research is needed to evaluate how each MASW testing parameter affects the full inversion of a data set. Additionally, a faster way to couple the receivers to the pavement is needed as that is the most time consuming portion of testing. Methods researched should include noncontact receivers.

The researchers attempted to determine the effect of lateral variability on Rayleigh wave propagation in Section 4, but the materials used proved to be too inconsistent or not cohesive enough. Possible future materials need to be cohesive and not require compaction.

To better establish a relationship between MASW obtained shear wave velocities and strain levels, additional research is needed on ASR affected concrete specimens with a diverse range of strain levels.

In order to build a more robust relationship between resonant frequency obtained shear wave velocities and strain levels, the current concrete prisms must be manipulated by introducing more alkalis to the curing environment. This will increase strain levels significantly and allow for more data points with time.

Works Cited

Aki, K., and PG Richards. "Quantitative Seismology: Theory and Methods WH Freeman and Company." San Francisco, California (1980) Print.

Al-Hunaidi, MO. "Insights on the SASW Nondestructive Testing Method." Canadian Journal of Civil Engineering 20.6 (1993): 940-50. Print.

Alzate-Diaz, Sara P., and John S. Popovics. "Application of MASW to Characterize Pavement Top Layers." Proceedings: Non-Destructive Testing in Civil Engineering (2009) Print.

"Arkansas." Map. Google Maps. Google, 08 March 2016. Web. 08 March 2016.

Bolt, Bruce A. "Nuclear Explosions and Earthquakes. The Parted Vail." (1976)Print.

Carino, Nicholas J. "The Impact-Echo Method: An Overview". Proceedings of the 2001 Structures Congress & Exposition. 2001. 21-23. Print.

Du Tertre, Antonin. "Nondestructive Evaluation of Asphalt Pavement Joints using LWD and MASW Tests." (2010)Print.

"Fayetteville, Arkansas." Map. Google Maps. Google, 08 March 2016. Web. 08 March 2016.

FHWA. "Falling Weight Deflectometer." Web. <https://www.fhwa.dot.gov/publications/research/infrastructure/pavements/ltpp/07040/images/figure6.jpg>.

Foti, Sebastiano. Multistation methods for geotechnical characterization using surface waves (2000) Print.

Gucunski, Nenad. Nondestructive Testing to Identify Concrete Bridge Deck Deterioration. Transportation Research Board, 2013. Print.

Hebeler, Gregory L., and Glenn J. Rix. "Site Characterization in Shelby County, Tennessee using Advanced Surface Wave Methods." MAE Center CD Release 06-02 (2007) Print.

Heisey, JS, II Stokoe, and AH Meyer. "Moduli of Pavement Systems from Spectral Analysis of Surface Waves." Transportation Research Record.852 (1982) Print.

Hobbs, Don W. "Alkali-Silica Reaction in Concrete." (1988)Print.

Jones, Ronald. "In-Situ Measurement of the Dynamic Properties of Soil by Vibration Methods*." Geotechnique 8.1 (1958): 1-21. Print.

Jones, R. "Surface Wave Technique for Measuring the Elastic Properties and Thickness of Roads: Theoretical Development." British Journal of Applied Physics 13.1 (1962): 21. Print.

Kreitman, KL, et al. "Nondestructive Evaluation of Reinforced Concrete Structures Affected by ASR". Proceedings of the 14th International Conference on Alkali-Aggregate Reaction. 2012. Print.

Lamb, Horace. "On Waves in an Elastic Plate." Proceedings of the Royal Society of London. Series A, Containing papers of a mathematical and physical character (1917): 114-28. Print.

Liang, Qing, and Chao Chen. "Comparative Analysis on Sensitivities of Love and Rayleigh Waves." (2007)Print.

Lin, S., and JC Ashlock. "Comparison of MASW and MSOR for Surface Wave Testing of Pavements". 27th Annual Symposium on the Application of Geophysics to Engineering and Environmental Problems (SAGEEP). 2014. Print.

Lin, Shibin. "Advancements in Active Surface Wave Methods: Modeling, Testing, and Inversion." (2014)Print.

Love, Augustus Edward Hough. Some Problems of Geodynamics: Being an Essay to which the Adams Prize in the University of Cambridge was Adjudged in 1911. CUP Archive, 1911. Print.

Martincek, G. "Dynamics of Pavement Structures E & FN Spon and Ister Science Press." Bratislava, Slovak Republic (1994) Print.

Miller, GF, and H. Pursey. "On the Partition of Energy between Elastic Waves in a Semi-Infinite Solid." Proceedings of the Royal Society of London. Series A, Mathematical and Physical Sciences (1955): 55-69. Print.

Nazarian, S., D. Yuan, and Vivek Tandon. "Structural Field Testing of Flexible Pavement Layers with Seismic Methods for Quality Control." Transportation Research Record: Journal of the Transportation Research Board.1654 (1999): 50-60. Print.

Nazarian, Soheil, et al. Use of Spectral Analysis of Surface Waves Method for Determination of Moduli and Thicknesses of Pavement Systems. 1983. Print.

Park, Choon B., et al. "Seismic Investigation of Pavements by MASW method geophone Approach". Proceedings of the SAGEEP. 2001. Print.

Park, Choon Byong, Richard D. Miller, and Jianghai Xia. "Imaging Dispersion Curves of Surface Waves on Multi-Channel Record". SEG Expanded Abstracts. 1998. 1377-1380. Print.

PCB. "Introduction to Piezoelectric Industrial Accelerometers." Web. <http://www.pcb.com/techsupport/tech_indaccel>.

Pessiki, Stephen Paul. "In-Place Methods to Estimate Concrete Strength: ACI 228.1 R-03".American Concrete Institute, 2003. Print.

Phillips, William J., Richard Deschenes, and Micah Hale. Alkali Silica Reaction Mitigation Using High Volume Class C Fly Ash (2015) Print.

Rivard, Patrice, and Francois Saint-Pierre. "Assessing Alkali-Silica Reaction Damage to Concrete with Non-Destructive Methods: From the Lab to the Field." Construction and Building Materials 23.2 (2009): 902-9. Print.

Rix, Glenn J., Kenneth H. Stokoe, and Jose M. Roesset. "Experimental Study of Factors Affecting the Spectral-Analysis-of-Surface-Waves Method." (1991)Print.

Roesset, Jose M., and Ko-Young Shao. Dynamic Interpretation of Dynaflect and Falling Weight Deflectometer Tests., 1985. Print.

Ryden, Nils, et al. "Lamb Wave Analysis for Nondestructive Testing of Concrete Plate Structures". Proceedings of the Symposium on the Application of Geophysics to Engineering and Environmental Problems (SAGEEP 2003), San Antonio, TX, April. 2003. 6-10. Print.

---. "Multimodal Approach to Seismic Pavement Testing." Journal of Geotechnical and Geoenvironmental Engineering 130.6 (2004): 636-45. Print.

Ryden, Nils, and Choon Byong Park. "Fast Simulated Annealing Inversion of Surface Waves on Pavement using Phase-Velocity Spectra." Geophysics 71.4 (2006) Print.

Ryden, Nils, et al. "Portable Seismic Acquisition System (PSAS) for Pavement MASW". Proc., Symp. on the Application of Geophysics to Engineering and Environmental Problems (SAGEEP 2002). 2002. Print.

Ryden, Nils, et al. "High Frequency MASW for Non-Destructive Testing of pavements "Accelerometer Approach". 14th EEGS Symposium on the Application of Geophysics to Engineering and Environmental Problems. 2001. Print.

Sargolzahi, Maryam, et al. "Effectiveness of Nondestructive Testing for the Evaluation of Alkali Silica Reaction in Concrete." Construction and Building Materials 24.8 (2010): 1398-403. Print.

Stanton, Thomas E. "Influence of Cement and Aggregate on Concrete Expansion." Engineering News-Record (1940). Print.

Stokoe, Kenneth H., et al. "Characterization of Geotechnical Sites by SASW Method." Geophysical characterization of sites (1994): 15-25. Print.

Stokoe, KH, Sung-Ho Joh, and RD Woods. "Some Contributions of in Situ Geophysical Measurements to Solving Geotechnical Engineering Problems". Proceedings. 2004. 97-132. Print.

Strutt, John William. "On Waves Propagated Along the Plane Surface of an Elastic Solid." Proceedings of the London Mathematical Society 17.1 (1885): 4-11. Print.

Swamy, RN, and MM Al-Asali. "Engineering Properties of Concrete Affected by Alkali-Silica Reaction." ACI Materials Journal 85.5 (1988): 367-74. Print.

Tran, Khiem T., and Dennis R. Hiltunen. "A Comparison of Shear Wave Velocity Profiles from SASW, MASW, and ReMi Techniques". Geotechnical Earthquake Engineering and Soil Dynamics IV. ASCE, 2008. 1-9. Print.

USGS. "Report on the Diagnosis, Prognosis, and Mitigation of Alkali-Silica Reaction (ASR) in Transportation Structures." 2015. Web. <https://www.fhwa.dot.gov/pavement/concrete/pubs/hif09004/asr11.cfm>.

Wood, Clinton Miller. The Impact of Source Type, Source Offset, and Receiver Spacing on Experimental MASW Data at Soft-Over-Stiff Sites. ProQuest, 2009. Print.

Yoon, Yungsoo. "Array-Based Measurements of Surface Wave Dispersion and Attenuation using Frequency-Wavenumber Analysis." Doctor of Philosophy Georgia Institute of Technology, 2005. Print.

Zywicki, Daren J., and Glenn J. Rix. "Mitigation of Near-Field Effects for Seismic Surface Wave Velocity Estimation with Cylindrical Beamformers." Journal of Geotechnical and Geoenvironmental Engineering 131.8 (2005): 970-7. Print.

Zywicki, Daren Joseph. "Advanced Signal Processing Methods Applied to Engineering Analysis of Seismic Surface Waves." (1999)Print.